BIOPHYSICAL STUDIES ON INFLUENZA A M2 PROTEIN

KEVIN CAMPBELL DUFF

Submitted in satisfaction of the requirements for the degree of PhD
in the University of Edinburgh, 1993.

Abstract

The influenza A M2 protein and, in particular, the proposed transmembrane domain, has been implicated in viral infectivity at two stages in the replicative cycle: viral uncoating and assembly. An identical function has been proposed for the protein at both points of interest, that is, that M2 acts as a proton channel. In order to work, this hypothesis assumes that M2 possesses a transmembrane domain, presumably in an α-helical conformation, that this domain orientates in a prescribed manner across the bilayer and that, indeed, M2 is able to translocate protons across the aforementioned bilayer. This thesis examines these assumptions experimentally using a synthetic, 25 amino acid peptide representing the proposed transmembrane domain of M2.

The work described herein may be divided into three main areas, each employing a separate biophysical technique. Circular dichroism was employed to assign an α-helical secondary structure to the M2 peptide. Neutron diffraction orientated this region precisely in the bilayer. Electrophysiological techniques observed directly, for the first time in viruses, proton translocation. The effects of amantadine, the only drug prescribed for use against influenza A infections, in each of these structural and functional investigations have also been recorded, providing revealing insights into the drug's efficacy.

M2 has structural analogues in other enveloped viruses and work such as that reported in this thesis may reveal a common pathway of viral infectivity for groups of enveloped viruses, therefore allowing the possibility of broad-spectrum drug therapies.

Acknowledgements

First and foremost, I would like to thank Dr Jeremy Bradshaw, my supervisor. The greatest accolade I can give is, 'without him this thesis would not have been possible'. I would also like to thank Prof Andrew Miller, head of Biochemistry, who initially gave me the opportunity of doing a PhD and who has constantly encouraged me and been enthusiastic about my results. His department may truly be said not only to promote learning amongst its students but also amongst its staff. Dr Richard Ashley and Dr Nick Price (not forgetting Ms Sharon Kelly) graciously allowed me and taught me how, to perform respectively, electrophysiological and circular dichroism experiments in their laboratories. Without them Chapters two and four would not exist.

Gratitude is extended to Dr Phil Sizer, who infected me with his belief that influenza is a 'sexy beast'. Mr Derek Notman and Mrs Oonagh Gray have produced excellent electronmicrographs for me over the last few years - I still owe them both a drink! Mr Colin Warwick tolerated my non-artistic input whilst managing to produce some beautiful figures despite me. Thanks to Mrs Maureen Pitkethly for supplying peptides at reduced cost because of the 'Scottish connection'. Also, Prof Arthur Duggan, who allowed me laboratory space in the Preclinical Veterinary Department. Thanks also go to Dr Anand Saxena for neutron beamtime, genuine interest in my project, and for inviting us along to his home on Long Island to sample his wife's excellent Indian cooking!

In addition, thanks to the lipid louts; Dr Peter Gilchrist, Mr (soon to be Dr) Andrew Cudmore, Dr Larry Hayward and, once again, Dr Jeremy Bradshaw. We managed to do the work *and* have fun!

Finally, heartfelt thanks to my wife Deanna, who has tolerated my occasional anxiety attacks with an honestly held (and quite mystifying) belief in my abilities. Love to her.

This thesis is lovingly dedicated to the memory of my mother, Ann.

"...an horizon is nothing, save the limit of our sight..."

Declaration

I declare that this thesis has been composed by myself and that the work described herein is my own except where stated.

List of contents

A The secondary structure of influenza A M2 transmembrane domain - a circular dichroism study

B The location of amantadine hydrochloride and free base within phospholipid multilayers: a neutron and X-ray diffraction study

C The transmembrane domain of influenza A M2 protein forms amantadine-sensitive proton channels in planar lipid bilayers

List of Exhibits

(titles comprehensively abridged)

Abbreviations

Ab	antibody
Ag	antigen
AIDS	acquired immunodeficiency syndrome
amantadine FB and HCl	1-amino adamantane (free base or hydrochloride)
Brookhaven	Brookhaven National Laboratory, Long Island, New York, U.S.A.
CD	circular dichroism
D_2O	deuterium oxide
DMPC	1,2-dimyristoyl-*sn*-glycero-3-phosphocholine
DOPC	1,2-dioleoyl-*sn*-glycero-3-phosphocholine
DOPE	1,2-dioleoyl-*sn*-glycero-3-phosphoethanolamine
DOPG	1,2-dioleoyl-*sn*-glycero-3-phosphoglycerol
DPPC	1,2-dipalmitoyl-*sn*-glycero-3-phosphocholine
EDTA	ethylenediaminetetraacetic acid
EM	electron microscopy
HA	haemagglutinin
HE	haemagglutinin esterase
HIV	human immunodeficiency virus
HPLC	high pressure liquid chromatography
ILL	Institut Laue Langevin, Grenoble, France
M1	matrix, membrane or major protein
M2	second (segment 7) influenza M protein discovered
MDCK	Madin-Darby canine kidney
MII	transmembrane domain of nicotinic acetylcholine receptor
MRC	Medical Research Council
mRNA	messenger RNA
NA	neuraminadase
NB	protein found in influenza B, similar to NA in influenza A
NMR	nuclear magnetic resonance
NP	nucleoprotein
NS1, NS2	non-structural proteins
OG	*n*-octyl glucopyranoside
PB1, PB2, PA	polymerase proteins
pH	potenz hydrogens
POPE	1-palmitoyl-2-oleoyl-*sn*-glycero-3-phosphoethanolamine

POPS	1-palmitoyl-2-oleoyl-*sn*-glycero-3-phosphoserine
rh	relative humidity
RNA	ribonucleic acid
RNP	ribonucleoprotein
SDS	sodium dodecyl sulphate
SH	small hydrophobic
SV5	simian virus 5
TFA	trifluoroacetic acid
UV	ultraviolet
WHO	World Health Organisation

Amino acid codes :

A - Ala - alanine
R - Arg - arginine
D - Asp - aspartic acid
G - Gly - glycine
H - His - histidine
I - Ile - isoleucine
L - Leu - leucine
P - Pro - proline
S - Ser - serine
W - Trp - tryptophan
V - Val - valine

CHAPTER 1 INTRODUCTION TO INFLUENZA

1. Introduction to influenza

1.1 Historical background

The epidemic is seldom mentioned, and most have apparently forgotten it. This is not surprising. The human mind always tries to expunge the intolerable from memory, just as it tries to conceal it while current.

H. L. Mencken

This is how Mencken (Sacks, 1985) described the great Spanish influenza pandemic of 1918-1919, the most devastating outbreak of disease since the Black Death of the Middle Ages. Just as the world was trying to recover from the carnage of the Great War the influenza virus struck. In a few short months approximately twenty-one million people worldwide died. Double the number of Britains slain in the war were killed by influenza, half a million Americans died, isolated villages in Alaska were destroyed down to the last person, and, in India alone, five million fatalities occurred. In terms of numbers of dead, it was the greatest visitation ever experienced by the human race.

Pestilences of many sorts have brought death and misery to mankind throughout history. Over the last one hundred years most of these plagues have been brought under control; the black death, cholera, yellow fever, typhus and smallpox no longer rage unchecked every few years. But influenza continues to flourish and to cause pandemics that periodically sweep around the world without restraint. In 1977, (before the identification of acquired immune disease [AIDS]) Beveridge described influenza as 'the last of the great plagues' (Beveridge, 1977).

The name 'influenza' was originally coined in an Italian document of 1504 and is a corruption of the Latin/Italian word *influentia* - 'a flowing from the stars of ethereal fluid affecting the character and destiny of man.' Thus the causative agent was thought to be astral in origin. However, the disease had masqueraded under various names before this; one of the first recorded epidemics being reported in classical times, 412 B.C., by Hippocrates and Livy. Quite a number of epidemics that were beyond reasonable doubt influenza were described in the Middle Ages. Definite pandemics took place in 1510 and 1580, and between these two dates, it was documented that, in 1562, Mary, Queen of Scots, 'fell acquainted' with influenza upon her arrival in Edinburgh from France. Indeed, the historical record clearly demonstrates that pandemics have occurred at intervals since ancient times. More recently, influenza deaths in Britain during the pandemic of 1847 exceeded those of the great cholera plague of 1832. In 1889-1890 the world suffered the Asian influenza pandemic. This influenza strain appears to have been highly virulent. In Europe the incidence was reported to be 40-50% and a total of around 1% of the population died. The 1918-1919 pandemic, as mentioned, was by far the most devastating in modern times but serious influenza outbreaks have still continued into the virological era. In 1968, the Hong Kong virus was first reported in China. During the following winter it became pandemic and the mortality in the U.S.A. was estimated at around eighty thousand, and, in the U.K., an estimated thirty thousand died in an eight week period alone. The winters of 1971, 1972 and 1975 all displayed increased influenza rates and associated deaths, indicating that

influenza viruses were highly active (Harris *et al.*, 1985). In 1989, an epidemic in the U.K. killed about twenty-five thousand people (O'Neill, 1991). And, most recently, in England and Wales the number of deaths attributed to influenza and pneumonia recorded for the winter of 1990 was ten thousand (Curwen *et al.*, 1990).

The influenza virus has also been implicated in other illnesses (Section 1.2). Schizophrenia, encephalitis lethargica and certain leukemias have been postulated to have, at least to a degree, an influenza aetiological input.

Such historical studies of influenza lead to the conclusion that epidemics on a global scale will continue to occur until more effective measures of combating the disease are devised and implemented. Charles Cockburn, head of the viral section of the World Health Organisation, wrote in 1973, "The influenza virus behaves just as it seems to have done for five hundred or a thousand years, and we are no more capable of stopping epidemics or pandemics than our ancestors were." Influenza pandemics could well become increasingly serious and there is no known reason why there should not be another catastrophic one like that of 1918 or even worse; the disease known as fowl plague, caused by an influenza virus, results in one hundred percent mortality in chickens.

1.2 The disease, its prevention and treatment

The onset of illness is usually rather abrupt and early symptoms such as headache, shivers and a dry cough occur 48 hours or more after the acquisition of infection. In most cases, a sudden rise in temperature from 37°C to 40°C is accompanied by intensification of

the headache, weakness and pain in the joints. Sleep is disturbed, a cough develops and the nose becomes obstructed but without production of a profuse discharge. With influenza B infections, nasal discharge does occur, and this, along with frequent sneezing causes a resemblance to the common cold. But with influenza A, a stuffy, blocked nose and dry throat are more often reported. The degree of prostration is very variable and is related both to age and the severity of the fever. The duration of the latter may average between one and five days. The dry cough is followed by limited expectoration and the voice may become hoarse. The involvement of the lower respiratory tract may be indicated by patches of rales over the lungs. Chest or cardiac complications may now occur and it is at this stage that sudden or unexpected deaths can result, particularly in the aged and the very young. Convalescence in those without previous illness is usually rapid once the fever has subsided but lassitude, depression and a painful cough may persist for several days.

Although these are the most readily recognisable symptoms of influenza A infection, the virus has also been implicated in other serious illnesses. Respiratory complications include primary (viral) pneumonia and secondary (bacterial) pneumonia. The latter may occur particularly in patients with a history of chronic lung disease (Scadding, 1937), the former has a high mortality rate (Hers *et al.*, 1958) and is thought to have been involved in the severity of the 1918 outbreak. Cardiac complications have also been described with reports of inflammatory myocarditis in previously healthy patients (Hers *et al.*, 1958; Martin *et al.*, 1959). Neurological problems may arise (Dubowitz, 1958) involving influenzal encephalitis.

Intriguingly, the neurological pandemic of viral encephalitis lethargica, that swept the world in 1918-1919, overlapped with the worldwide influenza outbreak. It is probable, but not certain, that the influenza pandemic in some manner paved the way for the encephalitis, and that the influenza virus potentiated the effects of the encephalitis virus, or lowered resistance to it in a catastrophic way (Sacks, 1985). Recent studies have also included linking schizophrenia with influenza (O'Callaghan *et al.*, 1991). In summary, it is postulated that in the first trimester, a pregnant woman exposed to influenza infection develops antibodies (Ab) to this virus. The foetal blood/brain barrier is not fully developed and maternal Ab can therefore travel through the placenta to the foetal brain. Here the Ab somehow recognises as antigen (Ag) an area of hippocampus implicated in schizophrenia. Subsequent tissue damage occurs (Prof R.M. Murray, Dept of Psychological Medicine, Institute of Psychology, Kings College Hospital, London, U.K.; personal communication).

Vaccine and drug therapy development against influenza has not been very successful. This is due to the unique properties of the virus itself. There are differences in epidemiological behaviour and host range between influenza types; studies have shown that influenza C virus may resemble A in its ability to infect animals as well as humans (Guo *et al.*, 1983), whilst for influenza B no consistent evidence is available which suggests the existence of extra-human reservoirs of infection. Host range may indeed have effects on viral structure. Influenza viruses are unique among the respiratory tract viruses in that they undergo significant antigenic change. Both of the surface antigens (Section 1.3) of the influenza

A virus undergo two types of antigenic variation: drift and shift. Antigenic drift involves minor antigenic changes in the haemagglutinin (HA) and/or neuraminadase (NA), while shift involves major changes in these molecules. Antigenic drift is due to point mutations in the gene leading to an accumulation of amino acid changes (Both *et al.*, 1983). The term 'shift' is applied to the emergence of a new influenza A virus possessing HA or NA antigens so different from those of previously prevalent viruses that it is designated as a new subtype. The change probably results from recombination between a human and an animal strain, both influenza A viruses. Host range may be seen to be of crucial importance (Webster, 1971). Influenza virus is therefore constantly changing, so rendering obsolete whichever current vaccine is in use. Each major shift has found a large proportion of the world population immunologically defenceless against the newly emerged virus. The World Health Organisation (WHO) operates an extensive network of laboratories around the world which remain continuously alert to the emergence of novel viral strains. These are then made available to commercial vaccine producers in order to update existing vaccines.

The conventional vaccine is an egg-grown, formalin- or ß-propiolactone-inactivated product incorporating the equivalent of 15-25 μg of HA of each of the latest prevalent strains of influenza types A and B (Potter, 1982). This polyvalent vaccine is injected intramuscularly in autumn or in winter during epidemics. Production costs are reduced and yields increased in vaccine manufacture by use of a genetic reassortment technique where the new strains of virus are mixed with an established laboratory 'master

strain' known for its high yield in eggs (Kilbourne, 1969). The vaccine is predominantly used with groups liable to the excess mortality mentioned above; namely, old people, people with respiratory, cardiac or renal disease, diabetes, anaemia or immunodeficiency. Side effects are not uncommon but their occurrance may be reduced by using disrupted (split-virus) vaccines, in which the envelope of the inactivated virion has been chemically disrupted. A particularly serious problem, the Guillain-Barre syndrome, was encountered in one of every one hundred thousand Americans vaccinated against 'swine flu' (H1N1) during a mass campaign in 1976-77 (Schonberger *et al.*, 1979), but no such association has been reported with any subsequent influenza vaccine. However, it is remarkable that despite decades of trials on all licensed vaccines the degree of protection which can be expected remains in doubt. More recent developments include the use of HA/NA virosomes, vaccinia virus incorporating the HA gene and even production of small antigenic peptides based on conserved sites on HA common to many strains of influenza (Mims and White, 1988).

Numerous studies of the drug amantadine (1-amino adamantane hydrochloride) (see Figure 3.4) since the pioneer work of Davies *et al.*, have continued to give relatively consistent results. Amantadine and its derivatives (eg. rimantadine) have been shown to be specific inhibitors of influenza A viruses both *in vivo* and *in vitro* and are effective in the prophylaxis and treatment of human infections (review by Tominack and Hayden, 1987). Although initially licensed in 1966 for use against H2N2 viruses and subsequently in 1976 for use against all human influenza A subtypes, it is still only

used on a very limited scale. However, rimantadine, which is as effective as amantadine and appears to cause fewer adverse reactions, is more widely used in the former U.S.S.R. (Zlychnikor *et al.*, 1981). Even though it is ineffective against influenza B infections, amantadine remains one of the few truly antiviral drugs available to the clinician. (For a full account of the mode of action of amantadine see Section 1.4).

1.3 The structure of the virion

Since the 1940's, when only a few viruses had been recognised, hundreds of viruses have been discovered and characterised, largely as a result of the exploitation of cell culture techniques. Taxonomic criteria for classifying viruses only began to be established in the 1960's and, presently, viruses of vertebrates are classified into about 20 families (Matthews, 1982). The influenza viruses are grouped under the myxoviridae. As the term myxo (from the Greek 'myxa', meaning mucus) attests, these viruses have an affinity for mucopolysaccharides and glycoproteins (in particular, sialic acid-containing receptors on cell surfaces). Influenza viruses A, B and C are further classified as being orthomyxoviridae due to the segmented nature of their genomes. Influenza A and B are morphologically identical, pleomorphic, enveloped viruses and are approximately 80-130 nm in diameter (Figure 1.1). Although they often appear roughly spherical in nature, filamentous forms do frequently occur in fresh isolates.

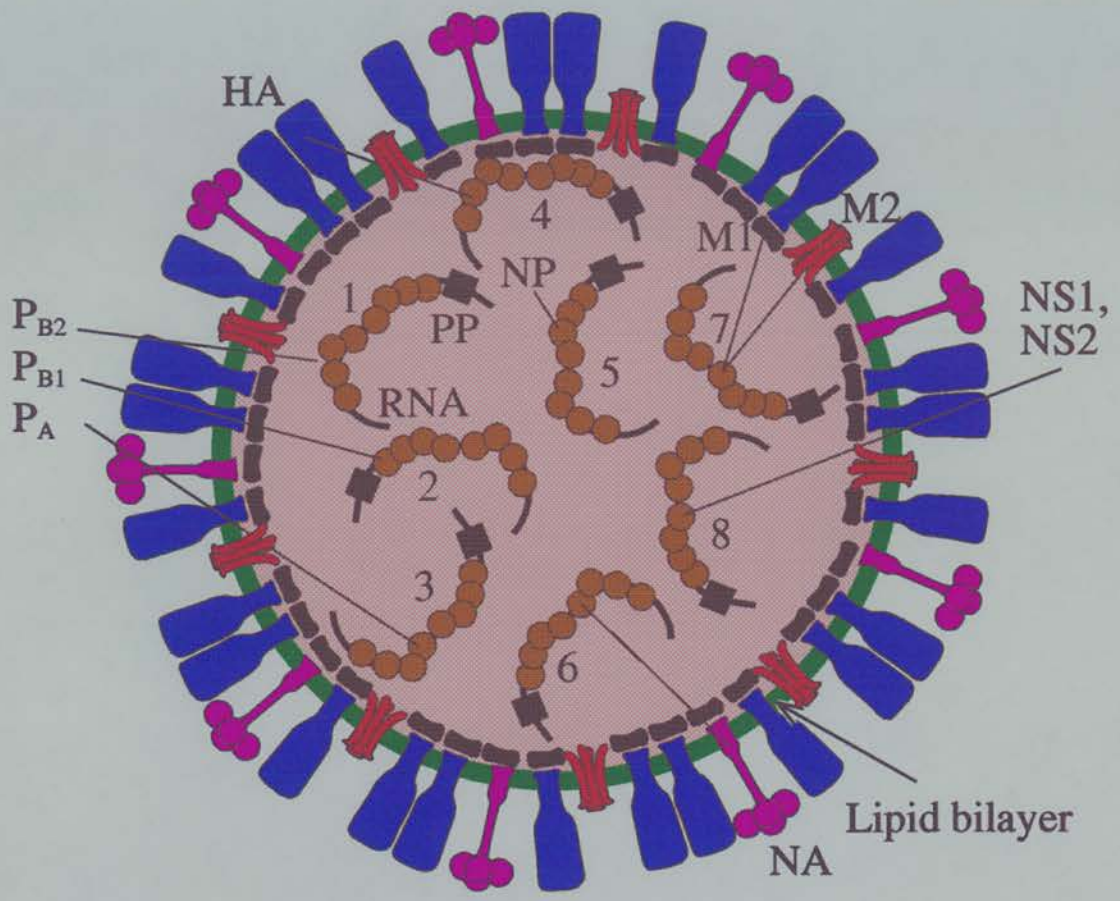

Figure 1.1 The structure of influenza A. Each gene segment points to its respective gene product. NB. Segment 5 codes for NP (represented by brown circle) and segments 1, 2 and 3 code for proteins which make up the PP (represented by black cube), both of which are ubiquitous to all other segments. See text for abbreviations.

The lipid envelope, which is derived from the host cell in which the virus has replicated, is studded with two morphologically distinguishable glycoprotein spikes in a proportion of approximately 4:1, namely the HA and the NA.

HA was the first membrane protein to have its three-dimensional structure resolved by X-ray crystallography (Wilson *et al.*, 1981). It is a trimer with molecular weight approximately 225 000. Cell attachment abilities reside within this molecule. Each monomer, HA_0, consists of two subunits, HA_1 and HA_2, linked by disulphide bonds. The amino terminus of HA_2 includes a highly conserved sequence associated with membrane fusion. HA is therefore responsible both for attachment to host cells via sialic acid receptors and for membrane fusion between the resultant endosome (see below) and the virus membrane (White *et al.*, 1982).

NA is a tetramer of total molecular weight 240 000. This enzyme catalyses the cleavage of the linkage between terminal sialic acid groups and adjacent sugar residues (Gottschalk, 1957). In general, the role of NA may be to facilitate the mobility of the virus both to and from the site of infection by enabling the virus to evade the protective mucoid layer of the host cell.

Both spikes are thought to penetrate through the lipid bilayer via anchors of hydrophobic amino acids and may make contact with the underlying electron-dense layer of matrix (M1) protein. M1 is the most abundant protein in the virion (35% of total) and forms a layer one or a few molecules thick which probably contributes in a major way to the structural integrity of the virion as well as being involved in viral assembly at the plasma membrane before budding. Enclosed within this matrix shell are the nucleoprotein (NP) and the

polymerase proteins (PB1, PB2 and PA) which are all closely associated with the single-stranded RNA. The NP appears to be involved in packing of the RNA. The three polymerase proteins constitute an RNA transcriptase enzyme (Kawakami and Ishitama, 1983) responsible for initiating RNA transcription in the infected cell. The virus genome consists of eight molecular species of single-stranded, negative-sense RNA of different coding potentials (Inglis *et al.*, 1976) which are replicated independently and are contained within ribonucleoprotein (RNP) structures.

Influenza B also codes for a glycoprotein similar, and in addition to, NA. This has been termed NB, and, as it does not appear to be incorporated into virions, its role in infection is not clear (Shaw and Choppin, 1984). Little is known of the molecular biology of influenza C; it has seven RNA segments and no separate HA and NA (instead it possesses a protein, HE [haemagglutinin-esterase], which bears both receptor recognition and cleavage activities).

In addition to the proteins described above, influenza A also codes for two nonstructural proteins, NS1 and NS2, whose functions are unknown, and a final protein M2. NS1 and NS2 are encoded in RNA segment 8 and are found to accumulate in large amounts in the nuclei of infected cells. Neither of the NS gene products are found in virions. It has been postulated that they may be involved in shutting-off host cell protein synthesis (Wolstenholme *et al.*, 1980). M2 is the subject of this thesis and will be discussed fully in the next section.

The cycle of infection of influenza A (Kingsbury, 1990) commences with initial attachment to host cell sialic acid moieties via HA (Figure 1.2) (Plate 1.1). The virus is internalised by receptor-mediated endocytosis and, in the endosome formed, is exposed to acidic conditions by the action of cellular proton pumps. At a pH specific for each influenza strain (usually between 5.5 and 6.0), the HA undergoes a conformational change whereby a fusion region is exposed. Fusion between the viral and the endosomal membranes takes place and the M1 dissociates resulting in release of the genetic components into the cell. Transcription occurs in the nucleus and is initiated by the viral-coded RNA polymerase complex. The negative-strand RNA is transcribed into positive-strand RNA (mRNA) by the polymerase and this is then translated into influenza proteins, or, it is further transcribed into negative RNA to supply the genetic components for future viruses. The nucleocapsid is assembled in the nucleus and the envelope is assembled on the infected cell surface. New virions are formed from nucleocapsid and envelope and bud-off from the host cell surface (Plate 1.2).

1.4 Influenza A M2 protein and its proposed role in the replication of the virus

In 1980, it was observed that, in addition to the open reading frame coding for M1, RNA segment 7 also included a second open reading frame that possibly encoded another protein (Winter and Fields, 1980). This protein was designated M2 and was subsequently identified in several infected cell types as a polypeptide of

approximate molecular weight 15 000. M2 was reported to be a nonstructural protein found only in infected cells and not in virions (Lamb and Chopin, 1981). In addition, examination of the predicted protein sequence of M2 suggested that it contained a region of amino acids (residues 25 to 43) that was sufficiently hydrophobic to interact with membranes (Lamb *et al.*, 1981). In 1985, Lamb *et al.* confirmed this and reported that influenza virus M2 was an integral membrane protein expressed on the infected cell surface. M1 is translated from a mRNA that is colinear with RNA segment 7, whereas M2 is translated from a spliced mRNA - the initiation codon and subsequent nine amino terminal amino acids of M1 and M2 are common to both, as they are encoded before the 5' splice junction. The remaining 88 amino acids of M2, encoded after the 3' splice junction, are translated from the second open reading frame. Such early work also revealed a high degree of amino acid conservation within the external NH_2-terminal residues, from avian through to human viruses, indicating that M2 has properties which are important to the biology of the viral infection in host animals.

Recent work has now identified M2 in virions using monoclonal Abs and, furthermore, has shown that such Abs bind to the extracellular NH_2-terminal domain and restrict the replication of influenza; a quantitative assay indicated 14 to 68 molecules of M2 per virion in the preparations used (Zebedee and Lamb, 1988). Other authors have reported electron microscopic evidence supporting the association of M2 protein with the influenza virion (Jackson *et al.*, 1991).

Subsequent research involving M2 has been inspired by the

Figure 1.2 The replicative cycle of influenza A - see text for details.

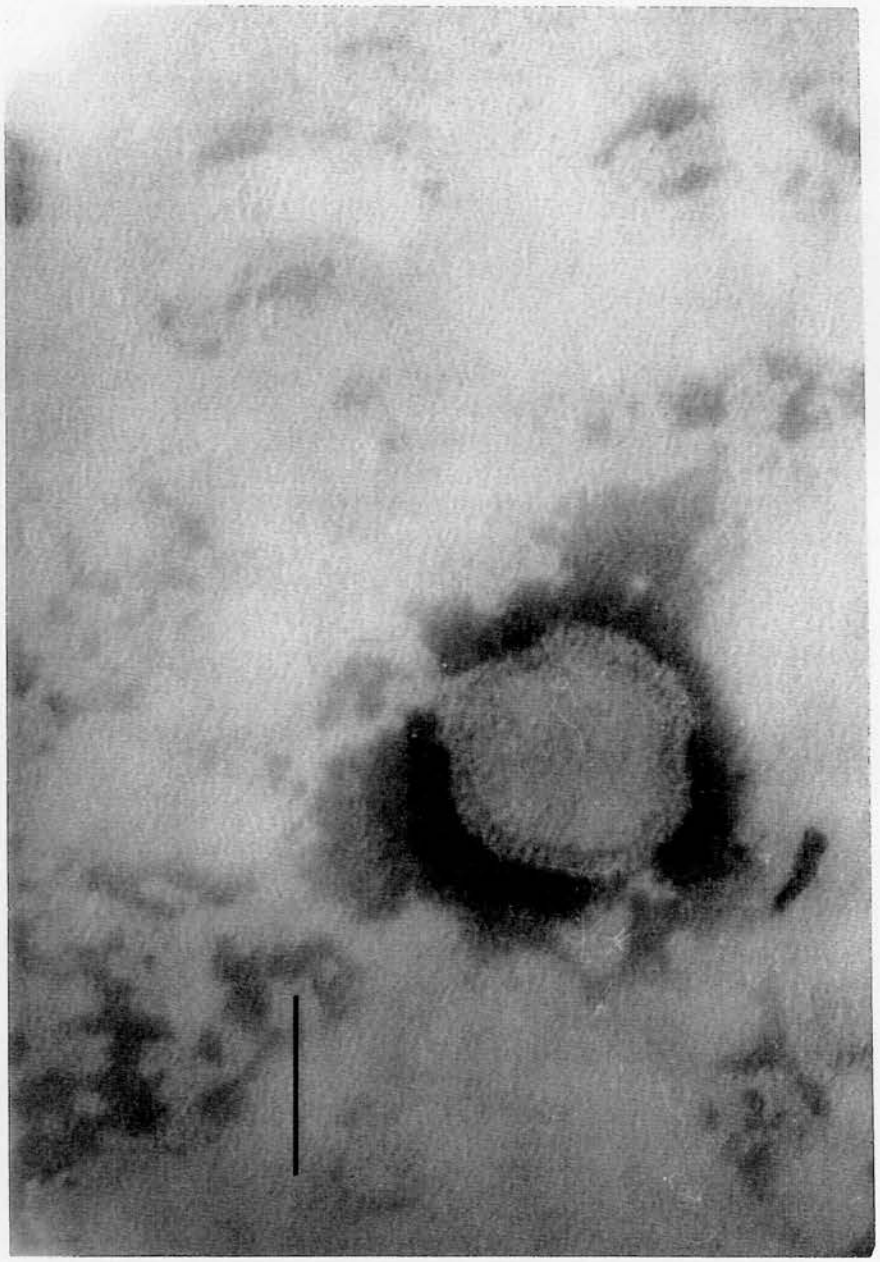

Plate 1.1 E.M. of influenza A virus (note the HA spikes). This plate was produced by applying the material to a 400 mesh copper grid (covered in carbon-coated Formvar) and stained with phosphotungstic acid (2% for two minutes). The size bar represents 100 nm.

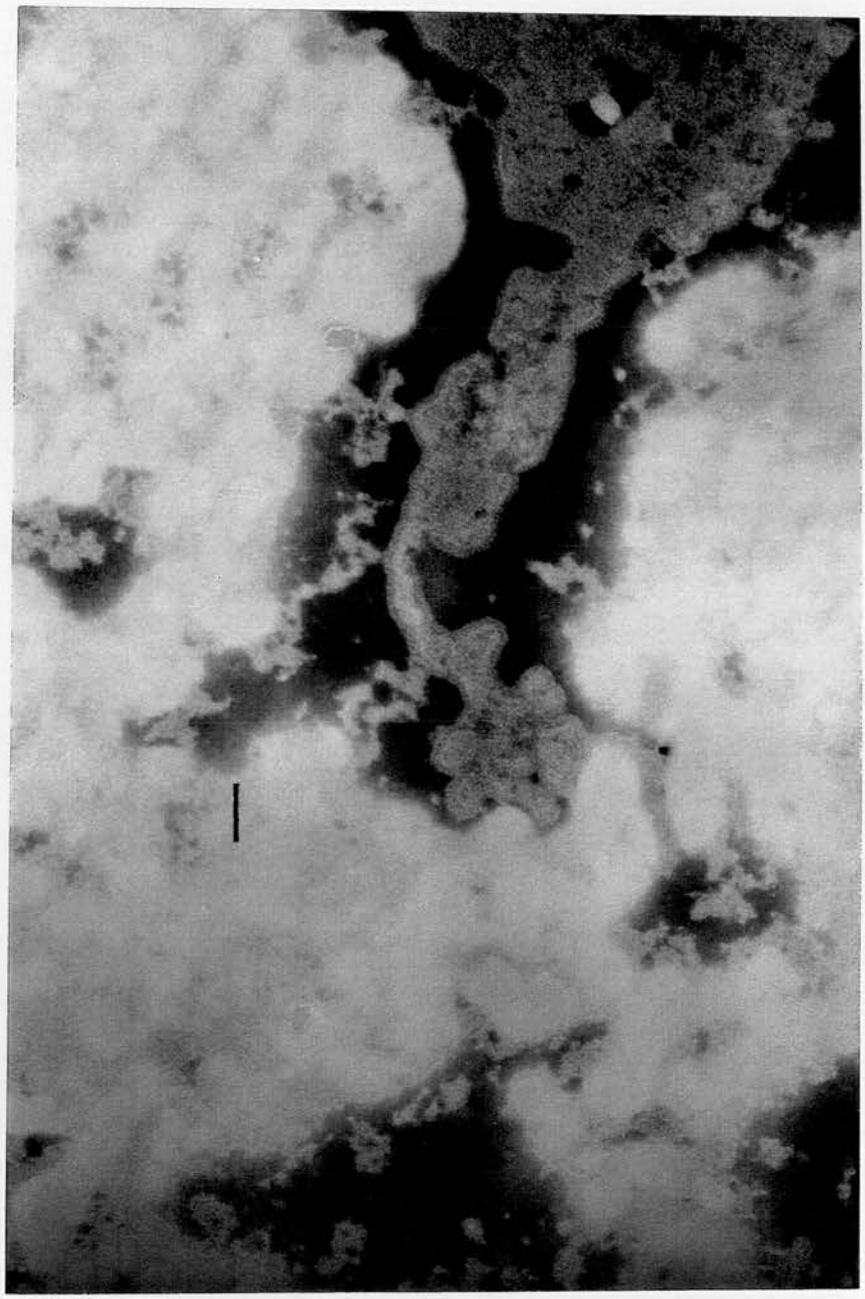

Plate 1.2 E.M. of budding viruses (single/groups of virus) from a fragment of cellular membrane (note the complete fringe of HA molecules). Preparatory procedure as for Plate 1.1. Bar indicates 100 nm.

action of amantadine upon the influenza virus. The replication of many influenza strains is inhibited by this drug and its related compounds, however, resistant viruses readily arise *in vivo* in chickens, mice and humans (Belshe *et al.*, 1988). Nucleotide sequence analyses have shown that in every case a mutation in the M2 protein is responsible for resistance (Hay *et al.*, 1985). The substitutions which confer resistance occur only in the hydrophobic, putative membrane-spanning region of the molecule, specifically at residues 27, 30, 31 and 34. Interestingly, if the 'membrane-spanning' domain adopts an α-helical structure then all the substitutions fall on one face of the helix near the luminal side of the membrane (Hay, 1989). The occurrence and predominance of certain substitutions are strain dependent and whether this reflects features of M2 itself or the properties of other virus components is not known. Genetic evidence therefore points to the postulated transmembrane domain of the M2 protein as the prime target of amantadine.

However, amantadine is not virucidal and it does not hinder viral absorption or penetration. Its effects have been shown to occur at two possible stages. The first occurs early during infection at the uncoating stage and the second occurs late in the cycle and prevents proper virus maturation (Hay *et al.*, 1986).

In cell culture, susceptibility to the early action of these drugs is a feature common to most human viruses; only certain equine and avian strains (H5 and H7) that infect, for example, chick embryo cells and MDCK cells, have so far been shown to succumb to the

late effect. However, the clearest indication as to the mechanism of drug action and the function of the M2 protein has come from studies of this latter phenomenon.

Inhibition occurs at the final stage in virus assembly by blocking the release of virus particles without interfering with bud formation (Ruigrok *et al.*, 1991). This appears to be the direct consequence of a specific alteration in the HA structure during its transport to the surface of drug-treated, infected cells. Addition of drug after the initial infection period does not significantly affect the synthesis of other virus components or the amount of HA synthesised, its posttranslational modification including glycosylation, acylation, and proteolytic cleavage, or its transport to the plasma membrane. However, the conformation of the molecule exposed on the cell surface is indistinguishable from that acquired following exposure of mature HA to a pH below about 5.5, as shown by several criteria, in particular, susceptibility to proteolytic digestion and reducing agents and recognition by monoclonal antibodies specific for the low pH form of HA (Sugrue *et al.*, 1990). Pulse-chase experiments have shown that the sensitive stage occurs some 20 minutes after synthesis of HA and coincides with the proteolytic cleavage of HA_0 to HA_1 and HA_2 (the mature, fuseogenic form of the HA molecule). This points to a compartment late in the transport pathway, such as the trans-Golgi or post-Golgi vesicles. The coincidence with protelytic cleavage is not particularly surprising in view of the nature of the phenomenon, since only the cleaved form of HA can undergo the irreversible conformational change upon exposure to low pH (Wiley and Skehel, 1987).

The fact that alterations in the primary sequence of M2 alone can abolish the effect of amantadine (the amantadine-resistant mutants) argues against a direct effect on HA and points to interference with an interaction between HA and M2 - either a direct structural interaction or some indirect interrelationship between the two proteins. Evidence favours the latter, and there are indications that the acidity of the cellular compartment relative to the pH at which the HA conformational transition occurs is important. Certain influenza viruses are insensitive to the action of amantadine in MDCK cells (which are epithelial) but are susceptible in chick embryo fibroblasts; whereas mutants possessing HAs that undergo the conformational transition at higher pH values of 6.0 to 6.4 (wild type, pH 5.6) are sensitive in both cell types. Of interest in this regard are reports of differences in the acidities of the cisternae and vesicles of the Golgi complex of different cells and, in particular, the lower pH in corresponding compartments of fibroblasts as compared to epithelial cells (Anderson and Orci, 1988). The Rostock virus HA, which undergoes the conformational change at pH 6.0, is affected by amantadine in MDCK cells and chick embryo fibroblasts whereas the Weybridge virus HA, which undergoes the conformational change at pH 5.6, is only affected by amantadine in chick cells. This may be because fibroblasts have a lower pH in their intracellular compartments than do epithelial cells and even in the presence of amantadine, the pH of the Golgi in epithelial cells is not sufficiently low to trigger the conformational change in Weybridge HA but is low enough to trigger the Rostock HA. In the fibroblasts, the pH is sufficiently low to trigger the HA of both strains.

Furthermore, the specific action of amantadine is counteracted by agents that elevate the pH of intracellular compartments involved in endocytosis and exocytosis. These include, for example, an extracellular pH greater than 8.5, millimolar concentrations of acidotropic amines, for example, methylamine and NH_4Cl, and low concentrations of ionophores such as monensin and nigericin. By analogy, the low concentration optimum of the specific action of amantadine and rimantadine, in the range of 0.05 to 5 μM, can be explained by the antagonistic action of higher drug concentrations. This may be because at higher doses these drugs themselves raise the pH of the Golgi by virtue of being weak bases and therefore the HA will not be exposed to low pH.

The conclusion reached from the above evidence is that, since M2 is instrumental in amantadine action, this protein, like the above compounds, effects a similar change in pH, which is blocked by the drug. This role of M2 is supported by observations that, in the absence of drug, cells infected with certain strains of virus, including HA mutants that undergo the conformational transition at higher pH values (as above), may express elevated levels of low pH HA that display a cell dependence and reversibility similar to that just discussed. This is also true if reassortant viruses are prepared containing a heterologous M gene. This further emphasises the important relationship between HA and an M gene product (presumably M2) in preserving the integrity of the HA, apparently by influencing the pH of certain vesicular compartments during its transport to the plasma membrane.

It may be postulated from these observations that the M2 protein forms a transmembrane channel involved in reducing the pH gradient across the membrane of normally acidic vesicles and that amantadine and rimantadine interfere by blocking ion flux (Hay, 1989). This is therefore analogous to the anticholinergic action of amantadine and related compounds (Warnick *et al.*, 1982) and is similar to that of other noncompetitive antagonists that block the ion channel of the nicotinic acetylcholine receptor. A further interesting parallel concerns the possible sites of amantadine interaction. Affinity labeling of the nicotinic acetylcholine receptor with certain noncompetitive antagonists indicated that their interaction with serine residues occurred towards the inner surface of the membrane, in homologous positions of the MII transmembrane segments of the four different polypeptide subunits of the pentamer (Changeaux *et al.*, 1987). The interaction of amantadine with an equivalent region of the virus M2 protein is indicated by the locations of the amino acid substitutions in drug-resistant mutants. The positions of these altered amino acids and the position of the polar and charged amino acids in wild-type and mutant viruses on the same face of an α-helical configuration of the postulated transmembrane domain of M2 would be consistent with its proposed amphiphilic nature. Recent evidence indicating that M2 polypeptides form disulphide-linked tetramers (Sugrue and Hay, 1991; Panayotov and Schlesinger, 1992) is consistent with the ability of the protein to form a transmembrane channel. The consequences of the amino acid substitutions are not known. They may alter the interaction of amantadine with M2, or, more drastically, change the protein structure itself. Studies of amphiphilic peptides have shown that similar changes in sequence

can dramatically alter their ion channel conductance and cation selectivity (Lear *et al.*, 1988).

From the above, it is possible to imply the mechanism of drug action early in infection - this being the stage at which most strains are affected. Since the same mutations in M2 abolish susceptibility to both early and late actions of amantadine and rimantadine, it is evident that the two actions have the same basis and are directed against a related function of M2.

The monitoring of virus/liposome interactions may be used as a model system for virus/endosome fusion. Concentrations of amantadine comparable to those found to be effective in cell culture specifically reduce the *rate* of *in vitro* membrane fusion between viruses whose replication is inhibited by amantadine and liposomes (Dr A.J. Hay, National Institute for Medical Research, Mill Hill, London, U.K.; personal communication). This is not accompanied by any reduction in the extent of fusion or the rate of the conformational change in the HA. It may be that this effect is exerted upon some feature of the uncoating process, for example, disassembly of the M1 protein shell (Bukrinskaya *et al.*, 1982). Subsequent observations that if monensin is added to this system then the rate of virus/membrane fusion *in vitro* increases, and that M1 solubilises at acidic pH (Gregoriades, 1973) lend support to the idea that, in endosomes, the M2 protein is involved in the transfer of protons across the viral membrane and that the resultant drop in pH destabilises the viral structure. Further support for this theory comes from recent work which showed that a lowered pH is required to dissociate the influenza M1 protein from the RNP's (Zhirnov, 1990). This is probably directly related to the *in vivo*

experiments that indicated that, in the presence of amantadine, M1 fails to dissociate from the RNP's (Martin and Helenius, 1991) and transport of the RNP's to the nucleus does not occur.

Thus, it appears that the role of M2 is important both in uncoating virus particles and in preserving the integrity of HA during its transport through acidic compartments to the cell surface (Figure 1.3).

Whilst this thesis was in preparation, Pinto *et al.* published a paper (May 1992) that is particularly noteworthy in that it shows monovalent cation flow (Na^+ and K^+) through M2 expressed in *Xenopus laevis* oocytes (see later). The electrophysiological study reported as part of *this* thesis was, in fact, submitted two months before the Pinto study was published (March 1992) and, in addition, is the first study to fully illustrate the Hay theory in that it shows, specifically, *proton* transport (Chapter 4).

1.5 Aims of thesis

It is the aim of this thesis to investigate fully the theory discussed in the previous section. It is therefore intended that a variety of biophysical techniques will be employed to assertain the structural and functional properties of influenza A M2 protein.

The unique attributes of influenza M2 protein have been described in Section 1.4 as being a function of the proposed transmembrane domain of that protein. The experiments reported here will therefore concern a synthetic peptide whose primary structure represents a 'transmembrane' sequence common to several strains of influenza A (see Section 2.7 for details).

Initially, the secondary structure of this M2 peptide will be investigated in liposomes, using circular dichroism (CD). Such studies are also intended to act as confirmation that the domain is indeed transmembraneous, will produce low resolution information on the gross positions of the amino acids, reveal any structural dependence based on the lipids used and show any effects on secondary structure upon the addition of amantadine.

Subsequently, the orientation of the M2 in phospholipid multilayers will be studied to high resolution with neutron diffraction. Both native (amantadine-sensitive) and mutant (amantadine-resistant) M2 peptides will be located, and amantadine will be added to both. The exact position of the M2/amantadine interaction will be investigated.

Finally, using electrophysiological techniques, it is proposed to test the theory that M2 is a proton channel. It is intended to study the effects of amantadine on any such channel activities.

In conclusion, the idea that viruses may code for ion channels is a novel one in biology. To date only one, Semliki Forest Virus, has been suspected of possessing such a potential, however, the protein responsible has not yet been positively identified (Schlegel *et al.*, 1991). In addition, other proteins have been named as structural analogues of M2 and these may be found to have functional similarities too. These include the NB protein of influenza B (Williams and Lamb, 1986), the SH protein of paramyxovirus SV5 (Hiebert *et al.*, 1985) and the *vpu* protein of HIV-1 (Terwillinger *et al.*, 1989). If groups of enveloped viruses in general are found to possess similar methods of uncoating and

reassembly then this information may open-up an innovative and potentially fruitful line of attack involving new, broad-based, anti-viral agents.

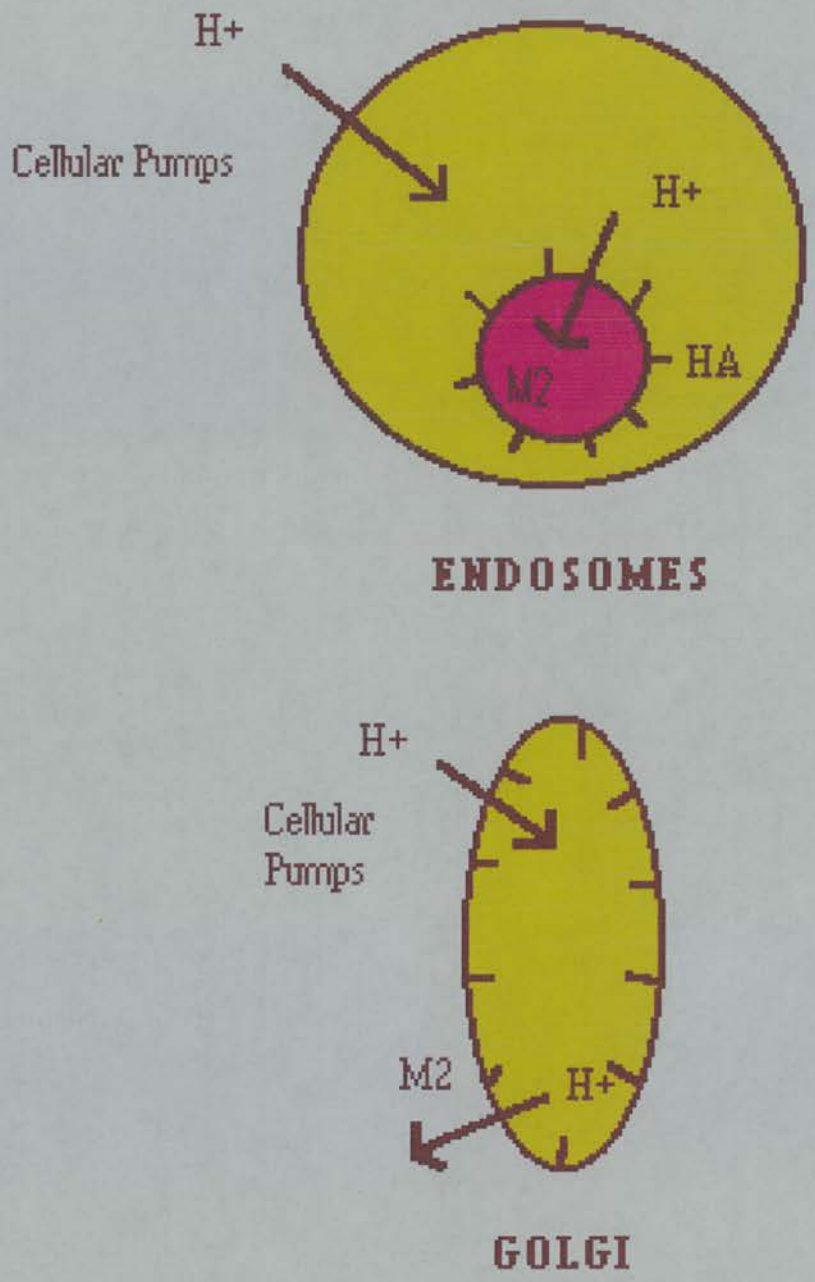

Figure 1.3 Theory of M2 action - role in virus uncoating and protection of HA in the Golgi (see Section 1.4).

CHAPTER 2 INVESTIGATION OF THE SECONDARY STRUCTURE OF INFLUENZA A M2 TRANSMEMBRANE DOMAIN IN PHOSPHOLIPID LIPOSOMES USING CIRCULAR DICHROISM

2. Investigation of the secondary structure of influenza A M2 transmembrane domain in phospholipid liposomes using circular dichroism

2.1 General introduction

The importance of conformation in the function of biological molecules is now an accepted fact. The specific three-dimensional organisation of such molecules, when known, has been shown in almost all cases to be intimately linked with function. The measurement of circular dichroism (CD) spectra has become a routine means of studying such molecular structures in solution. This spectroscopic technique represents one of the most sensitive and versatile probes of biopolymer conformation. Rapid progress has been made over the last two decades on both the experimental and theoretical sides of this chiroptical method. In the 1960's CD developed from a little-known and poorly understood phenomenon to a widely applicable method for studying the configuration and conformation of optically active molecules. Simultaneously, the understanding of the phenomena and the ability to make explicit calculations made rapid advances. Today experimental methods are at the point where CD can be measured at high sensitivity from the ultraviolet through to the infrared. Theoretical calculations on even quite complex systems can be done with considerable confidence at the semiquantitative level.

Examination of polynucleotides with CD has shed light on, amongst other things, base stacking and tilting which has helped define conformational assignments. CD has also been used, to a

lesser degree, to investigate the structure of various polysaccharides. In the field of protein chemistry, it has proved possible to investigate, in the far UV peptide bond absorption region, protein secondary structure, and, in the near UV aromatic sidechain region, protein tertiary structure. Other chromophores, for example haem groups, have characteristic absorptions and CD spectra. This therefore provides a sensitive analytical tool with which to investigate protein structure, amino acid substitutions and the effects of both ligand binding and solvent. Results may be obtained quickly and with relatively small amounts of sample.

2.2 CD theory

The basic CD experiment consists of placing a sample in a beam of alternating left and right circularly polarised light and recording the differential absorption of both components. (For reviews see Bayley, 1973; Woody, 1977; Campbell and Dwek, 1984.)

Production of circularly polarised light

Electromagnetic radiation may be thought of as possessing two wave motions at right angles to each other - a magnetic M component and an electric E component. The energies associated with M and E are equal, but most optical effects are concerned with the electric wave.

Although the amplitude of the E wave in Figure 2.1 oscillates in the zx plane, it could oscillate equally well in any direction perpendicular to the direction of propagation (z). Unpolarised light

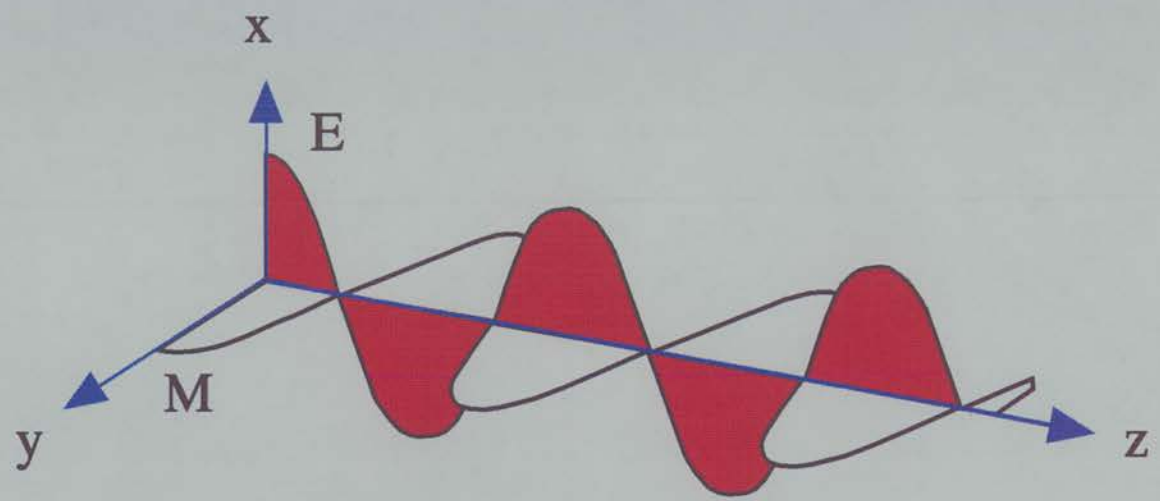

Figure 2.1 The electromagnetic wave. M represents the magnetic component and E represents the electric component - see text for details.

contains oscillations of the E components in *all* directions perpendicular to the direction of propagation. Plane or linearly polarised light has E oscillations in only one plane.

Plane-polarised E radiation of the sort described in Figure 2.1 can be considered to arise from a source that oscillates parallel to the x-axis. If the source also oscillates parallel to the y-axis in the same phase, then the two waves superimpose to produce a new, single plane-polarised wave. For example, if the two waves display identical amplitudes, the resultant wave will be orientated at 45° to the x-axis. If the two components do not have the same phase relationship, then the superimposition of the two oscillations does not lead to a fixed direction for E. For example, if the phase difference is $\pi/2$, as shown in Figure 2.2, then the path the E vector describes is a helical trajectory about the z-axis and the projection of this onto the xy plane describes a circle (Figure 2.3, a and b).

When the amplitudes of the two waves are equal, and if the phase difference is $\pi/2$, then the resultant wave is said to be *circularly* polarised. If the two components of oscillation along xy are unequal in amplitude, then the resultant wave is *elliptically* polarised. The polarisation is right-handed when the vector appears to rotate clockwise on looking in a direction opposite to the direction of propagation, and left-handed if the rotation is anticlockwise. Circularly polarised light may be produced if plane polarised light is passed through a quarter-wave plate, a transparent window made from a birefringent medium in which the velocities of the two plane-polarised waves differ, and is of a thickness such that the phase difference between the components of the emergent beam

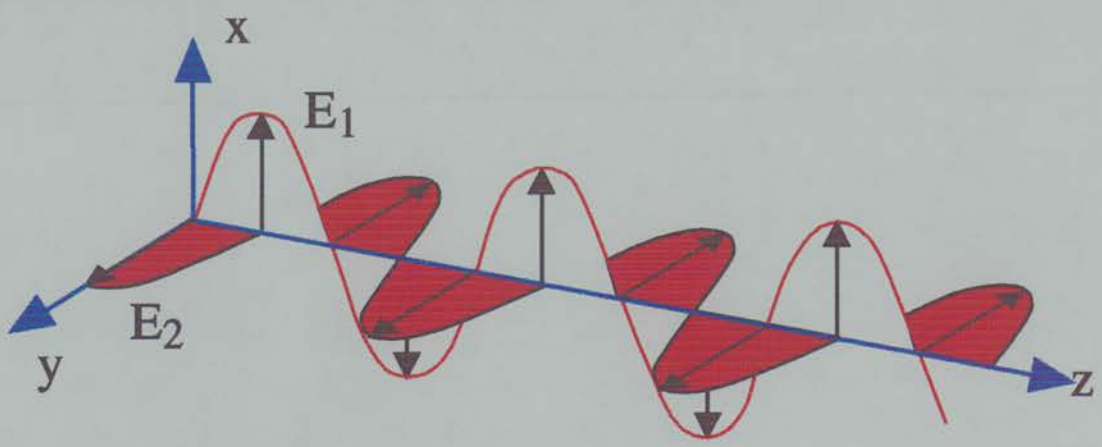

Figure 2.2 Circular polarisation. Two beams polarised along xz and yz, 90° phase shifted with respect to each other.

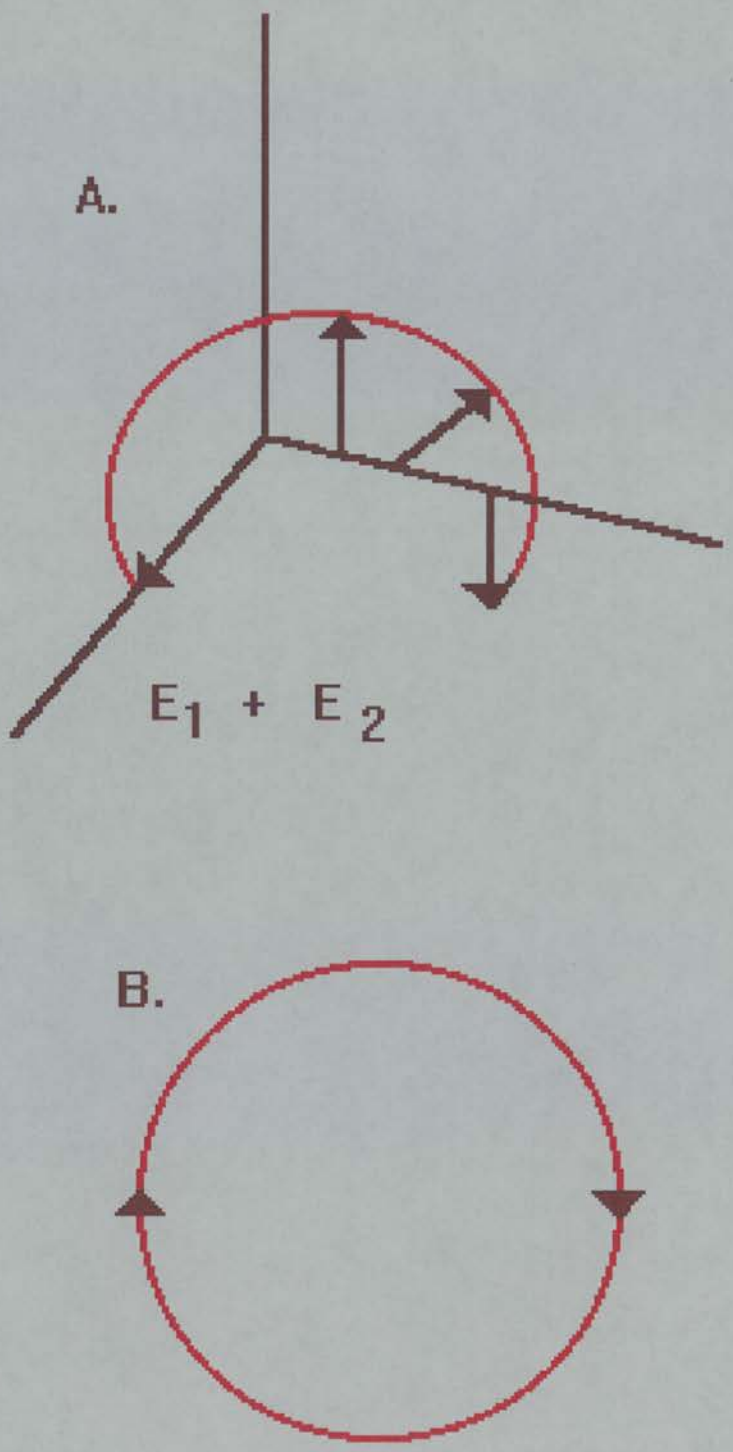

Figure 2.3 Illustration of (a) how two beams polarised along xz and yz, 90° phase shifted with respect to each other, generate a circularly polarised beam (b) when thay are superimposed.

is 90°. From the above, plane-polarised light may be considered equivalent to two circularly polarised beams rotating in opposite directions.

Optical activity

Many transparent substances affect the state of polarisation of light entering them. One such interaction that may occur between polarised light and matter is dichroism, which is a difference in absorption of left and right circularly polarised light.

Dichroism of circularly polarised light (CD) results when the absorbance of a medium varies with the direction of rotation of a circularly polarised measuring beam. Therefore, the experimentally observed parameter is change in absorbance (δA), which is defined as

$$\delta A = \delta\epsilon\,(Cd) = A_L - A_R \qquad 2.1$$

where A_L and A_R are the absorbances of the L and R beams, C is the concentration in g ml^{-1}, d is the path length in decimeters and ϵ is the molar extinction coefficient. CD is caused by an inherent helicity in the molecular structure of the medium, or to other forms of non-planar asymmetry (chirality). If plane-polarised light is transmitted through such a material, the circular components undergo different amounts of absorption. The emergent beam consists of elliptically polarised light (Figure 2.4), the major and minor axes of the ellipse being respectively the sum of and difference between the amplitudes of the emergent circular components.

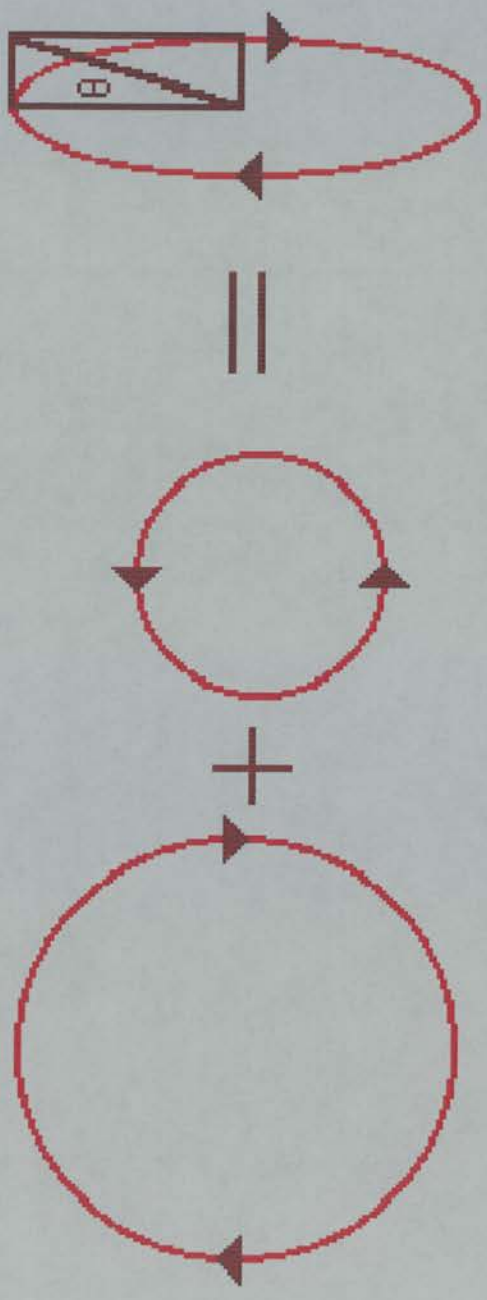

Figure 2.4 Resultant ellipticity due to differential absorption of the circular components of plane polarised light.

Although change in A is measured, the molar ellipticity is often reported. The ellipticity, Θ, is defined as the angle whose tangent is the ratio of the minor and major axes of the ellipse. The molar ellipticity, $[\Theta]$, is defined as -

$$[\Theta] = \Theta M/100\ Cd \qquad 2.2$$

where M is the molecular weight of the dichroic solute, C is its concentration in g ml^{-1} and d is the optical path length in decimeters.

These parameters can be related by the expression -

$$[\Theta] = 3300\ (\delta\epsilon) \text{ degree x } cm^2 \text{ x dmol-1} \qquad 2.3$$

Circular dichroism represents the manifestation of a specific phenomenon, the interaction between polarised light and an asymmetric structure. It exhibits a variation with wavelength and, near an absorption band, the refractive index of the absorbing medium undergoes large changes and the CD spectrum exhibits a Cotton effect, that is, a change in the direction of rotation or ellipticity with increasing wavelength, resulting in an S-shaped spectrum. The Cotton effect associated with each absorption band is easily identifiable in CD spectra, since differential absorption is only measurable within the band itself.

Molecular basis of optical activity

In general, spectrophotometric techniques involve the component molecules of the sample absorbing electromagnetic radiation of a specific wavelength and thereby entering an excited state. Such transitions from the ground state to the excited state involve a displacement of charge. A linear displacement with an electric transition dipole moment is denoted by μ. The transition can also have a circular component; this (rotating current) then generates a magnetic dipole moment m perpendicular to the plane of the circular motion (Figure 2.5).

Optical activity requires a finite μ and a finite m. This corresponds to a helical displacement of charge. The result is that left- or right-circularly polarised beams then interact differently with the molecules in solution. These interactions do not average to zero even in molecules randomly orientated in solution - the magnitude of the transition is proportional to the vector product of μ and m.

In the experiments discussed here, the required helical displacement of charge arises from the intrinsic nature of the chemical bonds. The amplitude and location of the Cotton effect at wavelengths between 180 and 240 nm, which is due primarily to the peptide linkages, are each specific to the conformation of the amino acid chain. Therefore, each protein secondary structure has a corresponding CD spectra, and, the spectra of a complex protein may be derived from the sum of the spectra of the component secondary structures. The proportion of each type of structure in the parent molecule may therefore be estimated using a multicomponent analysis (Chen *et al.*, 1974) which compares the experimental CD spectra with sets of reference proteins whose

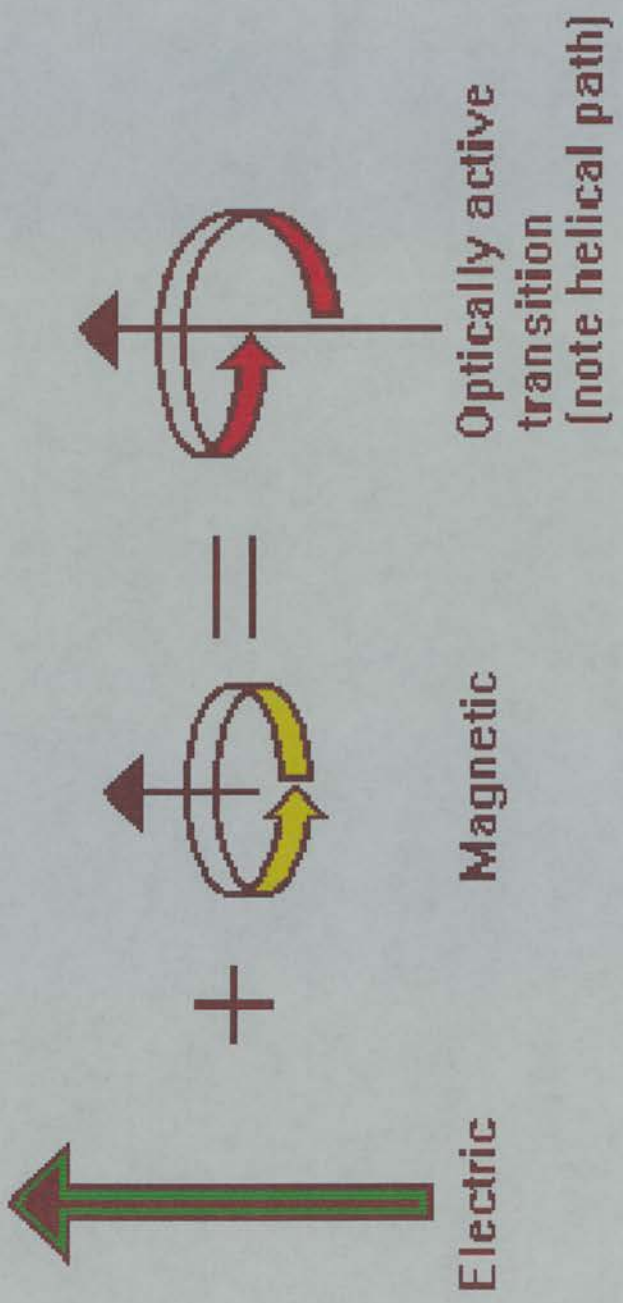

Figure 2.5 Helical displacement of charge can be considered to comprise a linear displacement plus a circular displacement.

secondary structure fractions are known from other sources, eg. X-ray diffraction data. In a liposomal sample, the weak CD spectra due to lipids are dominated by those of the proteins. Vesicles, liposomes and membrane fragments larger than 1 000 nm or so in diameter give rise to a slight red shift of the Cotton effect and a considerable reduction in its amplitude, but when these distortions are corrected for, reasonably accurate estimates of the component structures may be obtained.

2.3 Experimental hardware

CD arises from the differential absorption of left and right polarised light. Thus it could be detected by a double beam instrument that puts left in one beam and right in the other. In practice, it is possible to use a crystal that can be made to pass either left or right depending on the applied voltage of an electric field. This device, known as a Pockels cell, can thus produce a beam that is alternately switched between left and right polarised light. The beam then passes through the sample to a photomultiplier. The detected signal can then be processed to give a plot of change in absorbance versus wavelength. All experiments discussed in this section were recorded at Stirling University on a Jasco J-600 spectropolarimeter.

2.4 Introduction to the experimental section

Chapter 1 has presented a general background study of influenza and a more specific account of M2 and its potential importance. Chapter 2 will initiate the M2 studies described in this thesis by investigating, using CD, the secondary structure of M2 peptide incorporated into 1,2-dioleoyl-*sn*-glycero-3-phosphocholine (DOPC) liposomes. The CD work was carried out with Dr N. C. Price, Department of Biological and Molecular Sciences, University of Stirling.

2.5 The secondary structure of influenza A M2 transmembrane domain - an introduction

In protein structure prediction, the definition of what is and is not a transmembrane domain is unfortunately rather subjective. In essence, a transmembrane domain may be defined as such if it includes a region of hydrophobic amino acids bounded on either side by two charged residues. Initially, it was *suggested* that M2 contained a region of amino acids (25-43) that were sufficiently hydrophobic to interact with membranes (Lamb *et al.*, 1981; Lamb *et al.*, 1985). Subsequently, almost all papers referring to this protein have described such a *postulated* transmembrane domain as an *actual* transmembrane domain, without any definitive evidence over and above the sequence data.

The premise that such membrane-spanning regions often have an α-helical secondary structure is generally based on theoretical predictions and observations of such in bacterial photosynthetic

reaction centres (Deisenhofer *et al.*, 1985; Allen *et al.*, 1987; Roth *et al.*, 1989). In addition, specifically, when the M2 'transmembrane' domain is modelled as an α-helix the residues which are substituted in amantadine-resistant mutants all appear on the same face of the helix (Hay, 1989). Thus, it is an attractive assumption that this domain is indeed both transmembraneous and α-helical.

However, several caveats exist. An amantadine-resistant influenza virus has been isolated that contains a proline substitution (residue 30) deep in the proposed transmembrane domain - this is not usually thought to be compatible with a helical conformation (Hay et al., 1985). In addition, Pinto *et al.* (1992), observed that both deletion of four transmembrane residues and addition of one extra residue still permitted ion channel activity. The Pinto study concludes by stating '...clearly it is of importance to determine the structure of the transmembrane domain of the influenza virus M2...'

Therefore, this present study describes CD investigations of the secondary structure of influenza A M2 'transmembrane' domain reconstituted into DOPC liposomes. The results of adding amantadine at different concentrations and the effects of temperature on any secondary structure initially observed were also investigated. In addition, data have been collected regarding any M2 structural dependence with reference to the liposomal lipid-type used.

2.6 Materials

All chemicals, phospholipids and amantadine hydrochloride were purchased from Sigma Chemical Company Ltd. (Fancy Road, Poole, U.K.).

The M2 liposomes were prepared in a 10 mM Tris-hydrochloride, 0.1 mM EDTA buffer system, pH 7.4 (Section 2.7). All liposomes were determined to have protein concentrations between 0.1 and 0.3 mg ml^{-1} (results were corrected for concentration). Two concentrations of amantadine were added to the reconstituted liposomes, 4 μg ml^{-1} and 12 μg ml^{-1}. These were designated low and high concentration respectively.

Liposomal and control protein concentrations were determined colorimetrically following the Lowry modification of Markwell *et al.* (1981) using bovine serum albumin as standard.

2.7 Sample preparation for CD

The peptides

Synthetic, twenty-five residue, M2 peptides (amino acid sequence: SSDPLVVAASIIGILHLILWILDRL), corresponding to the predicted nineteen amino acid transmembrane sequence (25-43) plus a tail of three commonly occurring residues at each end, were produced. This sequence is common to several strains of influenza A (Ito, *et al.*, 1991; Belshe, *et al.*, 1988; Hay *et al.*, 1985). Mutants with a single amino acid substitution were also prepared - residue 27, V is replaced by A (Hay *et al.*, 1985). Some of these

peptides were deuterated for experiments described in Chapter 3. For a complete list of synthesised M2 peptides see Figure 3.7. In this chapter, only the first, above designated peptide, was used.

All influenza A M2 peptides used in this thesis were synthesised by F-MOC chemistry. This was carried out by the MRC Cellular Immunology Unit, Sir William Dunn School of Pathology, South Parks Road, Oxford, U.K. Finished peptides were subsequently sequenced at the MRC Immunochemistry Unit, Department of Biochemistry, South Parks Road, Oxford, U.K. and also at the Welmet Protein Sequencing Laboratory, Department of Biochemistry, Edinburgh University.

After synthesis, crude peptide was removed from the synthesis resin, deprotected and purified.

Deprotection and removal of the peptide from the resin involved the following procedure. (All glassware was acid-washed to minimise the possibility of contamination.) 0.3 g of the M2 resin was incubated at 30°C with a total of 3 ml deprotection cocktail (76% high purity trifluoroacetic acid [TFA], 20% ethanedithiol, 4% distilled water). Incubation occurred over ninety minutes and the tubes were shaken at least once every fifteen minutes. The resin was subsequently removed from the deprotected peptide by slow filtration through glass pipettes containing acid-washed glass wool. Approximately 0.75 ml of the filtered M2 eluent was collected in four tubes each containing 8 ml of ice-cold ether (the comparatively large volume is to stop the acidic TFA concentration increasing and holding the peptide in solution). The peptide was seen to precipitate on contact with the ether. The precipitated peptide was spun down in a MSE Centaur 2 centrifuge

(3 000 rpm for four minutes) and the supernatant aspirated-off. Finally, the peptide pellet was washed at least five times with the addition of 8 ml of ice-cold ether followed by centrifugation as above. After the last spin the tubes were aspirated and placed in a dessicator under vacuum for approximately twelve hours. Resulting samples were weighed.

These were then purified using reverse-phase HPLC. This was performed with a Beckman C-8 ultrapore preparation column (4.6 mm x 25 cm) fitted with a 2 ml injection loop. 1 ml of a 10 mg ml^{-1} sample (dissolved in 50:50, acetonitrile:water) was loaded per run and the following programme was developed -

Time(mins)	Function	Value(%)	Duration(mins)
0	%B	60	3
3	%B	75	5
8	%B	100	15
23	%B	100	15
38	%B	60	5
53	End		

NB. **Solvent A** - water / 0.01% TFA, **B** - acetonitrile / 0.01% TFA [Both solutions were filtered (0.2 μm filter) and degassed.] The flow rate was held at 3 ml min^{-1}. The elution profile is represented in Figure 2.6. The central peak was collected, lyophilised, sequenced and ascertained to be M2.

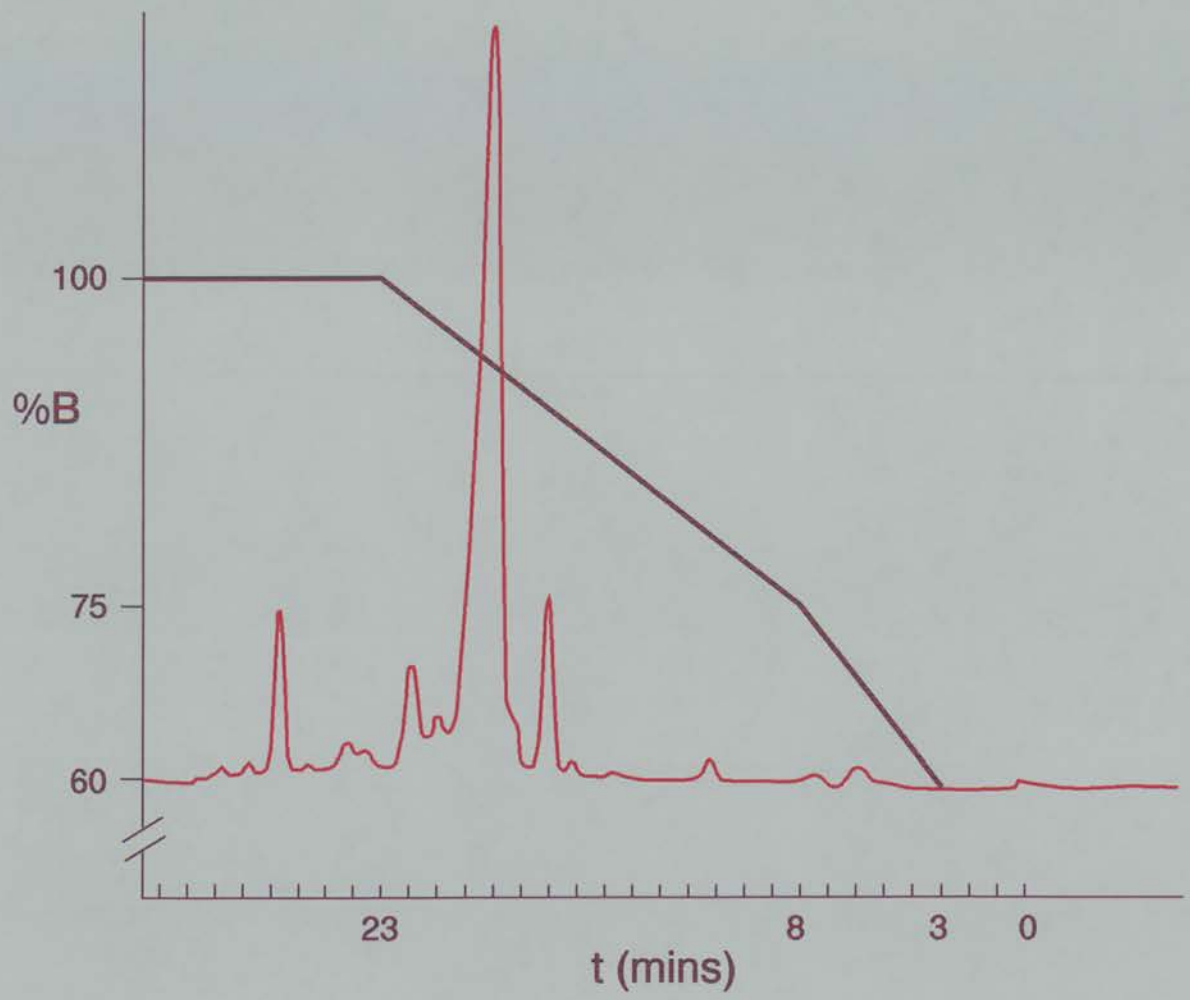

Figure 2.6 HPLC elution profile of M2 peptide - superimposed is the % acetonitrile (60-100%). [NB. Absorbance was measured at 275 nm; times relevant to the elution programme are shown.]

The liposomes

The native, undeuterated M2 thus prepared was reconstituted into phospholipid liposomes in the following manner. A molar ratio of 150:1 (lipid:protein) was chosen for the CD study and the detergent selected was *n*-octyl glucopyranoside (OG). One of the criteria for an adequate CD sample is a total protein concentration of approximately 0.2 mg ml^{-1}. After deducing the M2 molarity for such a concentration and calculating the corresponding lipid molarity, a solution of OG at a final molar concentration four times that of the lipid (Sizer *et al.*, 1987) was prepared in Tris-HCl buffer (10 mM Tris-HCl, 0.1 mM EDTA, 0.001% sodium azide, pH 7.4). Measured amounts of both peptide and dried lipid were separately dissolved in the detergent solution and sonicated in brief intermittent bursts to ensure thorough mixing and micelle formation. The two solutions were then added together and briefly sonicated again. This was followed by extensive dialysis against Tris-HCl (4 x 5 l for approximately ninety hours). The dialysate was observed to turn cloudy after twenty-four hours and, indeed, this phenomenon can be used to determine liposome formation spectrophotometrically (Huang *et al.*, 1969). The dialysate was transferred to Eppendorf tubes and centrifuged (Microcentaur 5 800 g for twenty minutes) to remove any possible multilamellar vesicles. The supernatant was used in all subsequent CD experiments.

2.8 Data analysis

CD spectra were recorded on a JASCO J-600 spectropolarimeter; analysis of the spectra in terms of secondary structure content was undertaken using the methods of Provencher and Glöckner (1981) (the CONTIN procedure), Chang *et al.*(1978) and Siegel *et al.*(1980).

2.9 Results and discussion

The far UV CD spectrum at 20°C (cell path length 0.02 cm) of M2 peptide incorporated into DOPC liposomes is shown in Figure 2.7 (green line). Under these conditions, satisfactory data could be obtained down to 200 nm; below this wavelength, the noise levels precluded accurate measurements of ellipticity. The spectrum shows the characteristic double minima at 223 nm and 209 nm of α-helices (Chang et al., 1978). Estimates of 92%, 79% and 100% α-helix were obtained using the methods of Provencher and Glöckner (1981), Chang *et al.* (1978) and Siegel *et al.* (1980) respectively. Although the exact values of these estimates should be treated with caution in view of the fact that data could only be collected down to 200 nm instead of 190 nm which is preferred (Provencher and Glöckner, 1981; Chang *et al.* 1978), it is clear that under these conditions the M2 peptide exists largely, if not completely, in an α-helical form. In addition, estimates of helix approaching 100% have been obtained both when M2 peptide is dissolved in 0.4% (w/v) sodium dodecyl sulphate (SDS) and 50%

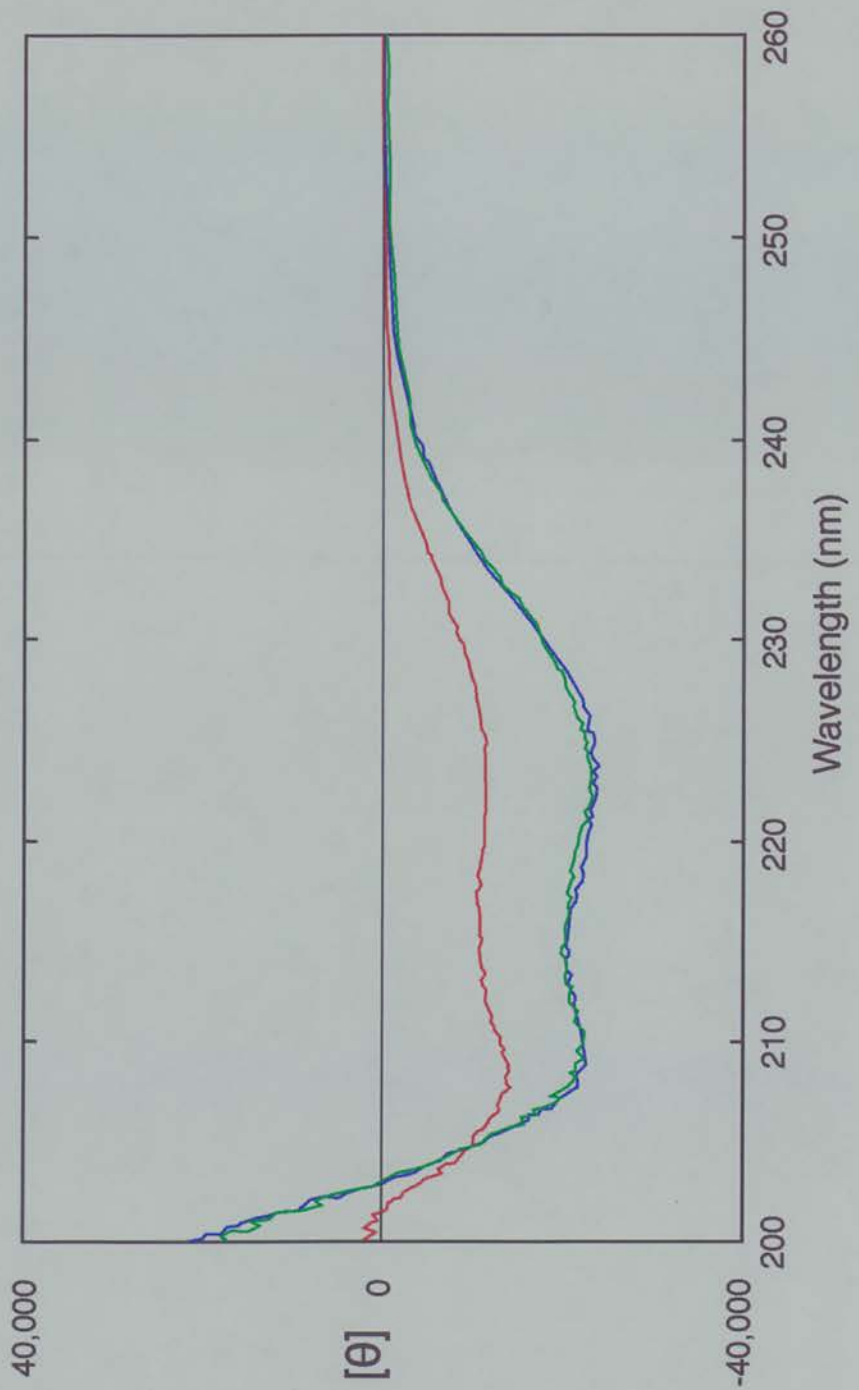

Figure 2.7 Far UV CD spectra of (i) M2 peptide in DOPC liposomes, at 20°C - green line (ii) M2 peptide in DOPG liposomes, at 20°C - red line (iii) M2 peptide in DOPC liposomes plus amantadine ('high' concentration), 20°C - blue line. For details see text.

(v/v) 2,2,2-trifluoroethanol (TFE) (Table 2.1). These solvents are commonly used to promote helix formation in peptides. Peptide reconstituted into lecithin liposomes (bovine brain PC) also displayed maximal helical conformation (Table 2.2). Such results are in direct contrast to that obtained when M2 is dissolved in buffer (Figure 2.8 - green line). In aqueous solution, the M2 peptide apparently did not adopt any stable secondary structure; the low value of the molar ellipticity at 225 nm (Table 2.1) is typical of a random coil.

The DOPC liposomal measurements were repeated at 37°C and no change was observed in the spectrum when compared with the 20°C data (Figure 2.8, blue and red lines, respectively).

On addition of amantadine to the liposomes, to give final concentrations of 4 μg ml^{-1} or 12 μg ml^{-1}, there were no significant changes in the CD spectra (see the molar ellipticity values in Table 2.1). Both low and high drug concentrations were used in order to examine any possible concentration dependence (Hayden and Hay, 1992). These results are significant in that they clearly demonstrate that amantadine itself has no discernible effect upon the helical nature of the M2 peptide (Figure 2.7, blue line) as was previously mooted (Hay *et al.*, 1986). This, along with recent direct findings that amantadine does indeed inhibit ion flow through M2 (Duff and Ashley, 1992; Pinto *et al.*, 1992) augments the thesis that the efficacy of amantadine is due to its channel-blocking abilities and not to any actual conformational interference with the transmembrane region.

The M2 peptide incorporated into 1,2-dioleoyl-*sn*-glycero-3-phosphoglycerol (DOPG) liposomes showed a considerably reduced CD spectrum (Figure 2.7 [red line] and Table 2.1). Analysis of

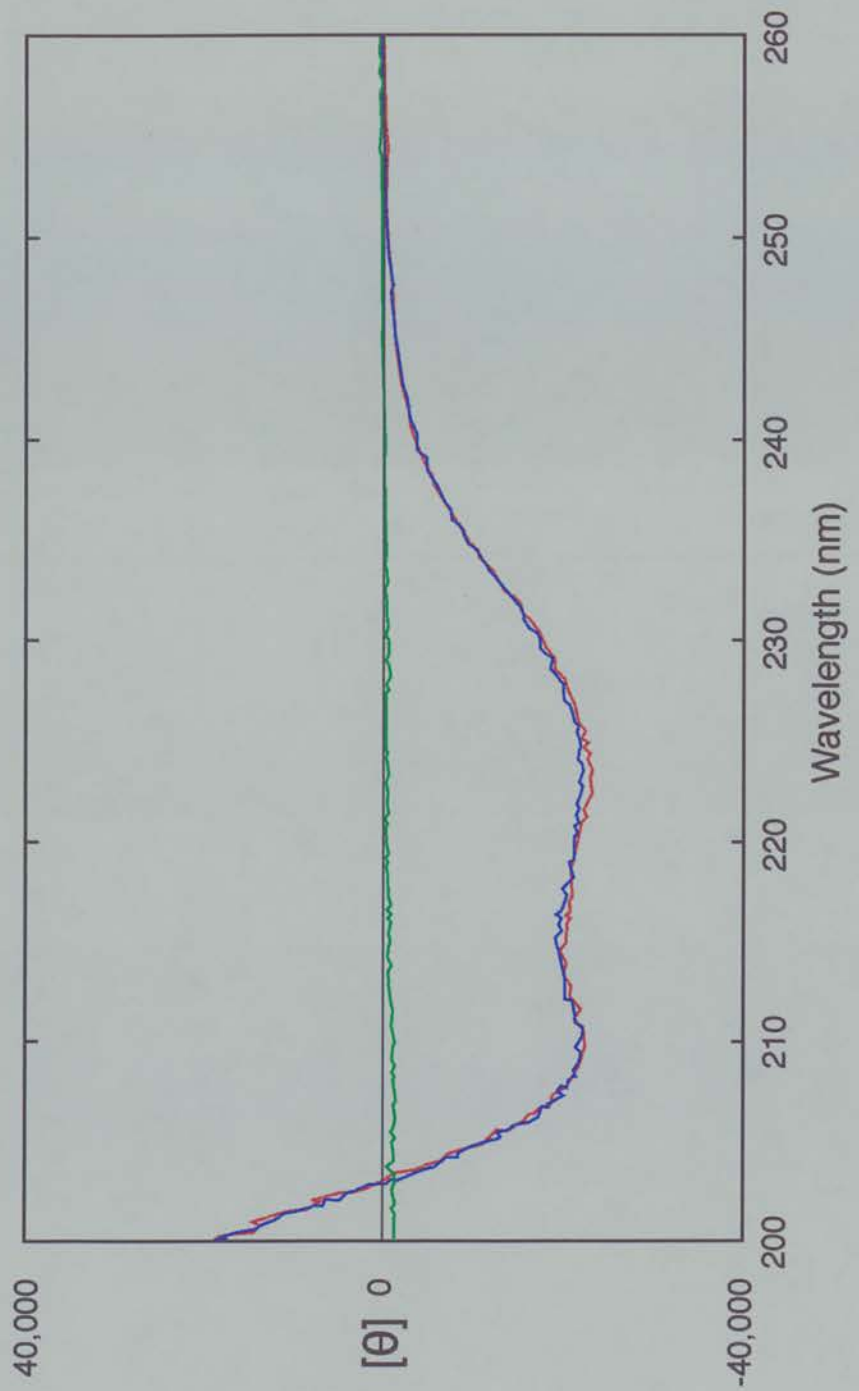

Figure 2.8 Far UV CD spectra of (i) M2 peptide dissolved in buffer, at 20°C - green line (ii) M2 peptide in DOPC liposomes, at 20°C - red line (iii) M2 peptide in DOPC liposomes, at 37°C - blue line. For details see text.

this spectrum by the CONTIN procedure (Provencher and Glöckner, 1981) yielded unacceptably high errors of estimates of secondary structure; the methods of Chang *et al.*(1978) and of Siegel *et al.*(1980) yielded values of 41% and 47% α-helix respectively, in accord with the reduced values of the ellipticity at 225 nm (Table 2.1). These experiments demonstrate a relationship between bilayer composition and the secondary structure of the peptide.

Whilst this is not intended to be a comprehensive, comparative study, these DOPG results, taken together with others, presented in Table 2.2, do invite comment. [%-helicities in Table 2.2 were calculated by taking a mean of α-helix values produced by the methods of Provencher and Glöckner (1981), Chang *et al.* (1978) and Siegel *et al.* (1980)]. From such data, it would appear that neutral lipid liposomes allow M2 peptide to adopt a more α-helical conformation than negatively charged lipids. If a 50:50 (molar) ratio of neutral and negative lipids was used then a slight rise in helical content was observed over and above the negative lipid-only results. Chain length does not appear to effect helicity. Such differences may also be due, in part, to differences in the lipid phase at 20°C. The lower M2 helical content characteristic of myristic and palmitic chains (dimyristoyl-PC [DMPC] and dipalmitoyl-PC [DPPC]) may be a result of these moieties adopting a crystalline (L_{β}') phase, whereas, at 20°C, DOPC and the mixed chains of lecithin adopt a fluid (L_{α}) phase (Tardieu *et al.*, 1973). The M2 peptide may be structurally constrained in the crystalline phase, where the lipid chains are slanting with relation to the bilayer surface, and unable to fully adopt its preferred conformation; in effect, the M2 'cylinder' would be trying to insert 'against the

grain' of the lipids. It may also be postulated that, with the negative lipids, the higher amount of α-helical structure shown by bovine brain L-α-phosphatidyl-L-serine (PS), which contains a variety of fatty acid chains, in comparison to the DOPG, is due to the mixed lipid tails associated with the PS somehow permitting the M2 molecule to adopt more secondary structure.

Epand *et al.*(1983) have demonstrated that the helical content of salmon calcitonin, a thirty-two amino acid peptide hormone, is dependent on the percentage of phosphatidylglycerol; altering the charge state of the membrane alters the helical content of the hormone. A similar phenomenon may also be found with peptide toxins where, for example, cardiotoxin and melittin are able to modulate lipid surface curvature and polymorphism in a lipid-specific manner (Batenburg and de Kruijff, 1988).

Regarding the caveats mentioned in Section 2.5, it would be interesting to examine with CD, M2 mutants that include either transmembrane proline substitutions or hydrophobic stretches that are apparently too short to cross a membrane. It may be that, if amino acids are deleted from a transmembrane domain then other residues, previously exterior to the bilayer, are pulled in; a proline substitution may indeed confer amantadine-resistance by disrupting any potential drug binding site without disrupting channel function. This would imply a degree of structural elasticity in tetramer formation in order to negate any helix-breaking effects due to the imino structure of proline.

Sample	Ellipticity at 225 nm
	(deg.cm^2.dmol^{-1})
M2 peptide/DOPC liposomes 20°C	-22 260
M2 peptide/DOPC liposomes 37°C	-21 660
M2 peptide/DOPC liposomes 20°C/aman 4μg ml^{-1}	-21 970
M2 peptide/DOPC liposomes 20°C/aman 12μg ml^{-1}	-23 190
M2 peptide/DOPG liposomes 20°C	-11 430
M2 peptide in 0.4% (w/v) SDS	-22 840
M2 peptide in 50% (v/v) TFE	-24 440
M2 peptide in buffer 20°C	-700

Table 2.1 Values of molar ellipticities at 225 nm for M2 peptide incorporated into liposomes. Molar ellipticity values were calculated from the observed CD spectra using a value of 110 for the mean residue weight. The error in the ellipticity values is estimated to be $\pm$5%.

Sample	% α-helicity
neutral lipids	
M2 peptide/DOPC	90.3
M2 peptide/lecithin liposomes	100.0*
M2 peptide/DMPC liposomes	52.0
M2 peptide/DPPC liposomes	37.8
M2 peptide/DOPE liposomes	40.5
negative lipids	
M2 peptide/DOPG liposomes	43.8
M2 peptide/bovine brain PS liposomes	51.9
mixed lipids	
M2 peptide/DOPC:DOPG liposomes	48.2

Table 2.2 Mean percent values of α-helical secondary structure for M2 peptide incorporated into liposomes composed of different phospholipids (see text for details). These were calculated from the observed CD spectra. The error is estimated to be ±5%.

N.B. (i) data were also analysed for ß-sheet, random coil and turn contributions, however, only the α-helical results displayed strongly consistent results (ii) * only performed once.

In summary, the transmembrane domain of M2 adopts an α-helical conformation in DOPC liposomes. This structure is not affected by the presence of the drug amantadine or by temperature. However, the secondary structure can be shown to be affected by lipid composition. In view of recent developments in the study of M2 protein, these results answer the questions raised regarding M2 in bilayers (Pinto et al., 1992; Hay, 1989; Hay et al, 1986); the transmembrane region adopts a predominantly α-helical structure and the efficacy of amantadine is not due to it altering this structure in any major way.

A possible model for such an α-helical conformation has been produced using the molecular modelling package SYBYL (Tripos Associates, 1991), as shown in Plates 2.1, 2.2 and 2.3. It is clear from this model that the peptide contains a large hydrophobic area which is consistent with its ability to exist in a membrane.

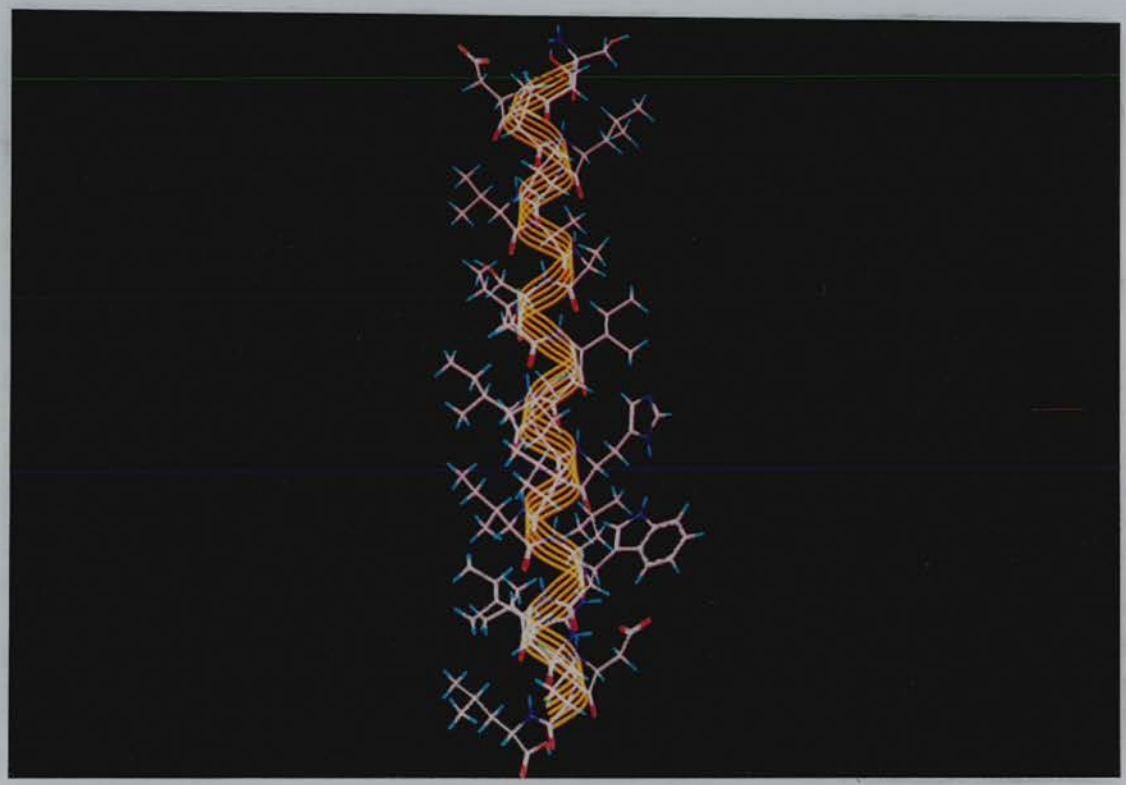

Plate 2.1 Influenza A M2 transmembrane domain modelled as an α-helical moiety (SYBYL) - the central ribbon represents the helix backbone.

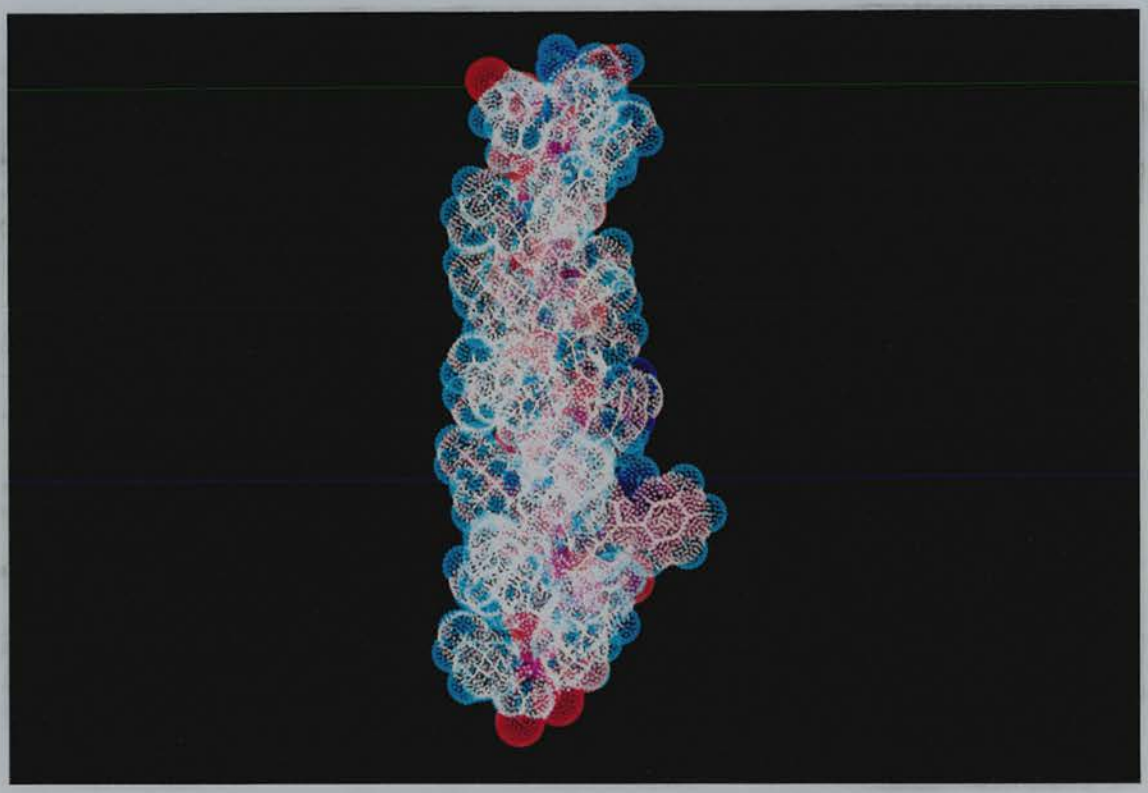

Plate 2.2 The transmembrane helix of M2 represented as a space-filled model.

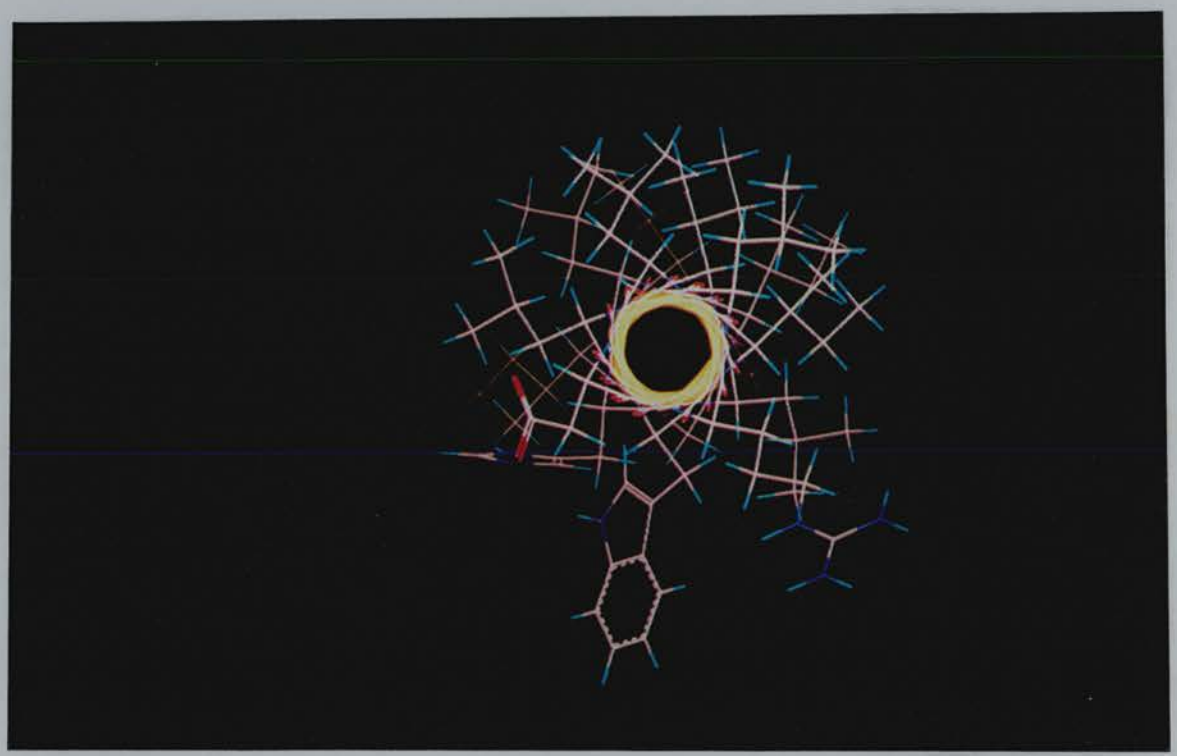

Plate 2.3 The M2 peptide shown as in Plate 2.1, but here it is orientated perpendicular to 2.1 in order to demonstrate the side-chain distribution.

CHAPTER 3 NEUTRON DIFFRACTION STUDIES CONCERNING THE RELATIVE POSITIONS OF AMANTADINE AND M2 TRANSMEMBRANE PEPTIDE IN DOPC MULTILAYERS

3. Neutron diffraction studies concerning the relative positions of amantadine and M2 transmembrane peptide in DOPC multilayers

3.1 General introduction

The amount of biological information obtained over the last forty years using neutron and X-ray diffraction has been enormous. The three-dimensional structure of thousands of different crystalline proteins have been determined and it would appear that such structures are identical in living cells. Such detailed information has greatly enhanced the understanding of enzyme mechanism and specificity, ligand-induced conformational changes and the role and evolution of protein structures. Nucleic acids have also been studied, both in fibre and crystalline form, yielding a wealth of information on base pairing and structure. Diffraction has been employed very successfully in the study of viral structure and composition. In addition, increasingly, this analytical tool is being turned on the very structures that underlie all cellular and enveloped virus integrity, namely, the membrane proteins and the membranes themselves.

3.2 Diffraction theory

The basic diffraction experiment consists of placing a specimen in a beam of radiation and recording the intensity of the scattered radiation as a function of angle. If the specimen consists of lipid bilayers which are completely disorientated with respect to the beam, then a diffraction pattern can be obtained by simply holding the

specimen stationary in the beam. Such a pattern is diffuse and characteristically circularly symmetrical. More information can be obtained if the lipid bilayers are orientated about an axis parallel to the beam. In practice, these are usually regularly stacked and hydrated. This results in a conformation of alternating layers of lipid and water.

Diffraction only occurs when the stacked bilayers are orientated at certain angles around an axis perpendicular to the incoming beam of radiation. This condition must be satisfied by the diffraction geometry. For a random dispersion of stacked membranes this condition is met since all angles are equally probable. For orientated multilayers such conditions can be met by preparing the sample on a curved support or by rotating a flat support. Specimens for neutron diffraction are conveniently prepared on a flat, quartz, microscope slide, therefore it is necessary to rotate the sample using a neutron diffractometer. In such a case, the neutron beam passes through the sample and the scattered radiation is recorded by a neutron detector; both sample and detector are rotated about a common axis.

If the lipid multilayers are regularly stacked, the diffraction pattern will consist of a series of sharp peaks which are approximately equally spaced. These peaks are commonly called Bragg reflections since their position on the pattern are described by Braggs Law -

$$n\lambda = 2d \sin\Theta_B \qquad 3.1$$

where n is the order number, λ is the radiation wavelength, d is the bilayer repeat distance (in nm) and Θ_B is the Bragg angle (which is equal to half of the angle dividing the incident beam from the diffracted beam).

The derivation of Braggs Law explains the conditions necessary for diffraction to occur. If radiation of wavelength \ is incident at an angle Θ_B upon a multilamellar array with a repeat distance d (this includes an interlipid layer of water), then at certain incident angles (the Bragg angles, Θ_B) the reflected waves will be in phase and thus constructively interfere. This constructive interference will occur between radiation reflected from points A and B in adjacent bilayers provided that the path length difference (CB+BD) is an integral number of wavelengths (Figure 3.1). W.L. Bragg was the first person to describe how diffraction from a regularly repeating structure could be considered in terms of 'reflections' from planes of equal scattering density (Bragg, 1913). In practice, only a small proportion of the incident radiation is scattered and, of that scattered radiation, in most cases there will have been a 180° phase shift. Therefore, it may be deduced that beam line flux will have an immediate bearing on scattering intensity and experimental time.

If equation 3.1 is rewritten then it may be observed that a reciprocal relationship exists between the structure under examination and its diffraction pattern -

$$2 \sin\Theta_B = n\lambda / d \qquad 3.2$$

Since, at low angles, $\sin\Theta_B \approx \Theta_B$, and the scattering angle $\Theta_S = 2\Theta_B$, it can be seen that -

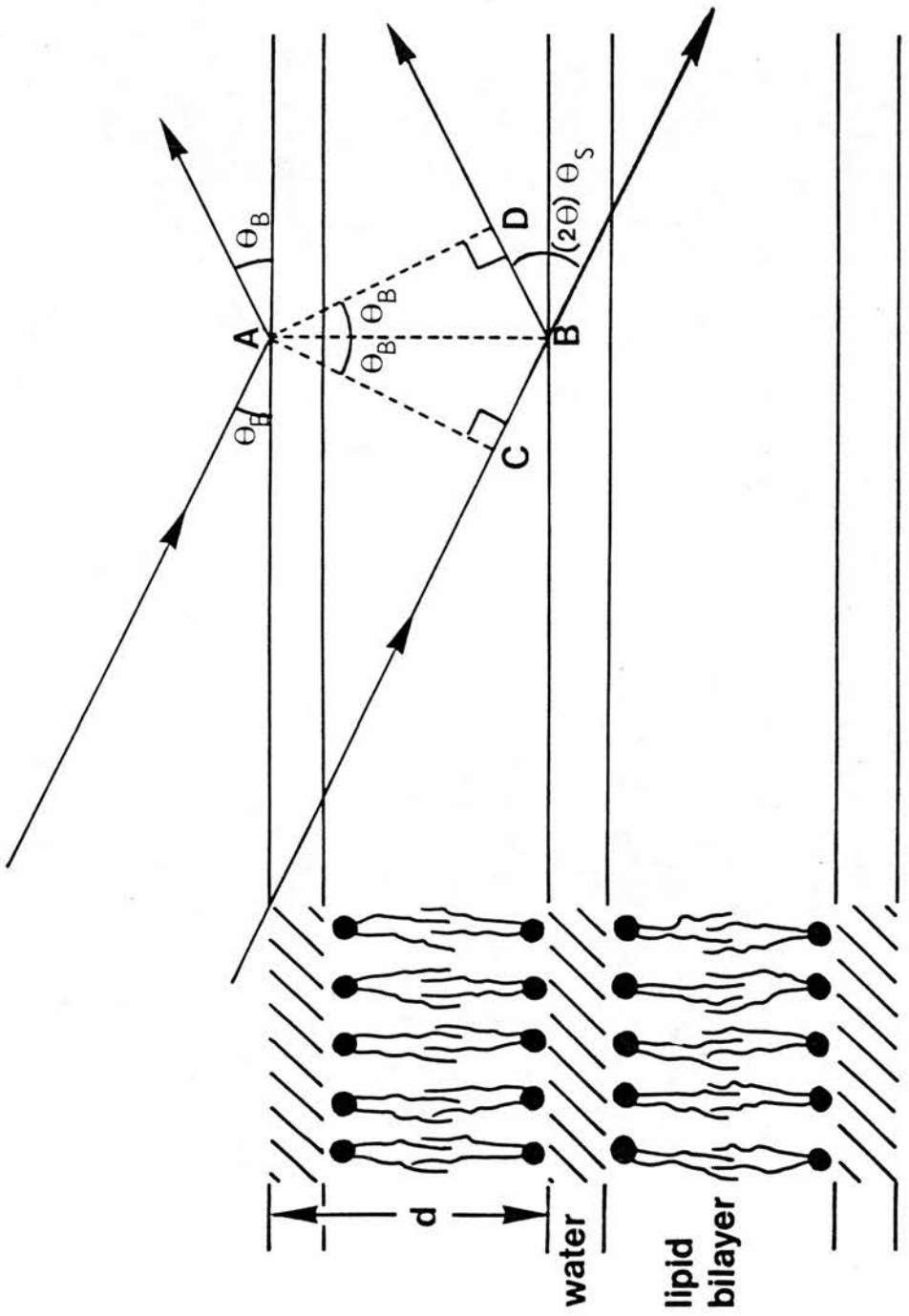

Figure 3.1 Diagram illustrating Bragg's Law - see text for details.

$$\Theta_S \approx n\lambda / d \qquad 3.3$$

Therefore, structures with large d repeats will diffract closer to the centre of the diffraction pattern than structures with small repeat distances.

As can be seen from Figure 3.1, if the angle between the main beam and the glass slide is Θ_B, then the angle between the main beam and the scattered beam is $2\Theta_B$. Thus, if the specimen rotates through Θ radians then the detector must be made to rotate through 2Θ radians. A diffraction pattern recorded in this manner is termed a Θ:2Θ scan. An advantage of this diffraction geometry is that the diffraction angle Θ_S (the angle between the main beam and the scattered beam) is obtained directly, whereas, when using X-rays and photographic film, this angle must be calculated by measuring the distance between the diffraction peak and the centre of the pattern and then using Bragg's equation.

It is possible to obtain a great deal of information regarding the multilayer structure by simply looking at its diffraction pattern and measuring the positions of the observed diffraction maxima. This approach reveals the bilayer repeat distance (d), whether the lipid experiences structural phase changes, any off-meridional peaks (indicating two-dimensional organisation) and whether more than one structural phase is present in the specimen. However, very much more information about the detailed structure of the bilayer can be obtained by *quantitatively* analysing the diffracted intensity. This is because the diffracted intensity describes the distribution of scattering matter in the lipid bilayer.

X-rays are scattered by electrons due to the interaction of electromagnetic radiation with the charged electron cloud. Neutrons, being uncharged, penetrate this cloud and are scattered by atomic nuclei. The radiation scattered from a sample is of two types: coherent and incoherent. It is the coherent radiation which interferes to produce the diffraction pattern whilst the incoherent radiation produces an isotropic background. Incoherent scattering is a function of nuclei in the sample which possess spin properties. These nuclei scatter neutrons differently for different spin orientations. The resultant background must first be subtracted from the diffraction peaks before the coherently diffracted intensity can be analysed.

For both X-rays and neutrons the strength of the coherent scattering from a particular type of atom is described by its coherent scattering amplitude. There are two important differences between X-ray and neutron coherent scattering amplitudes. Firstly, X-ray amplitudes are directly proportional to the atomic number, therefore hydrogen atoms are relatively transparent compared to the other atoms forming the bilayer. Secondly, with both X-rays and neutrons, there is a phase shift of 180° upon diffraction of the incident beam upon encountering biological molecules. However, there is an exception to this rule - neutrons diffracted by hydrogen exhibit no phase change (Bacon, 1975). By convention, the neutron scattering amplitude for hydrogen is therefore termed 'negative'.

X-ray and neutron scattering amplitude densities for water, lipid polar groups, hydrocarbon chains and methyl groups, amongst others, may be calculated as the sum of the coherent scattering amplitudes of the individual atoms divided by the molecular volume.

It may be seen from Figure 3.2 that, for X-rays, the scattering density distribution for a hydrated lipid bilayer will have peaks at the electron-dense phosphate groups and a trough at the centre of the bilayer where the terminal methyl groups are located, with water somewhere between the two. With neutrons, the scattering density distribution is slightly different with the main peaks occurring at the fatty acid ester region (due to the relative absence of hydrogen atoms here). These two techniques emphasise different physical features demonstrating the complimentary nature of X-ray and neutron diffraction.

However, a major difference may be seen in the neutron scattering density profile of a phospholipid sample if it is hydrated with deuterium oxide (D_2O) instead of water. By far the largest peak will now occur in the 'water' region. This example serves to illustrate the most important advantage in using neutrons to study bilayer systems, the use of hydrogen/deuterium exchange to localise certain molecular groups by introducing large changes in scattering density with minimal change in structure. Hydrogen/deuterium exchange offers two further advantages. Firstly, this change in scattering density at localised positions in the structure can help solve the phase problem (see below). Secondly, it is the incoherent scattering from hydrogen which causes much of the background encountered in neutron diffraction experiments. Thus, its replacement with deuterium greatly improves the signal-to-noise ratio.

Full analysis of a diffraction pattern involves the final production of an electron density profile or a neutron scattering density profile. Basically, these profiles represent the summation of

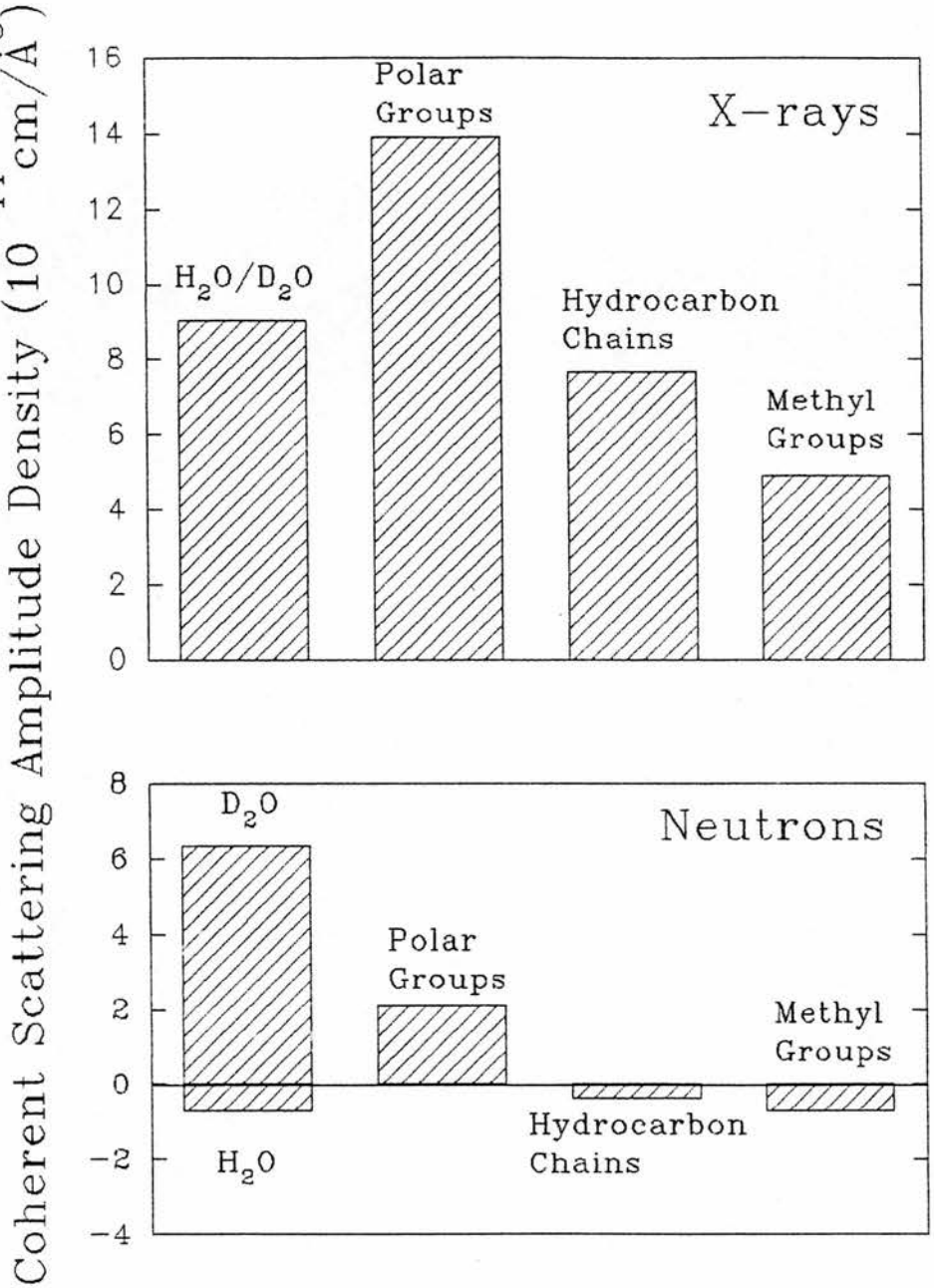

Figure 3.2 Neutron and X-ray coherent scattering amplitude densities for water and various portions of a typical phospholipid (see text). The scattering density histograms are both on the same absolute scale.

cosine waves calculated, in turn, by transforming the amplitude functions of the diffraction patterns into wave functions. These amplitude functions are the square root of the recorded intensity of each diffracted order. However, with centrosymmetric structures, it may be seen that in taking the square root of the intensity, the resulting amplitude may be either positive or negative; information has been lost concerning the sign of the amplitude. Reconstruction of a structure from its diffraction pattern is therefore only possible if we can determine both the amplitude and the phase of each diffracted beam (see below).

Transforming the amplitude function into a wave function which summates into the density profile is a process which may be performed using the Fourier transformation.

First, consider the diffraction from a single centrosymmetric structure with an arbitrary scattering density distribution ç(x) along a coordinate x. The scattered intensity from such a single structural unit is equal to the square of the Fourier transform of ç(x), that is -

$$I(R) = [F.T.\{ç(x)\}]^2 = [F(R)]^2 \qquad 3.4$$

where the intensity I(R) is measured along a coordinate R, which is simply related to distances from the centre of the diffraction pattern. This variable R, with dimensions of length^{-1} and usually called the reciprocal space coordinate, is related to the scattering angle Θ_S by -

$$R = 2 \sin(\Theta_S / 2) / \lambda \qquad 3.5$$

The Fourier transform of the distribution ç(x) is given by -

$$\text{F.T.}\{ç(x)\} \equiv F(R) = 2\int_0^\infty ç(x)\cos(2\pi Rx)dx \qquad 3.6$$

Because there is an identical inverse relationship -

$$\text{F.T.}\{F(R)\} = ç(x) = 2\int_0^\infty F(R)\cos(2\pi Rx)dR \qquad 3.7$$

then, if $F(R)$ is known at every value of R, the scattering density distribution ç(x) can be directly calculated.

For a random dispersion of N structures, which will scatter *independently*, the total diffraction intensity is N times the diffraction intensity from a single structural unit.

For a regular stack of N structural units, the scattered waves will only be in phase and thus constructively interfere at certain angles. At these angles the reciprocal space coordinate, R, will have values -

$$R = \{2\sin(\Theta_S / 2)\} / \lambda = \{2\sin(\Theta_B)\} / \lambda = n / d \qquad 3.8$$

using the definition of R (Equation 3.5) and Bragg's Law (Equation 3.1). At these values of R the total scattered amplitude will still be proportional to $F(R)$ (the Fourier transform of ç(x) for the single structural unit), but N times larger. Therefore, the scattering from a stack of structural units can best be described in terms of sampling the transform $F(R)$ of a single structural unit at discrete points

R = n/d. Since the intensities of these points will be proportional to N^2, compared to N in the case of a random dispersion, diffraction patterns from orientated multilayers are far quicker to record. Here, the Fourier transformation of a large stack of individual structural units with a repeat distance, d, only has values when the reciprocal space coordinate R = n/d.

When the Fourier transform is a continuous function, as in the case of a random dispersion of structures, then the scattering density distribution ç(x) can be evaluated using the integral in Equation 3.7. When, however, the Fourier transform is only sampled at discrete points, as in the case of a regular stack of structural units, it is more convenient to obtain ç(x) using the summation -

$$ç(x) = \{F(0)/d\} + (2/d)\,\Sigma F(n/d)\cos(2\pi nx/d) \qquad 3.9$$

A scattering density distribution calculated in this way is called a Fourier synthesis. The first term $\{F(0)/d\}$ is the mean scattering density over the repeat distance, d. The variation in scattering density about this mean level is given by the summation of cosine terms. As cosine terms of higher frequency are added to the synthesis (ie. as n increases), finer details can be resolved in the structure. In practice, the resolution which can be obtained is limited because only a finite number of reflections can be observed. Also, since $F(0)$ is proportional to the amplitude of the radiation scattered in the same direction as the main beam, it cannot be observed experimentally. This is not usually a serious problem however, since $F(0)$ only affects the mean level of the scattering density profile.

The amplitude of the Fourier transform, $F(R)$, cannot be directly obtained from the intensity distribution, I(R), since the intensity is the square of the amplitude. To obtain the amplitude, the square root of the intensity must be obtained. This is the origin of the phase problem -

$$F(R) = \pm I(R) \qquad 3.10$$

Phase information is often only available by indirect methods and elaborate techniques have been developed for its retrieval. The phase problem can be considerably simplified, however, if it can be shown that the diffracting object is symmetrical, since a symmetrical structure gives rise to diffracted beams which are always in phase or 180° out of phase.

It is important to appreciate that the reliability of a scattering density distribution usually rests far more upon the correct choice of signs than upon the precise determination of the diffracted intensities. Three main methods may be applied, either individually or in series, in order to phase complete data sets for all n values. Diffraction patterns of membranes which have been extensively studied using other techniques can frequently be phased by means of model building techniques. If a model of the expected membrane structure can be devised, its Fourier transform may be calculated and compared with the measured diffraction pattern. If the intensities of the theoretical and experimental transforms are in reasonable agreement, the phases of the experimental transform can be assumed to be those of the theoretical transform. If the agreement is poor the model is refined until a good fit is obtained.

A variation of the model building technique involves combining the measured amplitudes with all possible phases. Scattering density profiles are calculated for each combination, but only those consistent with plausible structures are accepted as being possible solutions. Providing a sufficiently detailed model is available, it is usually possible to assign phases to all but the highest orders.

Another phasing method which may be employed is to perform a series of multilayer swellings. An important relationship arising from Fourier theory is that the Fourier transform of a repeating function is that of the repeating unit sampled at multiples of the repeat frequency. Increasing the membrane spacing, by incorporating more water, results in a decreased sampling frequency, although the underlying diffraction pattern of the single membrane remains unaltered. If a series of swelling experiments are carried out, by altering cell humidity by using salt solutions of different concentrations to cause various degrees of swelling, the data can be combined to plot a continuous profile of diffraction and thereby obtain the Fourier transform amplitude distribution of a single repeating unit. The *relative* phases of different parts of the transform may be inferred if enough swelling points are used.

The most rigorous method for phasing diffraction patterns involves replacement of certain atoms in the specimen with atoms of relatively high scattering length. These atoms give rise to a pattern of scattering which modifies the diffraction pattern intensity distribution, and if their location is known, the phase distribution of the original pattern can be inferred. Obviously, the incorporated atoms must not perturb the original structure, ie. replacement must be isomorphous. A variation on this theme, used with neutrons, is

to exchange the solvent water with heavy water. Subtracting the phased amplitudes of, for example, lipid and water from lipid and heavy water leaves the difference scattering profile of the D_2O region between the lipid bilayers. With the correct choice of phase for both data sets, this distribution has been shown to be accurately described by a pair of Gaussian curves (Weiner *et al.*, 1991). The original lipid data sets can now be phased using the phases that produced the Fourier transform of the Gaussians upon subtraction.

If data sets are to be used in conjunction with each other, as above, then they must be properly scaled to each other with respect to amplitude. This may be achieved by using four or more data sets where it is possible to perform a complete set of subtractions resulting in the production of two pairs of D_2O Gaussians. The data sets can be rescaled to each other until both Gaussians are similar in size. Scaling on an absolute scale is also possible.

In conclusion, having obtained a set of amplitudes and having deduced their signs (these are now called structure factors), then the scattering amplitude density profiles may be produced using a simplified version of Equation 3.9 -

$$\varsigma(x) = \Sigma F(n/d) \cos(2\pi nx/d) \qquad 3.11$$

The term $F(0)/d$, which defines the mean scattering density, is missing since it will not have been observed and it is possible to leave out the factor 2/d in front of the summation if the amplitudes $F(n/d)$ are only to be put on a relative scale. Thus the experimentally derived profiles, $\varsigma(x)$, will also be calculated on a relative scale (the M2/Brookhaven data).

3.3 Experimental hardware

All neutron data in this thesis were obtained either at the Institut Laue Langevin (ILL), France or at Brookhaven National Laboratory, U.S.A. The initial amantadine study was undertaken on instrument D16, ILL and the subsequent M2 peptide work on instrument H3B, High Flux Beam Reactor (HFBR) at Brookhaven. Both instruments work on the same principles and comprise similar features. As an example, the details of H3B will be discussed.

From Figure 3.3 it can be seen that the instrument is made up of six main functional components. The collimator is inserted into the face of the nuclear reactor to allow release of a parallel beam of neutrons. The resulting 'white' neutron beam is monochromated by reflection from two thin-film monochromators. These multilayers typically have a periodicity of about 6 nm and, if placed in the direct beam, will themselves produce a beam of diffracted radiation of variable wavelength dependent on the angle of incidence. It is theoretically possible on H3B to adjust the wavelength over the range 1.7 - 4.5 Å, although for studies of the type described herein a value of around 2.45 Å was deemed suitable. A main beam shutter is next and this housing also incorporates a low efficiency fission detector which intercepts a small fraction of the neutron beam and may be taken to be a measure of the neutron flux. Data may therefore be either collected for a given period of time or for a specified neutron count. Data collection for a given number of monitor counts has the advantage that it automatically compensates for any changes in reactor flux. The main function of the collimator (Plate 3.1) is to reduce the size of the beam to meet the

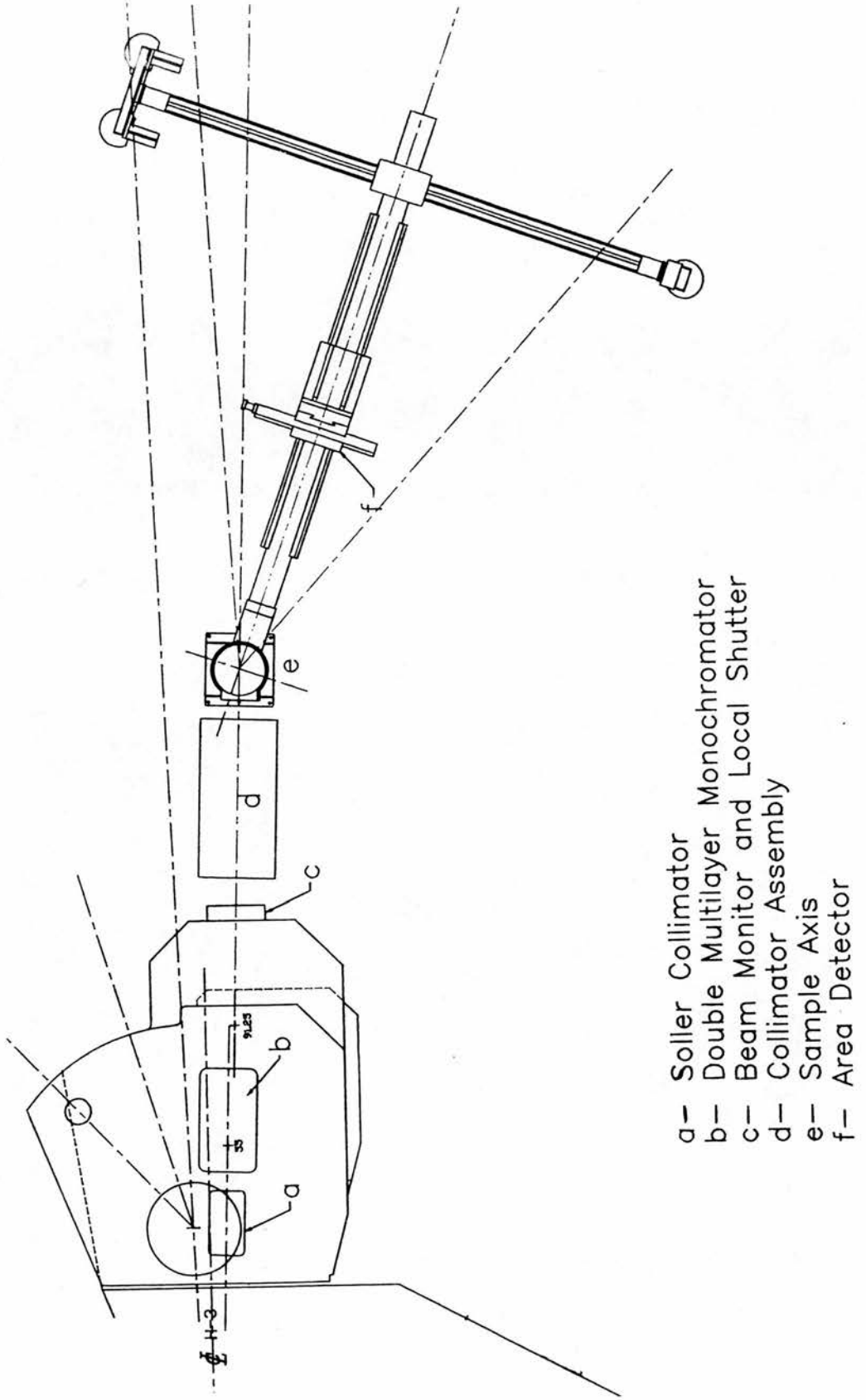

Figure 3.3 Membrane spectrometer H3B at Brookhaven National Laboratory (after 'Users Notes' compiled by A. Saxena.)

experimental requirements and to reduce the angular divergence of the beam. For a neutron beam reflected by a multilayer monochromator, the wavelength spread ([change in λ] / λ) is primarily determined by the angular divergence of the final beam, and its magnitude can be increased or decreased by adjusting the collimation accordingly. Lamellar samples are mounted on a goniometer and the slides are held vertically inside an aluminium can (Plate 3.2) during data collection which allows them to be kept at the desired temperature and humidity. Copper plates welded to the top and bottom of the can are connected to a constant temperature, circulating water bath. Humidity, and therefore bilayer spacing, is controlled by placing small water baths filled with a solvent (either D_2O, H_2O, or a mixture of both) and/or salt inside the can. This can is mounted on a shaft attached to a rotational stage and its motion is dictated by the geometry of the Θ:2Θ scan. Finally, the diffracted intensities are collected with a gas filled area detector. A few channels close to each edge of the detector record spurious counts and are not therefore considered in data analysis. These channels are removed from all consideration by defining a 'useable area'.

3.4 Introduction to the experimental section

Chapter 2 presented CD data collected on the secondary conformation of native M2 transmembrane peptide incorporated into liposomes. Chapter 3 locates to high resolution the position of M2 peptide in the bilayer and its orientation with regard to amantadine.

Plate 3.1 Membrane spectrometer H3B (HFBR) at Brookhaven National Laboratory, overall view. Note the detector, temperature control bath and the location of the reactor.

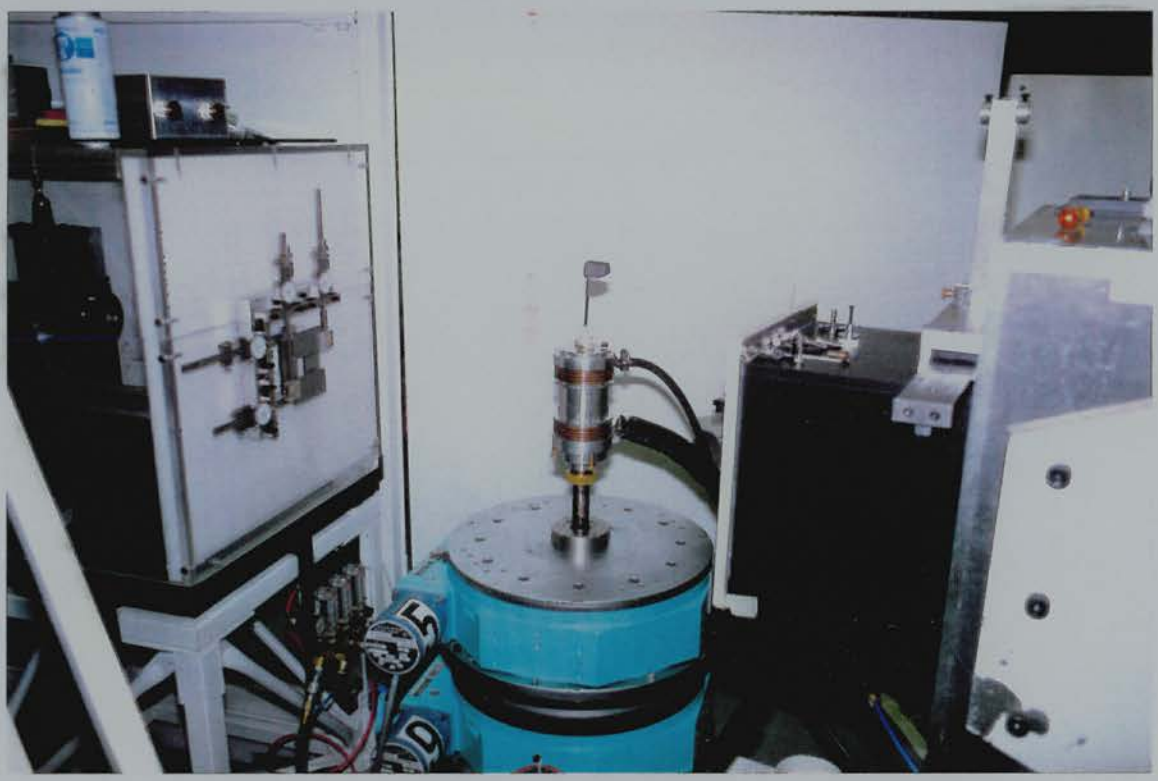

Plate 3.2 Membrane spectrometer H3B (HFBR) at Brookhaven National Laboratory, detail of lamellar sample can - collimated beam comes from the left, the detector is on the right.

Such experiments were repeated using amantadine-resistant mutant M2 transmembrane sequences (see Section 2.7 for details of peptide preparation).

A useful preliminary study to such work was undertaken in order to locate both amantadine hydrochloride (HCl) and amantadine free base (FB) individually in bilayers of DOPC. Such a study has value in itself as amantadine may have properties other than its pharmacological ones.

Section 3.5 will therefore describe this preliminary study whilst Section 3.6 will be concerned with the bilayer position of M2 (both native and mutant) and with any interactions between the M2 peptides and amantadine. The diffraction work was carried out with Dr J.P. Bradshaw, Department of Biochemistry, University of Edinburgh.

3.5.1 The location of amantadine HCl and FB within phospholipid multilayers - an introduction

Amantadine (1-aminoadamantane hydrochloride) is licensed for the prophylaxis of influenza A infection and for treatment of both influenza and Parkinson's disease (Oxford and Galbraith, 1980; Obeso and Martinez-Lage, 1987). In the case of influenza, the efficacy of amantadine is postulated to involve interruption of viral-host cell membrane fusion and/or interference in haemagglutinin maturation (Hay, 1989; Sugrue *et al.*, 1990). The mechanism of action of amantadine in Parkinson's disease is probably related to its ability to increase presynaptic synthesis and release of dopamine. This effect is potentiated by the drug inhibiting dopamine reuptake

(Gilman *et al.*, 1990). These therapeutic processes are thought to include the involvement of the hydrophobic, lipophilic properties of the molecule (Phonphok and Rosenthal, 1991).

Amantadine studies undertaken so far have been wide-ranging, including its effect on influenza infection and, more recently, its specific molecular effect on the viral protein which is implicated in this drug-induced prophylaxis, namely M2 (Sugrue and Hay, 1991). However, other work has been published in which amantadine has been reported to affect bilayer stability. A recent study has noted the role of amantadine in the stabilisation of clathrin-coated membrane vesicles, similar to those formed upon initial viral penetration by influenza, Semliki Forest and vesicular stomatitus virus (Phonphok and Rosenthal, 1991). However, others have reported that, although tromantadine (an amantadine derivative: N-1-adamantyl-N-[2-(dimethylamino) ethoxy] acetamide-hydrochloride) appears to stabilise phospholipid bilayers, amantadine itself slightly lowers the temperature of the bilayer to hexagonal phase transition. Also, NMR studies have shown that amantadine is perturbing to the organisation and motional properties of phospholipids in the bilayer phase (Cheetam and Epand, 1987). These results indicate an amantadine-mediated increase in disorder. It can therefore be seen that a certain degree of ambiguity exists in the interpretation of the available data.

As a prerequisite to further mechanistic studies of amantadine, and in order to examine the ambiguous results reported above, a series of experiments were undertaken to investigate the location of the drug within bilayers of DOPC. To reduce possible ambiguity in the results a single lipid species was used; DOPC being the most

physiologically representative. Positional differences between amantadine hydrochloride (HCl) and amantadine in its free base form (FB) have also been examined.

In addition, this section describes the use of a specific deuterium labelling technique to locate amantadine in synthetic multilayer membranes using neutron diffraction. These results are both quantitatively and qualitatively supported by, and are discussed in relation with, a concomitant X-ray diffraction study using unlabelled amantadine. [The X-ray work was undertaken by another member of the group (Andrew Cudmore).]

3.5.2 Materials

DOPC was purchased from Sigma Chemical Company Ltd. (Fancy Road, Poole, U.K.) and confirmed to be a single species by thin layer chromatography. Amantadine was obtained from the same source in both FB and HCl forms. Deuterated amantadine FB was obtained from Dr M. R. Alecio of the Shell Research Centre (Sittingbourne, Kent, U.K.).

3.5.3 Sample preparation for neutron diffraction

Good sample preparation is of paramount importance in diffraction studies as correct multilayer orientation and hydration are prerequisites for diffraction data collection. In addition, if data sets are to be analysed in conjunction with each other, then all such samples must be prepared in a rigorous, reproducible manner.

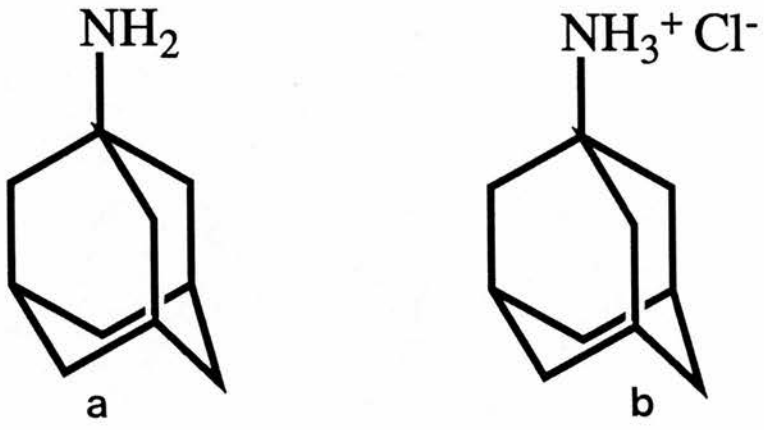

Figure 3.4 The two forms of 1-aminoadamantane used in this study: (a) amantadine free base (b) amantadine hydrochloride.

Orientated phospholipid bilayer stacks were prepared as follows. Samples comprising 20 mg of DOPC in chloroform, as supplied by Sigma, were dried-down under oxygen-free nitrogen. The lipid was then dissolved in approximately 0.5 ml of methanol. Any amantadine added (5% molar ratio with respect to the DOPC) to the final sample was dissolved separately in a similar volume of methanol. The solutions were then whirlimixed, added together and whirlimixed again. The sample was slowly applied to a quartz glass microscope slide using a fine-tipped stretched pipette, allowing each layer of solvent to dry partially in a stream of warm air from a hairdrier before the addition of more sample. After all the solvent was applied to the slide, it was given time to dry (usually about ten minutes) and then a further application of methanol was spread over the sample. This step produces a smooth, even finish. After subsequent drying, the slide was placed *in vacuo* for at least two hours. This drives-off any residual organic solvent. The multilayers were then rehydrated by transfering the quartz slide into a dessicator over the rehydration solvent of choice. This dessicator was placed in an oven at 20°C (at which DOPC adopts the L_{α}-phase) for at least four hours. Subsequent to this, after moving the sample from its dessicator into the sample-can for the experiment (which contained identical conditions to the dessicator), a re-equilibration time was allowed for conditions to stabilise before data collection commenced. From studies performed previously at the ILL, it was known that this period never exceeded fifteen minutes, therefore, re-equilibration was allowed to proceed for at least thirty minutes. In effect, this time is to allow the multilayers to replace any solvent that they may have lost, during transfer between

containers, by absorbing moisture from the humid atmosphere inside the can. During this period the equilibration process was monitored by recording the angular position of the third or fourth order of lamellar diffraction which increased as the multilayers dehydrated and decreased as they took up water from the atmosphere. Each sample was judged to have achieved equilibrium when there was no further shift in the position of the Bragg peaks and the calculated lamellar repeat distance was that predicted for the experimental conditions by previous X-ray work. Any sample which did not fulfil both of these criteria was discarded.

When changing the D_2O:H_2O ratio, the samples were allowed to dry out in normal atmospheric conditions for about an hour before being replaced in a dessicator containing the next solvent. Each recorded diffraction pattern consisted of up to eight well defined orders. The mosaic spread of each sample was determined using the D16 software.

3.5.4 Neutron data analysis - ILL

Corrections : Once the diffracted intensities had been corrected for detector response and background, then integrated, the following corrections were applied -

(1) Lorentz factor. The Ewald construction is a mathematical tool which enables the prediction of the geometry of diffraction (Ewald, 1921). If the diffracting sample is taken to be the centre of a sphere of possible diffraction, then only on the circumference of this sphere, and where it complies with Bragg's Law, is it

possible to observe intensities. Higher orders will be correspondingly less intense as the sphere curves away from them. The Lorentzian factor corrects for this -

$$C_{Lor(n)} = \sin(2\Theta_n) \qquad 3.12$$

(2) Absorption. When the angle of diffraction is low, the incident and diffracted beam have a significant path length within the sample and thus will be subject to a greater degree of absorption than when the angle is high and the corresponding path lengths low. Moreover, the degree of absorption will also be affected by the H_2O/D_2O composition of the sample. The appropriate correction for absorption by the lipid film, was applied -

$$C_{Abs(n)} = 1/(\sin\Theta_n/2ut)(1-\exp[-2ut/\sin\Theta_n]) \qquad 3.13$$

where $u = (6.04-0.75mf)$, mf being the mole fraction of D_2O (Worcester and Franks, 1976). The mass of lipid on each slide, the area over which it was spread and the unit cell size, as determined by diffraction, were used to calculate a value of 30 μm for t, the thickness of the lipid film.

(3) Sampling by the Detector. As a result of lattice disorder in the sample, the diffraction peaks may be so wide that the whole of each diffraction peak is not recorded by the detector, and a correction must be applied to the data to account for this. In this study the mosaic spread of each sample was small enough to ensure

that each diffraction peak was regular in shape and contained wholly within the central part of the detector so no correction was applied in this case.

The final neutron structure factor amplitudes were therefore calculated as -

$$|F_{(n)}|^2 = I_n C_{Lor(n)} C_{Abs(n)} \qquad 3.14$$

where I is the measured intensity.

Phasing : Neutron scattering profiles may only be obtained upon solving the individual phases of the recorded amplitudes. In this study two different techniques were employed to phase the neutron data sets: D_2O/H_2O exchange and isomorphous replacement.

Neutron data are routinely phased by carrying out experiments hydrated at various H_2O/D_2O ratios (Worcester and Franks, 1976; Büldt *et al.*, 1979; Franks and Leib, 1979; Jacobs and White, 1989). This method was used in the present study, with additional phasing information coming from a variation of the isomorphous derivative technique (Büldt *et al.*, 1978) in which use was made of the presence or absence of amantadine in the multilayers. Assigning phases to the neutron data proceeded by altering the sign of the individual structure factors until a result was achieved in which both the differences caused by replacing H_2O with D_2O and the DOPC/amantadine minus DOPC differences were consistent within each set of comparable data.

The two diffraction techniques, X-rays and neutrons, emphasise different features within the bilayer structure, and further confirmation that the correct phases had been assigned was given by the fact that the two methods agreed and thereby showed the complementary nature of the techniques.

White and his co-workers (Wiener *et al.*, 1991) have produced an elegant method for scaling neutron data. This approach was used in the present study and basically involved using the size of the D_2O and the amantadine distributions to scale the different sets of data to each other. The results put the profiles on a 'relative absolute' scale in which they are scaled with respect to the unit cell contents, but not on an absolute per volume scale.

3.5.5 Results

Table 3.I gives the corrected, scaled neutron diffraction structure factors for all three samples, DOPC, DOPC with amantadine HCl, DOPC with amantadine FB, at 0% and 100% D_2O. Figure 3.5 shows reconstructed transbilayer profiles of DOPC alone (a, b) and difference profiles defining the distribution of amantadine HCl (c, d) and FB (e, f) respectively. The dotted line represents the neutron data with the bold line representing the complementary X-ray data. The difference profiles were calculated by subtracting structure factors of pure DOPC from those of DOPC with 5% (mol) amantadine and placed on a relative absolute scale using the method of Wiener *et al.*, 1991. The horizontal scale is distance, measured from the bilayer centre, in Ångströms. Figure 3.6 contains difference neutron density scattering profiles showing

the distribution of water between bilayers of (a) pure DOPC, (b) DOPC with amantadine HCl and (c) DOPC with amantadine FB, all at 20°C. Also shown are Gaussian distributions fitted to the water profiles in reciprocal space over all eight observed orders of diffraction, using a development of the method of Wiener *et al.*, 1991. Each curve consists of the sum of two Gaussians with the following parameters: (a) Z (distance from the centre of the bilayer) = ± 26.53 ± 0.35 Å, AW (1/e halfwidth) = 8.82 ± 0.20 Å; (b) Z = ± 26.04 ± 0.55 Å, AW = 8.75 ± 0.25 Å; (c) Z = ± 25.58 ± 0.45 Å, AW = 8.65 ± 0.25 Å. The difference between the observed and modelled water profiles may be taken as an approximation of error in the reconstructions. Each graph therefore also shows this difference, plotted on an enlarged scale, corresponding to that used in Figure 3.5 (right hand side).

The mosaic spread of the DOPC bilayers ranged from 0.4° to 0.6°, these very low values being quite characteristic of unsaturated fatty acyl phospholipids. The mosaic spread was not significantly changed upon the addition of amantadine.

3.5.6. Discussion

DOPC

Figure 3.5 displays both X-ray and neutron scattering density profiles across the phospholipid bilayer with the water component occupying the outer region of the graphs. With X-rays, the DOPC profile (a) agrees with previously published data (Bradshaw *et al.*, 1989; Weiner and White, 1991) in that it displays the classic phospholipid leaflet form with a main peak representing the electron-

DOPC	Amantadine HCl	D-Amantadine Free Base	%D_2O 0% D_2O	100% D_2O
20			1) -6.47 2) -12.09 3) 5.16 4) 0.34 5) -1.44 6) 0.33 7) -0.30 8) 0.00	-89.31 25.56 -4.34 1.00 -2.84 0.77 -0.67 0.00
20	0.25		1) -19.74 2) -8.66 3) 3.17 4) 0.00 5) -1.37 6) -0.18 7) 0.26 8) -0.30	-61.22 10.02 -1.68 0.32 -1.86 0.06 0.15 -0.27
20		0.25	1) -13.55 2) -17.65 3) 6.53 4) 0.00 5) -1.98 6) 0.33 7) 0.00 8) 0.00	-96.41 18.80 -2.76 1.21 -2.97 0.57 -0.16 -0.15

Table 3.1 Relative absolute neutron structure factors of lamellar arrays of pure DOPC and DOPC with 5% (mol) amantadine HCl or FB at 98% rh and 20°C. The accuracy is estimated to be ± 0.15 units.

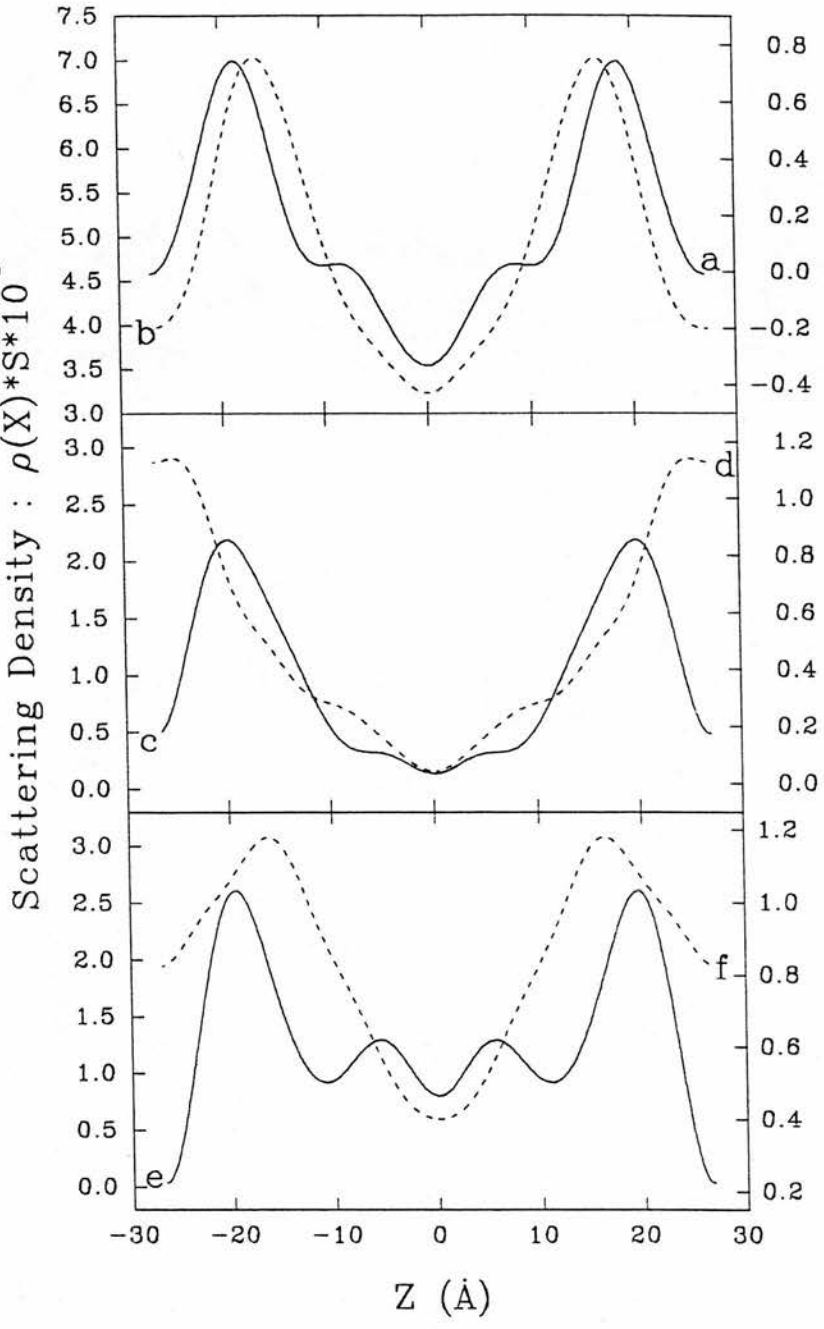

Figure 3.5 Reconstructed trans-bilayer scattering profiles (neutron - dotted lines, X-ray - bold lines). (a) and (b) represent pure DOPC, (c) (d) and (e) (f) represent difference profiles of amantadine HCl and FB respectively. [NB. X-ray data produced by A. Cudmore.]

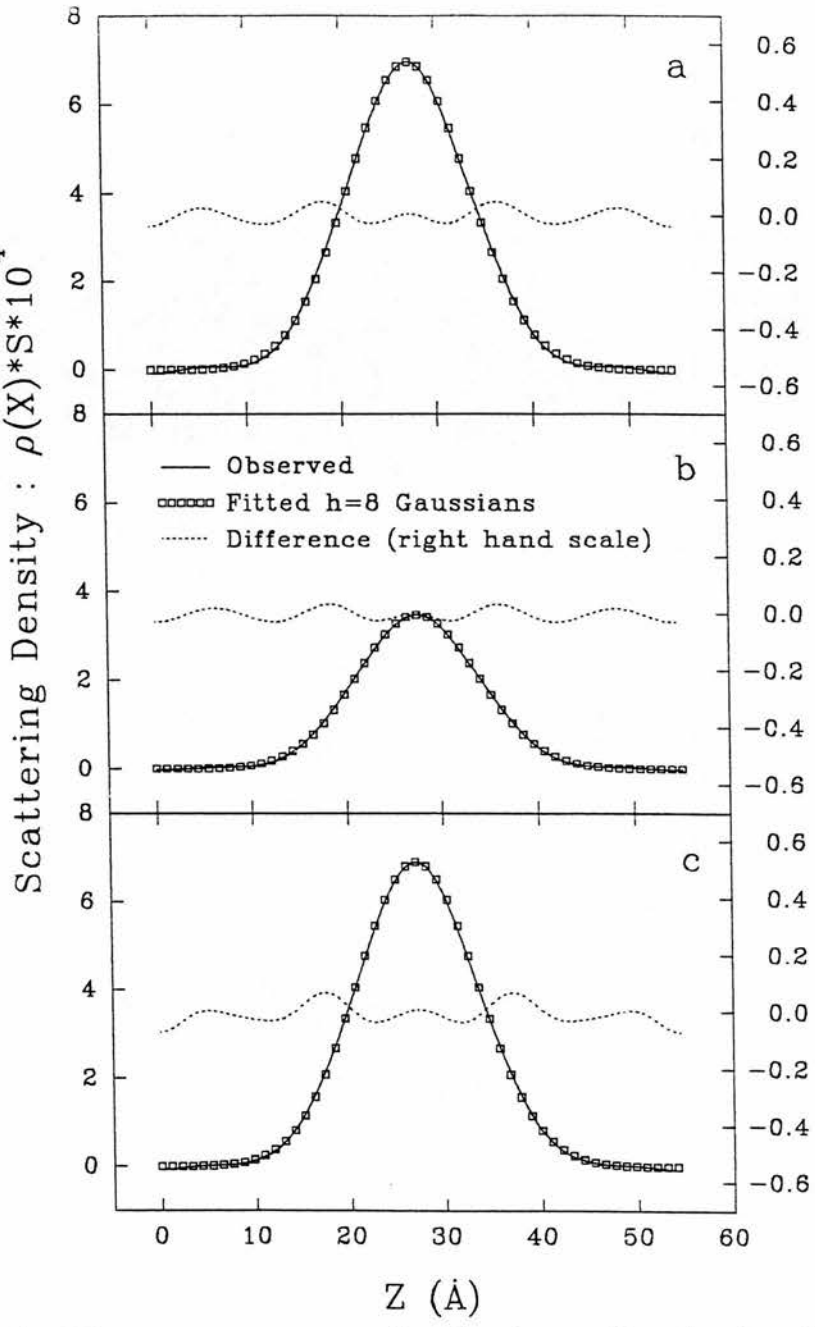

Figure 3.6 Difference neutron scattering density profiles showing the distribution of water between bilayers of (a) pure DOPC, (b) DOPC with 5% (mol) amantadine HCl and (c) DOPC with 5% (mol) amantadine FB, all at 20°C. Included are Gaussian distributions fitted to the diffraction patterns of the water profiles. For details see Section 3.5.5.

dense region which encompasses the phosphate groups and fatty acyl ester bonds. A secondary peak appears within the hydrophobic region which corresponds to the double-bond in the oleic acid chains. It can be seen from (b) that less detail results from the neutron data. This is probably due to the lower contrast characteristic of neutron scattering (all these diffraction experiments were sampled through eight orders so this phenomenon does not involve the X-ray data being collected to a higher resolution than the neutron).

The differences between the X-ray and neutron profiles are due to inherent atomic scattering differences across the unit cell (see Section 3.2). X-rays are more strongly scattered by the phosphate groups in the repeat motif whereas maximum neutron scattering corresponds to the fatty acyl ester bond positions (Franks and Lieb, 1981). Profile (b) clearly displays this scattering dichotomy with the neutron data peak appearing markedly closer to the hydrophobic interior of the bilayer than the X-ray result (a). The sharper X-ray profile displays a second, highly-defined peak in the fatty acyl chain region of the leaflet.

Amantadine HCl

Figure 3.5 (c) to (f) are difference profiles which were calculated by subtracting the lipid and water structure factors from the lipid, water plus amantadine structure factors and therefore represent *only* the amantadine distribution across the bilayer. They are displayed in the same orientation as the pure DOPC but it can be seen that these profiles, both X-ray and neutron, are substantially

different from the DOPC data. Amantadine, in both its hydrochloride and free base forms, appears to have been incorporated into the multilayer system.

The highest peak in the X-ray profile (c), representing the greatest distribution of amantadine HCl, lies between the phosphate and ester linkages. This surface location is also represented in the neutron profile (d) but its shape has changed with additional density encroaching into the water. It is proposed that the difference between the X-ray and neutron profiles is due to the relatively higher scattering length of nitrogen for neutrons compared to that for X-rays, which emphasises the amine group in the neutron profiles. These results therefore orientate amantadine HCl in the bilayer; the hydrophobic, cyclic region of the drug located between the phosphate and ester linkages of the phospholipids with the NH_3+ group protruding into the water space.

Importantly, this interpretation is supported by changes in the distribution of water between adjacent bilayers when amantadine HCl is added. Figure 3.6 shows difference profiles representing the location of the deuterons of heavy water, calculated by subtracting neutron scattering profiles of multilayers containing H_2O from corresponding ones hydrated with D_2O. It can be seen that incorporation of amantadine HCl into the DOPC bilayers reduces the area under the water profiles, indicating that the drug is displacing some of the water from the system.

Both profiles (c) and (d) of Figure 3.5 include additional features in the lipid tail region which may be caused by termination error; ie. errors caused by not collecting all possible orders of diffraction. The resolution of the present study procludes

unambiguous assignment of these features to the presence of amantadine deep within the bilayer, but it should be noted that evidence from the FB profiles (see below) indicates that full penetration of the bilayer by a proportion of the amantadine can occur. This is particularly noticeable in the neutron profiles and is either a product of the relatively high concentration of drug used saturating preferential surface sites, or it may represent amantadine which has reverted to the uncharged, FB form by deprotonation.

Amantadine FB

At this resolution, both amantadine peaks are in the same position in the X-ray profile (e) as in the amantadine HCl result (c). Positionally, therefore, the data are identical. However, there is a difference in the proportional representation of amantadine across the bilayer with relatively more now appearing in the fatty acid tail region of the phospholipids. The neutron results (f) agree with these findings. Here the main scattering density at the surface location has moved slightly into the bilayer reflecting the fact that the amantadine FB is deuterated on the hydrophobic carbons only and that the NH_2 amine group is unlabelled and therefore scatters much less intensely compared to the labelled mass; it can be observed as a shoulder on the water side of the main peak. This observation again orientates the amantadine with its NH_2 group at the lipid/water interface.

Profiles (e) and (f) clearly show that a proportion of amantadine has penetrated almost to the centre of the bilayer. The height of the profiles above zero can only be explained in terms of a considerable mass of drug being present in this region. Consistent

with this finding, the amount of water associated with the bilayers containing amantadine FB is much greater than that for bilayers containing amantadine HCl (Figure 3.6) and almost equates with that present in the bilayers in the absence of either form of amantadine. Clearly a proportion of the drug has moved away from the water-penetrated surface of the bilayers to take up a deeper location in the bilayers. This evidence, taken together with the HCl results, leads to the proposal that the interaction between amantadine and DOPC bilayers takes the form of an equilibrium between two possible regions. One of these is located at the water-bilayer interface, the other is less defined and broadly represents the fatty acid tail region. The balance of this equilibrium between the two sites appears to depend upon the starting protonation state of amantadine. However, this does not necessarily imply that the initial charge state of the amine is preserved throughout the experiment. This result compares with tetracaine where its interaction with phospholipids is also reported to be influenced by the charge state of the drug (Smith *et al.*, 1991, Shimooka *et al.*, 1992).

Amantadine/Phospholipid interactions

If the optical parameters and the sample dimensions are kept constant throughout a series of diffraction experiments then the mosaic spread may be used as a measure of the macroscopic order of each sample; the smaller the mosaic spread, the less the degree of disorder in the system (Schwartz *et al.*, 1975; Blaurock and Nelander, 1976). The values obtained for stacked bilayers of pure DOPC in this study are in good agreement with previous observations (Bradshaw *et al.*, 1989, White *et al.*, 1991). The

mosaic spread did not change upon the addition of 5 % (mol) amantadine, which indicates that the interaction between the drug and the bilayer did not disturb the macroscopic order. There was no evidence of phase separation in the multilayers containing amantadine. It seems that, under these experimental conditions, amantadine does not markedly perturb the bilayer system.

It has been reported that amantadine reduces the extent of dissociation of clathrin from coated vesicles (Phonphok and Rosenthal, 1991) in a study which used relatively small amounts of the amine. The ability of amantadine and related compounds to stabilise or destabilise phospholipid bilayers has also been extensively investigated. Cheetam and Epand (1987) concluded from NMR studies that amantadine perturbs the organisation and increases the fluidity of bilayers. This present neutron study, using a much lower drug:lipid molar ratio, does not indicate any such perturbation but it may be that this anomaly reflects the different drug concentrations used in such studies.

Another variable involves the lipid type used. The work reported here employed DOPC which has a large headgroup and two unsaturated chains giving the phospholipid a quasi-hourglass shape, creating an area of increased steric freedom in the neck region when the lipids are formed into a bilayer. The amantadine may be accomodated within such an area, fitting in between the phospholipid molecules. These data, which indicate that the cyclic carbon component of amantadine orientates on the hydrophobic side of the phospholipid headgroup, support this model. This would suggest

that the effects of amantadine upon bilayer structure and stability are likely to be complex and to be dependant upon intrinsic and environmental factors.

X-ray work (carried out by A. Cudmore) shows that the bilayer repeat distance was reduced by up to 2.5Å at low humidities (Duff *et al.*, 1993). A similar effect is produced by the addition of 1,2-dioleoyl-*sn*-glycero-3-phosphoethanolamine (DOPE) (Bradshaw *et al.*, 1989) to DOPC, where the smaller PE headgroup allows the choline moiety of DOPC to lie in a more perpendicular orientation and therefore closer to the plane of the bilayer surface (Dr J.P. Bradshaw, Biochemistry Department, University of Edinburgh, U.K.; personal communication). Amantadine may have a similar effect on DOPC. Unfortunately, the relatively low contrast between the PC headgroup and water makes it impossible to determine the headgroup conformation with the present data. However, this also means that any drug-induced changes in headgroup conformation will not have an adverse effect on the profile subtractions. Future neutron work using specifically deuterated phospholipid headgroups may be able to resolve this question.

The finding reported here that uncharged, amantadine FB has the ability to penetrate more easily into the bilayer is supported by diffusion data performed on other similar compounds (Miller and Lenard, 1981). This phenomenon could be related to the zwitterionic nature of DOPC, the lipid chosen for our study. Further work could investigate the possible relationship between the lipid composition of the bilayer and the nature of its interaction with

amantadine. For example, including a proportion of negatively-charged lipid may induce major changes (Kim, *et al.*, 1991) particularly with the charged amantadine HCl.

3.6.1 Introduction to M2 work

Using the same basic techniques employed above to locate amantadine, the study presented in the rest of this chapter determined the orientation of the M2 peptide (using deuterated and undeuterated moieties, Section 2.7) in DOPC multilayers. In addition, interactions with deuterated amantadine FB were investigated.

From the CD results, it appears obvious that the M2 transmembrane domain must cross the liposomal bilayer. However, it *could* be argued that the peptide may orientate in an α-helical conformation adsorbed onto the surface of the vesicle and that therefore, if this situation holds, it is not transmembraneous. This diffraction work, in producing neutron scattering profiles across the phospholipid bilayer, will clarify this point. In addition, by using the same methods used to locate amantadine, namely, scattering differences and a variation of the isomorphous derivative technique, the relative position of amantadine to the M2 peptide will be identified. Also, the use of amantadine-resistant mutant sequences will show how an amino acid substitution effects the amantadine population with regard to the M2.

3.6.2 Materials

DOPC was purchased from Sigma Chemical Company. Deuterated amantadine FB was obtained from Dr M R. Alecio of the Shell Research Centre. Influenza A M2 peptides were synthesised at the MRC Cellular Immunology Unit (see Section 2.7). Peptides with sequences displayed in Figure 3.7 were used.

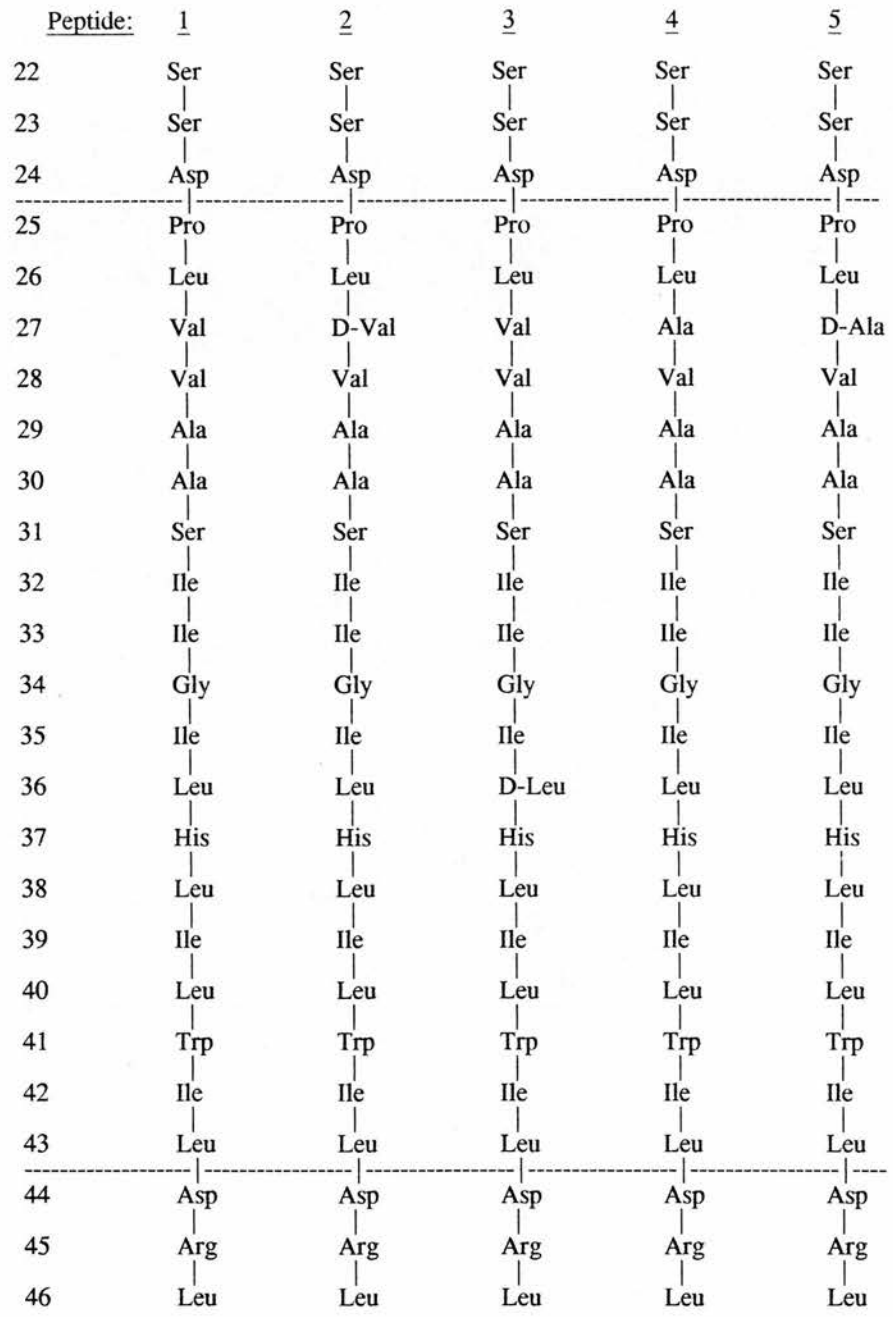

(Peptide 1 is wild-type with 2 and 3 being the identical sequence but labelled on, respectively, amino acids 27 and 36. Peptide 4 is amantadine-resistant with 5 being the identical sequence but labelled on amino acid 27. The amino acids between the dotted lines are thought to be within the membrane.)

Figure 3.7 Recipe sheet of five peptides - amino acid abbreviations described in Abbreviations. See Section 3.6.2 for details.

Sequence 1 is wild-type with 2 and 3 having the same primary structure but being labelled with deuterated amino acids (Section 3.2) at residues 27 and 36 respectively. The valine is labelled with deuterium instead of hydrogen at each methyl group and at its other non peptide-bond hydrogens giving it 8 deuterons. The leucine is labelled in an similar manner giving it 10 deuterons. Sequence 4 represents an amantadine-resistant mutant with residue 27 being substituted by an alanine (Hay *et al.*, 1985). In sequence 5 this amino acid is deuterated at its hydrogens (4 deuterons). It was sequence 1 that was used exclusively in Chapters 2 and 4.

3.6.3 Sample preparation

Sample preparation was as described in Section 3.5.3 for the amantadine neutron experiments. The M2 peptides and amantadine FB were added at, respectively, 1% and 2% (molar ratio with respect to the lipid). Deuterated amantadine FB was used in this study since the much lower concentration, in respect to Section 3.5, dictated that greater contrast was necessary.

3.6.4 Neutron data analysis - Brookhaven

The ILL data is partially prepared for subsequent analysis by the in-house software, however, at Brookhaven (where data discussed in this section were collected), the individual diffraction peaks must be manually integrated together and subtracted from the background scatter. Although this means more time must be spent preparing the Brookhaven data for subsequent analysis it also means

that new, more accurate methods of treating the data may be introduced at this early stage.

Initially, the data was collected in small, discrete packets across the x and y-axes of the detector. The first step in data analysis was to summate these packets of information into a coherent set of data. This involved calculating where each peak lay (this can also be observed) and selecting which data correspond with what peak. This may be termed an x,y-axes integration and was carried out as follows.

The information, which is in the form of a three-dimensional detector pattern, was collapsed onto a two-dimensional spectrum. This spectrum consisted of a graphic representation of the diffracted intensities where the x-axis represented scattering angle and the y-axis represented intensity. The areas of Bragg scattering appeared as discrete peaks.

These peaks were defined from the background and the area under them measured. A commercial program, Sigmaplot (Jandel Scientific, Corte Madera, California, U.S.A.), is available that is capable of achieving this. The background was calculated by base-line fitting and the area under each peak measured by fitting Gaussian curves to the spectrum. When a best-fit was achieved, the area under the Gaussian was recorded.

A complete scan of the sample across the Bragg plane was built-up by adding together, in the x-axis, the collected peaks. In practice, this was accomplished by recording the diffraction peaks only, ie. by placing the sample only where scattering was expected ($2\Theta_B$). However, it is possible that some peak intensity may be missed on either side of the peak due to slight angular orientation

errors regarding the sample slide itself (Θ) or by limiting the scan too severely. These missing data were corrected for by assuming, at first, that all nineteen data files (the small discrete packets mentioned earlier) representing each peak were present. Then it became a simple matter to assign the area under the previously fitted Gaussian an arbitrary value of 100%. The programme then calculated the percentage of the theoretical peak represented by the actual collected nineteen files. If this result (z) was less than 100%, then the observed intensity was scaled-up by 100 / z.

The d repeat was calculated for each data set by measuring the distances between the peaks, the sample to detector distance and then applying the Bragg equation (the wavelength was already known). Intensity files were created which contained all the data necessary for future analysis, ie. the order number (one through four in these data), its corresponding intensity and the d repeat.

The next stage involved creation of amplitude files from the intensity data. The intensity data was corrected and then square-rooted to amplitudes.

Corrections : The corrections described in Section 3.5.4 were applied. In addition, an acceptance angle factor was included because on H3B the beam is narrower than the sample, in contrast to the ILL where it is wider.

Acceptance angle. The area of specimen sampled by the beam is dependent upon the relative angle of the slide to the beam. If the slide presents a very low angle (Θ_B) to the incident beam, the area illuminated represents most of the sample. At 90° the area of sample illuminated is the cross-sectional area of the beam itself.

This means that the diffraction peaks recorded for the lower orders will be correspondingly higher than they should be. As long as the neutron beam is narrower than the maximum projected width of the sample slide and the neutron flux is constant across the width of the beam, the angular correction factor, takes the form -

$$C_{Ang(n)} = \sin\Theta_n \qquad 3.15$$

Phasing : The Brookhaven data were phased in a novel manner. Each sample was run at four different D_2O concentrations (0, 33, 66 and 100%). It may be deduced that, therefore, the scattering density of the region between the bilayers (representing the H_2O or D_2O) will progressively increase with increasing D_2O concentration. Even order reflections will increase in amplitude whilst odd orders will decrease. [NB. However, if the water layers peak at $\pm$ d/2, rather than at the origin, the odd numbered orders will behave in the opposite manner - a shift in the origin of d/2 is equivalent to changing the signs of the odd orders.] This phasing method is shown in Figure 3.8. Such a method is possible with 0 and 100% D_2O data points but the use of only two points does not produce a straight line which inspires confidence.

Subsequent to this four-point method, a variation on the isomorphous replacement technique was employed where the peaks corresponding to amantadine were used as end-points in Fourier subtractions and phases were assigned in order to obtain such profiles. Excellent agreement was achieved between these complementary phasing approaches.

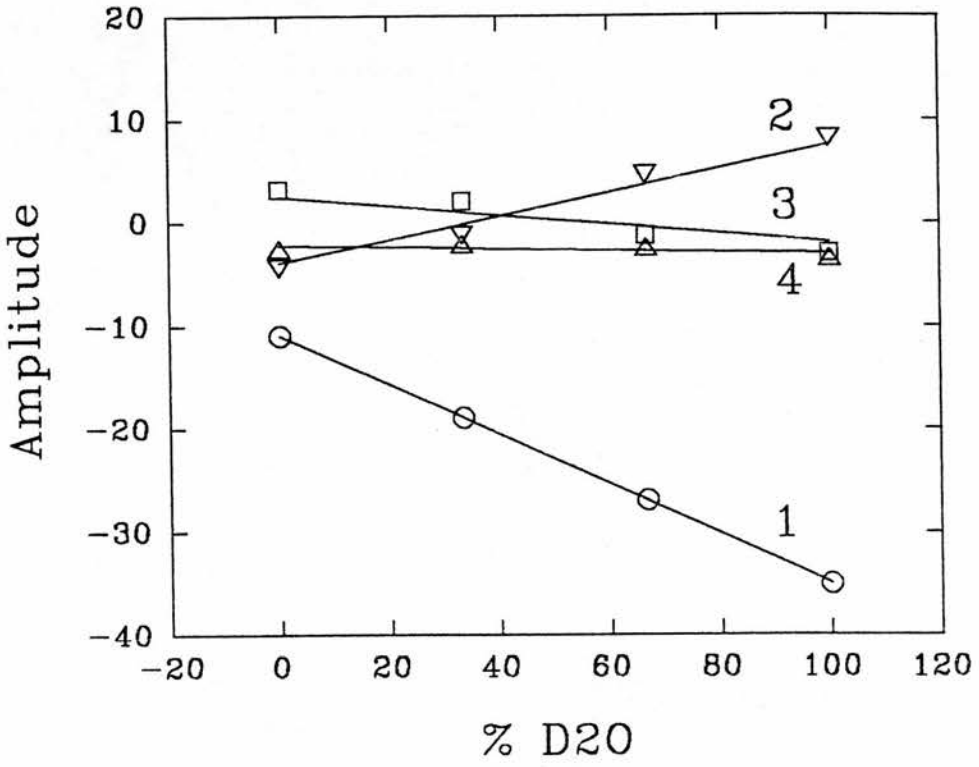

Figure 3.8 An example of the D_2O phasing method. The amplitudes change linearly with the % of D_2O - with positive slopes for even orders and negative slopes for odd orders (see Section 3.6.4). The numbers refer to order number (n).

3.6.5 Results

Table 3.2 gives the corrected, scaled neutron diffraction structure factors for all samples. It should be noted that structure factors were obtained for each sample at 33 and 66% D_2O, in addition to the results shown at 0 and 100%. However, as these data were used only in assignment of phase and **not** in subsequent Fourier subtractions they are omitted in the interests of clarity and brevity. It was the 0% data that was used in the subtractions. 100% data are presented in Table 3.2 when used in subtractions to produce water peaks. Difference neutron scattering profiles are shown in Figures 3.9 through 3.13. These profiles were calculated as in Section 3.5.5. Also shown are Gaussian distributions fitted to specific profiles in order to provide an accurate reconstruction free of termination error (Section 3.5.5).

The mosaic spread of the DOPC bilayers ranged from 0.4° to 0.6°. This was not significantly changed upon the addition of either peptide or drug.

3.6.6 Discussion

DOPC

Figure 3.9 displays the DOPC phospholipid bilayer profiles with the water component occupying the outer region of the graphs (such an orientation is followed in all subsequent difference profiles - except for water profiles). Profile (a) is the DOPC result obtained in Section 3.5 (ILL, $20^{\circ}C$) and (b) is that calculated here (Brookhaven, $37^{\circ}C$). The profiles are similar, with (b) showing

DOPC	M2	D-M2 DVal27	D-M2 DLeu36	M2 Mutant	D-M2 Mutant	D-Aman F.Base	Structure Factors 0% D_2O	100% D_2O
20							1)-10.93 2) -3.87 3) 2.51 4) -2.22	-22.04 5.24 -1.88 -1.94
20	0.7						1) -5.02 2) -3.60 3) 2.82 4) 0.34	-32.50 4.63 0.16 2.61
20		0.7					1) -2.65 2) -3.21 3) 1.98 4) 0.59	
20			0.7				1) -4.91 2) -3.35 3) 2.94 4) 0.81	
20	0.7					0.1	1) -5.94 2) -2.03 3) 1.97 4) -2.35	
20						0.1	1) -5.24 2) -3.39 3) 2.69 4) -1.24	
20				0.7			1) -4.56 2) -1.47 3) 2.14 4) 0.03	-32.04 6.75 -0.52 2.30
20					0.7		1) -1.52 2) -1.13 3) 2.26 4) 0.50	
20				0.7		0.1	1) -6.11 2) 0.33 3) 1.33 4) 2.19	

Table 3.2 Relative neutron structure factors of lamellar arrays of various mixes of DOPC, five different M2 peptides (1% molar) and amantadine (2% molar) - 98% rh, 37°C.

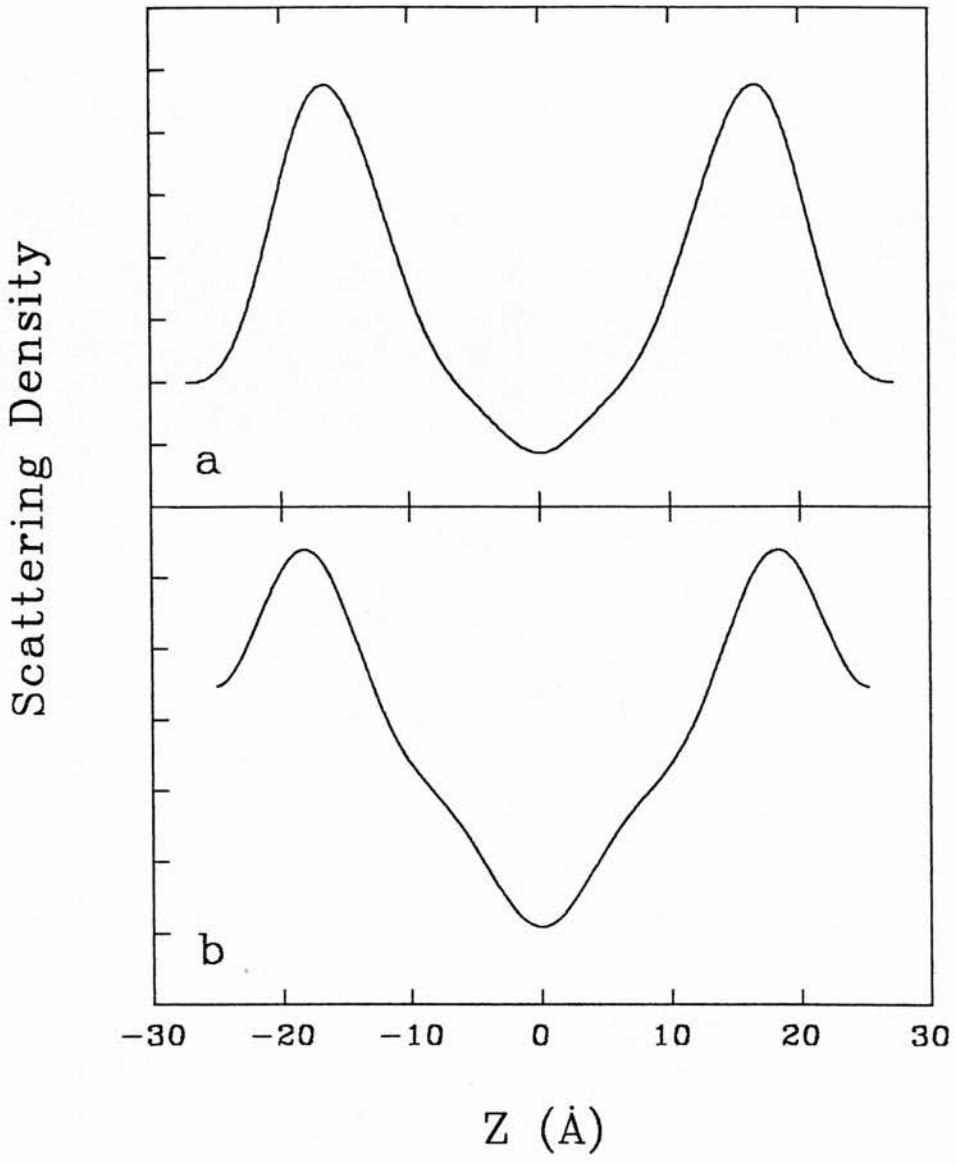

Figure 3.9 Reconstructed trans-bilayer neutron scattering profiles. (a) represents pure DOPC, 20°C (from Section 3.5) and (b) represents pure DOPC, 37°C. Both at 100% rh. (No vertical scale is shown as (a) is scaled absolutely and (b) is scaled relatively [two different data sets]. Therefore, comparisons between the two may only be made in the shapes of the profiles and not the scattering lengths.)

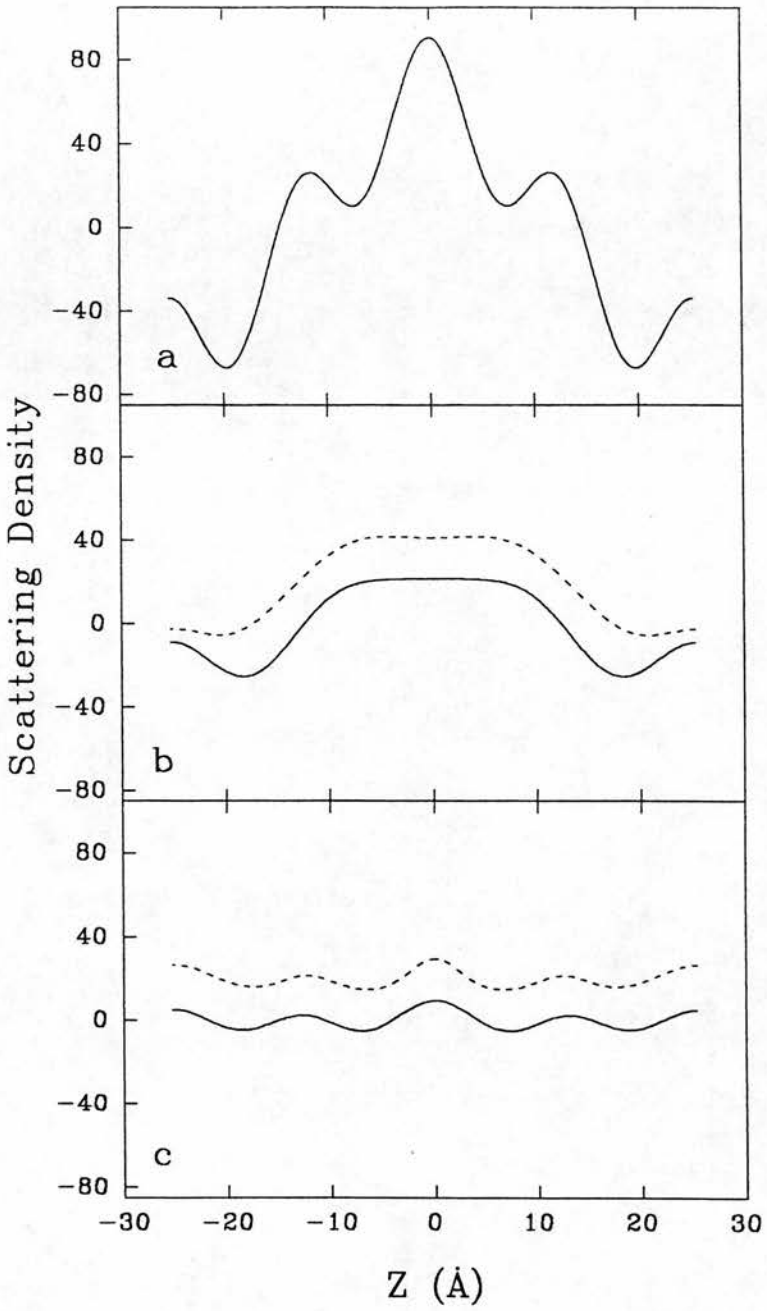

Figure 3.10 Difference neutron density scattering profiles. (a) represents the distribution of native M2 peptide, (b) and (c) represent, respectively, the d27 and d36 labels. Gaussian distributions are shown fitted to (b) and (c).

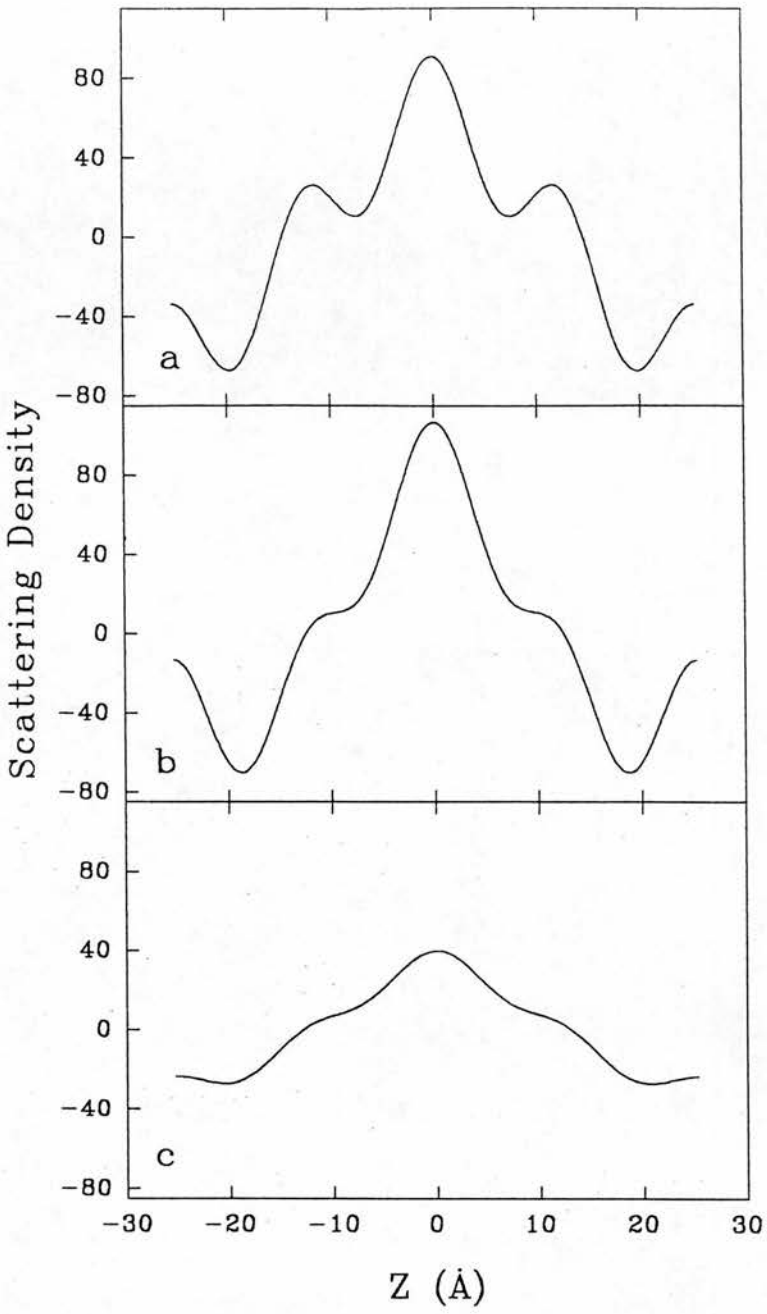

Figure 3.11 Difference neutron density scattering profiles. (a) represents the distribution of native M2 peptide, (b) and (c) represent, respectively, the distribution of M2 mutant and the label position on deuterated M2 mutant.

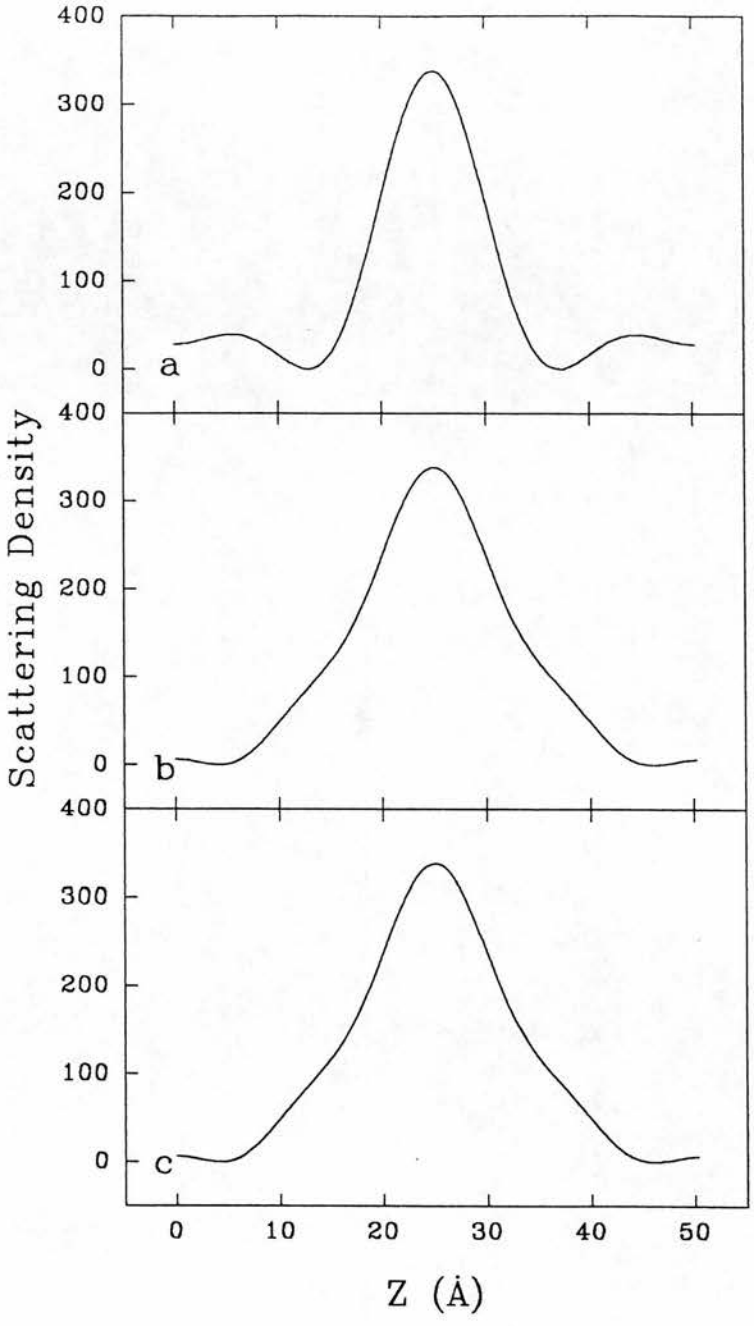

Figure 3.12 Difference neutron density scattering profiles showing the distribution of water associated with bilayers containing (a) DOPC only (b) DOPC plus 1% native M2 and (c) DOPC plus 1% mutant M2.

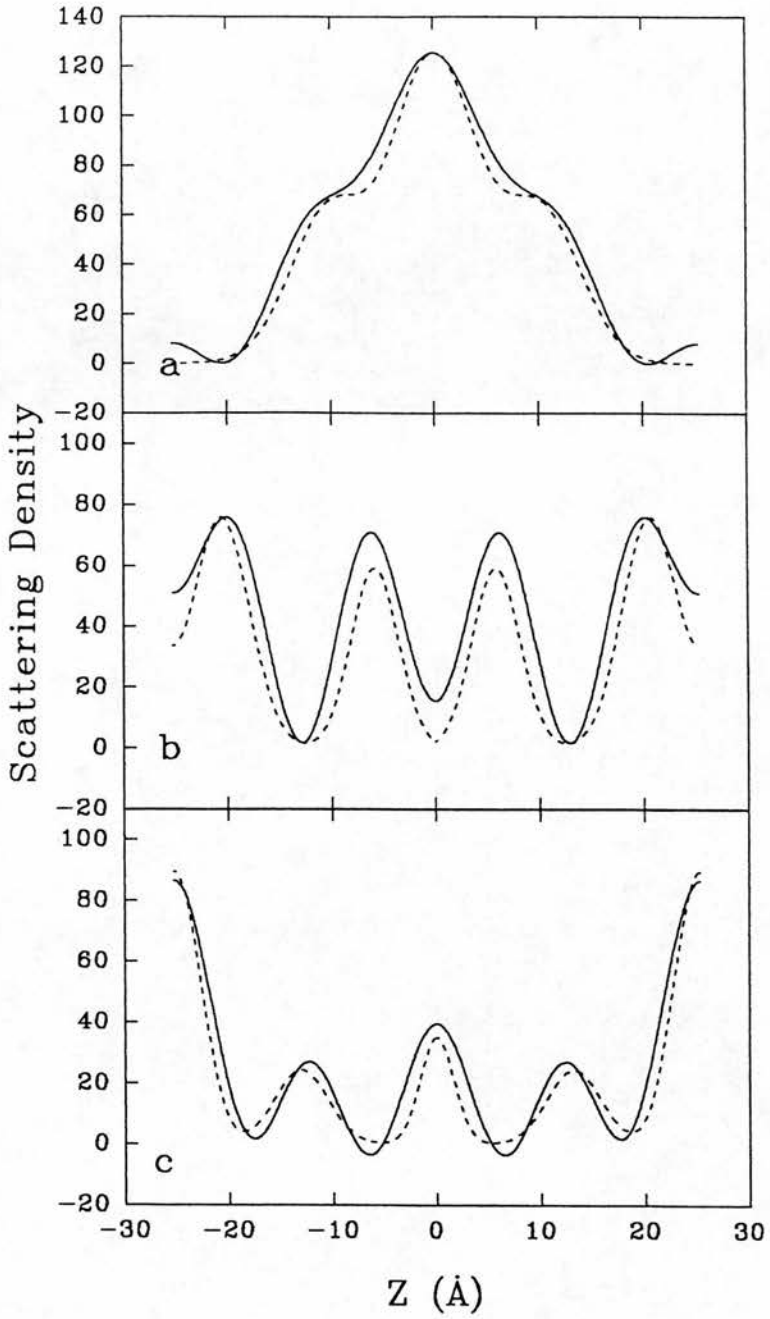

Figure 3.13 Difference neutron density scattering profiles. (a) represents the distribution of amantadine when associated with DOPC, (b) and (c) represent, respectively, amantadine distributions associated with DOPC plus 1% native M2 and DOPC plus 1% mutant M2. Gaussian distributions are shown fitted to all three.

more detail in the fatty acid tail region. Maximum neutron scattering corresponds to the fatty acyl ester bond positions (Franks and Lieb, 1981; Section 3.5.6). Profile (b) was used in all subsequent subtractions.

M2 peptide

Figure 3.10 (a) represents the native, undeuterated M2 peptide population. Almost all of the scattering density can be seen to be located within the bilayer region indicating that the proposed transmembrane domain of influenza A M2 protein does indeed span the membrane. The small peak in the water region may indicate a population of water-soluble M2.

Figure 3.10 (b) shows the position of the d27 label (produced by subtracting the native, undeuterated peptide from the native, deuterated (d27) peptide). The mass of label lies predominantly in the bilayer, however, if Gaussian fitting is applied, it may be seen that two separate populations may be defined - one peaking 8 Å each side of the centre of the bilayer (the two parts of this population are summed in the Fourier profile making it appear to peak in the *centre* of the bilayer) and the other, much smaller one peaking in the middle of the water region (24 Å from the bilayer centre). This result corresponds to the deuterated valine position in the peptide (peptide insertion into the bilayer will occur in both possible orientations perpendicular to the plane of the lipids) and also with some label appearing in the water. The relative amounts of label represented by each population may be calculated by simply measuring the Gaussian widths at half height, multiplying this by their heights, and then dividing one by the other. Such a

calculation shows that approximately 9% of the total label may be found in the water. This relatively low amount may be explained if some of the peptide is excluded from the lipid phase, perhaps because the concentration used is too high, or if an equilibrium is set-up where M2 moves into and out of the bilayer (but at any one time it is ten times more likely to find peptide associated with the lipid [diffraction is a time-averaged technique]).

The d36 profile, Figure 3.10 (c), includes a large peak in the centre of the bilayer, where it would be expected (deuterated leucine). However, two other substantial peaks may be observed. Gaussian fitting confirmed that this result represented a three-component population. Such a phenomenon cannot be explained and it may be that one or more of the other six leucines were deuterated in error. Since all of these peptides are extremely hydrophobic, many difficulties were reported in their synthesis and purification - the d36 peptide was the first to be prepared.

In summary, it may be said that the native M2 peptide was observed to be transbilayer and that the d27 label could be isolated to a single, discrete population identifiable within this region.

Figure 3.11 displays similar difference profiles but with the mutant M2 peptide instead of the native (the native, undeuterated M2 is shown again (a) for comparison). The mutant sequence (b) can be seen to be transbilayer. The profiles differ slightly in that, with the mutant, the hump observed approximately 12 Å from the centre of the bilayer is smaller. This area is where the valine to alanine substitution was engineered.

Profile (c), which represents a deuterated mutant M2 minus mutant M2 subtraction, can be seen to be very similar to the non-

deuterated M2 profile. It proved impossible to locate a discrete mass of label in the mutant, labelled peptide (as was done with the native d27 data). This may be an anticipated result of using small amounts of label to ensure isomorphism. The labelled amino acid in the mutant sequence was alanine, d4. The amount of deuterium incorporated into the deuterated, mutant peptide was therefore half that incorporated into either of the other two labelled sequences. It would appear that such levels of labelling are not enough and that the resulting profile (c) simply displays the tiny difference between the M2 mutant concentrations in the two samples due to experimental error in preparation.

In summary, the mutant M2 is also transbilayer and the two profiles, native and mutant, are extremely similar but with, importantly, slight observable differences in the region of the amino acid substitution.

Additional information on the nature of the peptides was obtained by subtracting the DOPC/M2 data collected at 0% D_2O from the DOPC/M2 data collected at 100% D_2O. The resultant difference profile is the water peak [Figure 3.12 (b) and (c)] associated with the M2 peptides. (Note that the water is shown in the centre of the profile and not at the periphery as in the other results.) This was compared with the profile obtained by subtracting the DOPC-only data collected at 0% D_2O from the DOPC-only data collected at 100% D_2O. This subtraction also results in a water peak but one that is produced in association with phospholipid bilayers alone [Figure 3.12 (a)]. Profiles (b) and (c) may be seen to be much wider, graphically demonstrating that, in bilayers incorporating M2, water is free to penetrate at least 12 Å into the

bilayer at both sides of the lipid face. This may be compared with about 5 Å in lipid-only systems. At this resolution, it may be seen that the M2 peptides form an *almost* continuous channel across the bilayer. Although the peptides used in these studies were monomeric, it must be assumed that some form of equilibrium functions in which, for example, tetrameric channels are being continuously formed and dissociated, thereby allowing the inclusion of solvent (see Chapter 4).

Amantadine and M2 peptide

Figure 3.13 (a) shows the amantadine FB distribution in lipid-only systems. This can be described by two Gaussians; the first and larger of the two centred on the middle of the bilayer, and the second centred 10 Å on either side of the first, ie. halfway down the fatty acid moieties. Such a result is in broad agreement with that obtained in Section 3.5.6, where amantadine FB was reported to be located deep in the bilayer. However, Figure 3.13 (a) shows that more of the amantadine FB has penetrated into the centre of the lipid environment than was observed in the previous study. It is thought that this relative distribution dichotomy is probably due to experimental differences in amantadine FB concentration and temperature between the two studies. [NB. The ILL data were gathered on 5% (mol) amantadine FB and at a temperature of 20°C, whereas the Brookhaven data were gathered on 2% (mol) amantadine FB and at a temperature of 37°C.]

The difference distributions of amantadine associated with native [Figure 3.13 (b)] and mutant M2 (c) are shown. It is immediately apparent that both of these profiles are quite different

from each other and, indeed, quite different from the amantadine distribution in the lipid-only system (a).

When native M2 is present (b), the population profile of drug appears as two discrete peaks in contrast to that described in (a). Gaussian fitting to difference profile (b) indicates that these peaks are centred 6 Å and 20.5 Å from the middle of the bilayer - the amantadine now appears to adopt a much more specific orientation. Recent molecular modelling studies, which have examined possible tetrameric associations of the M2 transmembrane domain and its interactions with amantadine (Sansom and Kerr, 1993), have identified a minimum in the vicinity of the Ser_{31} oxygen atoms when energy interactions were evaluated as amantadine was moved along the length of the channel. This was shown to derive from a favourable electrostatic interaction between the cationic amine group and the ring of Ser_{31} O atoms. In addition, van der Waals contacts were observed between the Val_{27} side-chains and the amantadine ring. It was shown that the ring fits into a pocket formed by the Val_{27} side-chains (the M2 was modelled as a tetramer) and at the same time the protonated amine group forms favourable electrostatic interactions with the Ser_{31} oxygens. (It was concluded that the combination of a steric cut-off at Ile_{42} and the favourable interaction at Val_{27}/Ser_{31} provided a molecular explanation for block of M2 channels by amantadine.)

This thesis has already indicated that Val_{27} (the d27 label data) may be found 8 Å from the centre of the bilayer (see above). It can be calculated that the Ser_{31} lies approximately 6 Å from this (one amino acid in an α-helix represents a translation of 1.5 Å). If the amantadine molecule is placed in the position described in the

reported modelling study, between the Val and Ser, then its spatial centre will occur at approximately 5 Å from the middle of the bilayer (ie. midway between the two amino acids). As reported at the start of the previous paragraph, amantadine was located 6 Å from the centre of the bilayer. Interestingly, because the mass of deuterons occur on the fused ring (the opposite end from the amine head), the scattering centre of deuterated amantadine does not correspond with the spatial centre. Indeed, the *centre of scattering density* of the molecule is displaced towards the adamantane-ring, thereby off-setting the centre of scattering density by approximately 1 Å in the direction of the Val_{27} - exactly as observed in these neutron diffraction experiments. Therefore, remarkably, all detectable amantadine in the bilayer appears to be in the position, with regards native M2, that Sansom and Kerr (1993) have proposed as the site of channel blockade.

No amantadine was observed in the water region in the lipid-only data, however, considerable amounts appear in this area when native M2 is present (the 20.5 Å peak). The drug may be interacting at the lipid/water interface (as was observed in Section 3.5) or it is possible that it may be in contact with the other amino-terminal serines that project out into the water (Figure 3.7). NB. Amantadine analogues have been shown to interact with serines in the nicotinic acetylcholine receptor (see Section 1.4).

In contrast to the above, when mutant M2 (Val_{27} becomes Ala_{27}) is considered [Figure 3.13 (c)], it may be seen that, instead of discrete populations of amantadine as in (b), the drug distribution is much more generally dispersed across the bilayer with a maximum at the centre of the water layer - perhaps again interacting

with the terminal serines. Indeed, it now requires three Gaussians to describe this new distribution. This result may be interpreted as demonstrating that the mutation results in a more general membrane flow-through of drug.

It is important with diffraction data not to over-interpret scattering profiles, especially if fewer orders have been used, however, regarding the above results, it is tempting to postulate that here we are observing the mechanism of action of amantadine-sensitivity and resistance in influenza A.

CHAPTER 4 ELECTROPHYSIOLOGICAL STUDIES OF INFLUENZA A M2 TRANSMEMBRANE DOMAIN AND THE EFFECTS OF AMANTADINE

4. Electrophysiological studies of influenza A M2 transmembrane domain and the effects of amantadine

4.1 General introduction

Nearly all cells contain macromolecular pores embedded in their cellular plasma membranes. These include ionic channels, carriers and pumps. Their functions include the transport of necessary ionised substrates and the transmission of signals. Within multicellular organisms, ion pores produce the sparks of electrical activity that are recognised as the essence of life itself, they control the muscular movements of organisms and, in sensory organs, the pores translate physical or chemical stimuli into electrical signals for the nervous system. Even cells not directly connected to the nervous system, such as those in the blood, the immune system, the liver and other organs, use ion pores for both transport and transmission processes.

During the twentieth century, major cellular roles have been discovered for most of the inorganic ions endogenous to the body fluids. None are passively distributed across the cell membrane. Each has been assigned, by evolution, at least one special regulatory, transport or metabolic task. And, importantly, each ion has at least one transport pore.

Since the 1950's biologists have been able to study the electric currents arising from these ions fluxes at a macroscopic level. Only since the 1970's, however, could they examine the individual ion pores themselves. This advance was due to the development of a sensitive, electrophysiological technique known as patch-clamping.

This initial technique has been developed and refined over the years and has produced a family of related electrophysiological processes. One such development involves the reconstitution of protein into planar lipid bilayers and the recording of single-channel currents.

Over the last fifteen years such techniques have helped in the study of, for example, the effects of acetylcholine on sodium channels, how K^+ and Ca^{2+} channels are controlled, signalling mechanisms at a cellular level and the role of pore-formers in intracellular signalling. As the number of channels that have been isolated and defined grows, it would appear that such electrophysiological techniques will help reveal the major role such pores play in the control of almost all cellular processes.

4.2 Electrophysiological theory

Introduction

Ionic channels may be regarded as excitable molecules. They are specifically responsive to some stimulus: a membrane potential change; certain ligands, small molecules or ions; mechanical deformation, and so on. Once activated, the channel response, called gating, is apparently a simple opening, or closing, of the pore. The open pore has the important property of selective permeability, allowing some restricted group of small ions to flow passively down their electrochemical gradients at a very high rate - usually greater than a million ions per second. This high throughput actually aids in defining channels as opposed to other pore-forming transporters that, in some manner, *actively* cross the

membrane. In addition, channels may be observed to restrict ion flow to downhill fluxes and are not coupled to any energy input systems.

Physical definitions

Much of what has been discovered about ionic channels has been deduced from electrical measurements. In order to study the results of electrical experiments, some essential principles must be observed. (Detailed reviews on electrophysiological theory appear in Sakmann and Neher, 1983; Miller, 1986; Stein, 1986; Stein, 1990; Hille, 1992.)

All matter is made up of charged particles. They are normally present in equal numbers, so most bodies are electrically neutral. A mole of hydrogen atoms contains Avogadro's number ($N = 6.02 \times 10^{23}$) of protons and the same number of electrons. Quantity of charge is measured in coulombs (abbreviated C), where the charge of a proton is $e = 1.6 \times 10^{-19}$C. Avogadro's number of elementary charges is called the Faraday constant: $Fc = Ne = 6 \times 10^{23} \times 1.6 \times 10^{-19} \approx 10^5$ C / mol. This is thus the charge on a mole of protons or on a mole of Na^+, K^+, or any other monovalent cation. The charge on a mole of Ca^{2+}, Mg^{2+}, or on other divalents cations is 2 Fc and the charge on a mole of Cl^- ions or other monovalent anions is - Fc.

Electrical phenomena arise whenever charges of opposite sign are separated or can move independently. Net flow of charge is called current and is measured in amperes (abbreviated A), where one ampere corresponds to a steady flow of one coulomb per second. By the convention of Benjamin Franklin, positive current

flows in the direction of movement of positive charge. Hence if positive and negative electrodes are placed in Ringer's solution (physiological saline), Na^+, K^+, and Ca^{2+} ions will start to move toward the negative pole, Cl^- ions will move toward the positive pole, and an electric current is said to flow through the solution from positive to negative pole. Michael Faraday named the positive electrode the anode and the negative the cathode and, in his terminology, anions flow to the anode, cations to the cathode, and current from anode to cathode. The size of the current will be determined by two factors: the potential difference between the electrodes and the electrical conductance of the solution between them. Potential difference is measured in volts (abbreviated V) and is defined as the work needed to move a unit test charge in a frictionless manner from one point to another. To move a coulomb of charge across a 1 V difference requires a joule of work. In common usage the words 'potential', 'voltage', and 'voltage difference' are used interchangeably to mean potential difference, especially when referring to a membrane.

Electrical conductance is a measure of the *ease* of flow of current between two points. The conductance between two electrodes in salt water can be increased by adding more salt or by bringing the electrodes closer together, and it can be decreased by placing a nonconducting obstruction between the electrodes, by moving them farther apart, or by making the solution between them more viscous. Conductance is measured in siemens (abbreviated S and formerly called mho [reciprocal Ohms]) and is defined by Ohm's law in simple conductors -

$$I = gE \qquad 4.1$$

Current (I) equals the product of conductance (g) and voltage difference (E) across the conductor. The reciprocal of conductance (resistance, symbolized R) is measured in ohms (abbreviated Ω). Ohm's law may also be written in terms of resistance -

$$E = IR \qquad 4.2$$

Homogenous conducting materials may be characterized by a bulk property called the resistivity (abbreviated p). It is the resistance measured by two 1 cm^2 electrodes applied to opposite sides of a 1 cm cube of the material and has the dimensions ohm · centimeter (Ω· cm). Resistivity is useful for calculating resistance of arbitrary shapes of materials. For example, for a right cylindrical block of length l and cross-sectional area A with electrodes of area A on the end faces, the resistance is -

$$R = pl/A \qquad 4.3$$

Resistivity decreases as salts are added to a solution. Consider the following examples at 20°C: frog Ringers solution 80 Ω · cm, mammalian saline 60 Ω · cm, and sea water 20 Ω · cm. Indeed, in sufficiently dilute solutions, each added ion gives a known increment to the overall solution conductance, and the resistivity of electrolyte solutions can be predicted by calculations from tables of single-ion equivalent conductivities, like those in Robinson and Stokes (1965). In saline solutions the resistivity of pure phospholipid bilayers is as

high as 10^{15} $\Omega \cdot$ cm, because although the physiological ions can move in lipid, they far prefer an aqueous environment over a hydrophobic one. The electrical conductivity of biological membranes comes not from the lipid, but from the ionic channels embedded in the lipid.

To summarise what has been discussed so far, when one volt is applied across a 1Ω resistor or 1 S conductor, a current of one ampere flows; every second, 1/Fc moles of charge (10.4 μmol) move and one joule of heat is produced. Ohm's law plays a central role in membrane biophysics because each ionic channel is an elementary conductor spanning the insulating lipid membrane. The total electrical conductance of a membrane is the sum of all these elementary conductances in parallel. It is a measure of how many ionic channels are open, how many ions are available to go through them and how easily the ions pass.

In addition to containing many conducting channels, the lipid bilayer of biological membranes separates internal and external conducting solutions by an extremely thin insulating layer. Such a narrow gap between two conductors forms, of necessity, a significant electrical capacitor.

To create a potential difference between objects requires only a separation of charge. Capacitance (C) is a measure of how much charge (Q) needs to be transferred from one conductor to another to set up a given potential and is defined by -

$$C = Q/E \qquad 4.4$$

The unit of capacitance is the farad (abbreviated F). A 1 F capacitor will be charged to 1 V when +1.0 C of charge is on one conductor and -1.0 C on the other. In an ideal capacitor the passage of current simply removes charge from one conductor and stores it on another in a fully reversible manner and without evolving heat. The rate of change of the potential under a current I_C is obtained by differentiating Equation 4.4 -

$$dE/dt = I_C/C \qquad 4.5$$

The capacity to store charges arises from their mutual attraction across the gap and by the polarization they develop in the insulating medium. The capacitance depends on the dielectric constant of that medium and on the geometry of the conductors. In a simple capacitor formed by two parallel plates of area A and separated by an insulator of dielectric constant e and thickness D, the capacitance is -

$$C = e\epsilon_0 A/D \qquad 4.6$$

where ϵ_0, called the polarisability of free space, is 8.85×10^{-12} $CV^{-1}m^{-1}$. Cell membranes are parallel-plate capacitors with specific capacitances near 1.0 $\mu F/cm^2$. According to Equation 4.6, this means that the thickness D of the insulating bilayer is only 23 Å (2.3 nm), assuming that the dielectric constant of hydrocarbon chains is 2.1. Hence the high electrical capacitance of biological membranes is a direct consequence of their molecular dimensions.

Working formulae

It may be intuitively seen that, in channel systems, the ions on both sides of the membrane will seek equilibrium. However, if the ionic concentration on one side of the barrier is due to two or more populations of counterions and the channel is permeable to only one of these types, then an interesting phenomenon may be observed. The diffusional forces causing net diffusion of the permeant ion are countered by a growing electrical force tending to oppose the ions flow. The potential builds up until it finally reaches an equilibrium value, E_K, where the electrical force balances the diffusional force and the system no longer changes. Equilibrium potentials are important in describing biological membrane potentials. If a mole of an arbitrary ion S with charge Z_S is considered then -

$$E_S = E_1 - E_2 = RT/Z_S Fc \ \ln [S]_2/[S]_1 \qquad 4.7$$

where E_S is the membrane potential difference, R is the gas constant, T is the temperature in Kelvin, and Fc is Faraday's constant. Side 1 is usually defined as being intracellular and side 2 as being extracellular. This equation is known as the Nernst equation (Nernst, 1888) and it describes how ionic equilibrium potentials vary linearly with the absolute temperature and logarithmically with the ionic concentration ratio. Equilibrium potentials change sign if the charge of the ion is reversed or if the direction of the gradient is reversed, and they fall to zero when there is no gradient.

So far, the membrane has been discussed as a capacitor and the channel as a conductor. However, if Ohm's law is tested with this

capacitor/conductor system which includes an ionic concentration gradient across the membrane, then it may be seen that current in the pores goes to zero at E_S and not at 0 mV. This is because of the effect of the concentration gradient. The current/voltage law becomes -

$$I_S = g_S (E-E_S) \qquad 4.8$$

where I is current, g is the conductance and the electromotive force is E_S and, therefore, the net driving force on the S ion is $E-E_S$ and not E. To a first approximation this linear law works, but many pores are known to have nonlinear current/voltage relations when open.

Simple current/voltage measurements can be used to gain much information on ionic channels. With reference to a simplified system (Figure 4.1) it can be seen that if a positive potential is applied to electrode (1) then the positive ions will, if possible, cross the membrane from A to B. As the potential difference across the membrane is increased then the current, or number of ions flowing, will also increase. If the polarity of the electrodes is reversed then the current flow will also reverse. This may be graphed on an I/E, or, as they are more commonly termed, I/V plot (Figure 4.2, red line). When the plot passes through the origin it denotes that the channels are nonselective or that there is no effective ionic gradient. If the slope of the I/V plot decreases (Figure 4.2, blue line), then the equivalent conductance, and hence the number of open channels, differs correspondingly. Thus conductance gives a useful measure of how many channels are open in an area of membrane.

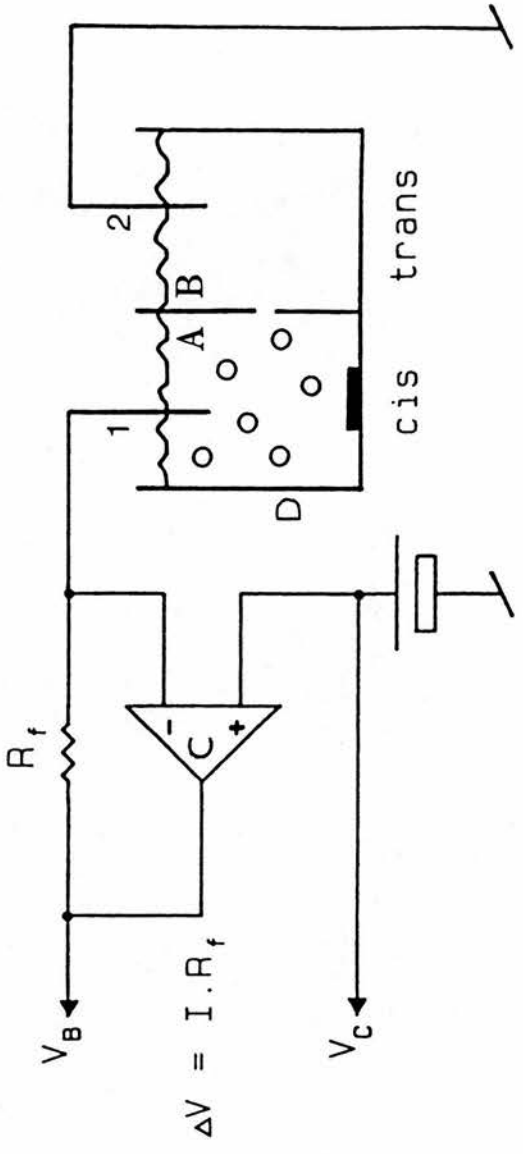

Figure 4.1 Electrophysiological apparatus (see text for explanation).

If the I/V plot has the same slope but a different zero current potential (Figure 4.2, green line), then the channel has equal conductance but a different electromotive force. This indicates that the channel is either different from the other channel described above, with a different ion selectivity, or, that it is the same channel but now it is bathed on both sides with different concentrations of its permeant ion. Therefore, zero current potentials are useful in studies of selectivity.

In summary, it may be said that, in a situation where there is only one ion diffusing across a membrane, a transmembrane potential will be set up that, when equilibrium is reached, is a function of the ratio of the concentrations of the diffusing ion at the two sides of the membrane. However, if more than one type of ion is able to diffuse then the ion concentration ratios will not be exactly those given in the Nernst equation (Equation 4.7). This problem is solved by the Goldman-Hodgkin-Katz (GHK) voltage equation (Hodgkin and Katz, 1949), which relates the overall membrane potential to a diffusion potential contributed by each ion, which is determined by the concentration of the diffusing ion at each membrane face and by the permeability of the ion across the bilayer in question. Essentially, each ion tends to develop a membrane potential given by its concentration ratio across the membrane. The extent to which it reaches this potential depends on what fraction of the total amount of charge carried across the membrane is carried in the form of that particular ion, ie., on its permeability and its concentration -

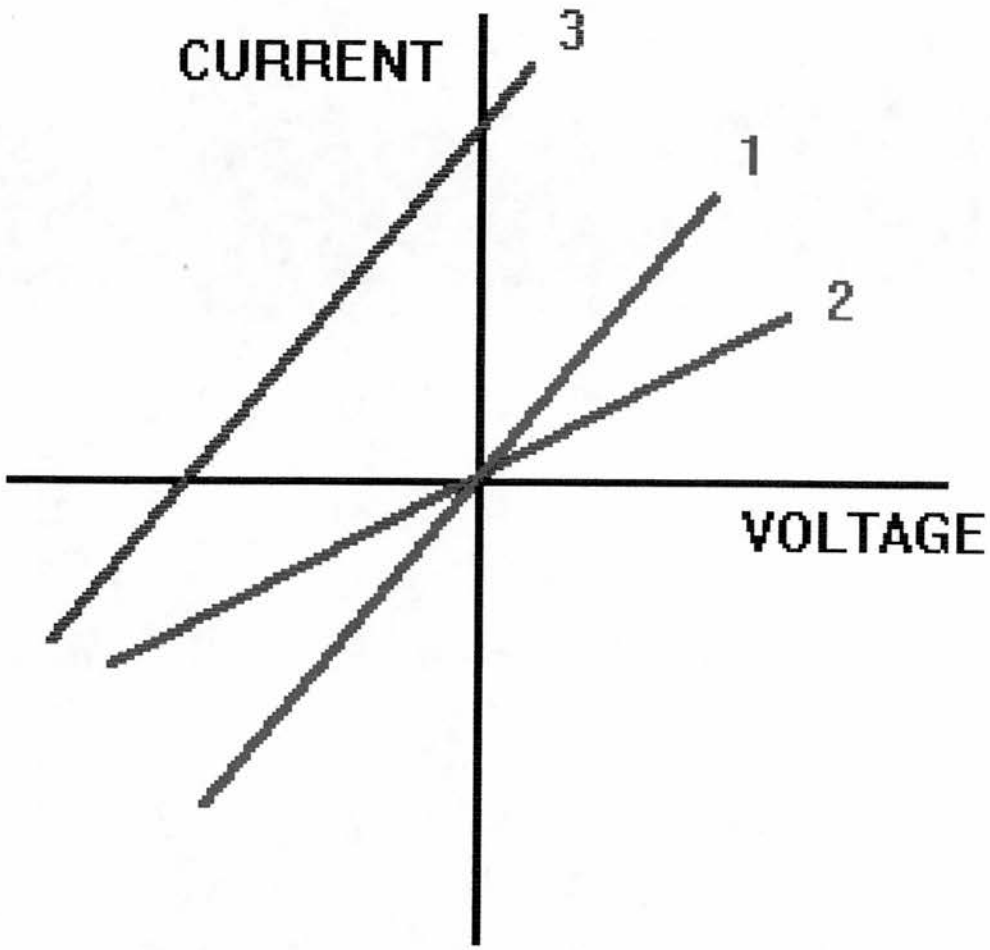

Figure 4.2 Specimen I/V plots. Red line (1) represents double the amount of open channels as the blue line (2). The green line (3) shows a data set with a different zero current potential. See text for full explanation.

$$E = RT / ZFc \ \text{In} \ \frac{\{Px\,[x_{II}] + Py\,[y_{II}] + Pz\,[z_{II}]}{\{Px\,[x_{I}] + Py\,[y_{I}] + Pz\,[z_{I}]} \qquad 4.9$$

where P is the permeability of the ions x, y and z, and [x], [y] and [z] are the concentrations of these ions at sides I and II of the membrane.

To understand this equation (Equation 4.9) consider some special cases: (a) When only one ion can permeate (say, x), P exists for that ion but is zero for all others. Equation 4.9 therefore reduces to the Nernst equation (Equation 4.7). (b) When one ion (say, y) is *overwhelmingly* permeant, all other values of P are insignificant and, once again, Equation 4.7 is recovered. (c) It also follows that an ion that is present at a very low concentration relative to other permeant ions will contribute very little to the potential, although it might well be as permeant as the other ions. The current flow (and it is this parameter that determines the potential) depends on both permeability and the absolute concentration of an ion.

4.3 Experimental hardware

The equipment used in the experiments discussed in this chapter may appear simple in description. However, that is only a superficial impression and, underneath, a great deal of electronic ingenuity is employed, predominantly in order to produce and maintain an extremely low background noise so that the movement of a few elementary charges may be detectable. It is not the aim of this section to describe the experimental hardware in such detail -

further information may be obtained from advanced electrophysiological texts (eg. Hamill *et al.*, 1981; Sakmann and Neher, 1983).

The basic experimental set-up is illustrated in Figure 4.1. The perspex block, D, consists of two chambers, designated *cis* and *trans*. The solution in each chamber is in contact with an electrode. By convention, the *cis* chamber (A) is the side to which the peptide, drug, etc. is added and the *trans* chamber (B) is opposite. The lipid membrane is positioned so that it effectively blocks the gap between these chambers (Section 4.7), and the ion channel under scrutiny must be incorporated into this barrier. Thereafter, the solutions of one or both chambers may be carefully changed by perfusion in order to examine the channel characteristics of the protein.

It may be seen from Figure 4.1 that, for example, when both chambers are filled with solutions of equimolar cationic concentration and a positive voltage is applied to the *cis* microelectrode, if the particular reconstituted ion channel permits, then cations (current) will flow from *cis* to *trans*. From Equation 4.2 it is observed that, if the resistance of the system has not changed, then the potential difference will now decrease. It would therefore prove difficult to characterise any ion channel electrophysiologically if the applied voltage was constantly changing.

However, it is possible with suitable electronic circuitry to hold the membrane potential steady at any given voltage. This is accomplished by connecting the recording electrodes to a device called a feedback amplifier (Figure 4.1, C) which compensates for any potential change sensed by these electrodes by applying a back-

off potential to keep the voltage constant (V_B). This arrangement is known as a voltage-clamp (V_C), and the designated value of V is called the command voltage. By setting different command voltages and measuring the injected current that is required to maintain them, it proves possible to investigate systematically the membrane conductance as a function of the membrane potential. The ions that carry the transmembrane current can be identified by monitoring the effect of changing the concentration of specific ions in the *cis* and *trans* chambers.

The recorded current flow is low-pass filtered to remove high frequency noise, displayed on an oscilloscope and simultaneously recorded onto magnetic tape.

4.4 Introduction to the experimental section

The work described so far in this thesis has concentrated on *structural* studies of the M2 transmembrane domain. Chapter 2 presented CD data concerning the secondary structure of the M2 peptide incorporated into liposomes and Chapter 3 defined the position of both the peptide and amantadine within the bilayer. It is intended that Chapter 4 will detail studies of the *functional* properties of the molecule. Specifically, using reconstitution techniques, native M2 peptide will be incorporated into voltage-clamped planar lipid bilayers and the transmembrane domain will then be examined electrophysiologically in order to determine whether it possesses any proton channel properties.

4.5 Introduction

In 1989 it was proposed that influenza A M2 protein forms a transmembrane channel which is involved in reducing the interior pH of the virus at the uncoating stage and, in addition, that M2 reduces acidification of post-Golgi vesicles involved in the transport of haemagglutinin (HA) during viral assembly (Hay, 1989). The method by which the protein achieves these results was suggested to be by allowing the passage of protons.

The elegant experiments which led to this conclusion, described in Section 1.4, were all, in effect, circumstantial. Although it certainly appeared likely that M2 was a channel, definitive evidence was lacking. Indeed, it was not until two years later that workers reported the presence of the first ion channel to be found in *any* virus - Semliki Forest Virus (Schlegel *et al.*, 1991).

Recently, it has been stated that other viruses possess proteins with sequences analogous to M2 (Section 1.5). There may, therefore, exist a functional similarity too. It is possible that groups of enveloped viruses use similar strategies within their infectivity cycles and this would mean that they could be challenged with broad-based, anti-viral therapies. Therefore, it would appear important, and timely, to determine exactly what M2 may be capable of and how.

In response, this present study, which has been carried out with Dr Richard Ashley, Department of Biochemistry, University of Edinburgh, describes electrophysiological investigations of the possible function of influenza A M2 transmembrane domain reconstituted into planar lipid bilayers. The effects of adding

amantadine to this system and altering the pH and the constituents of the bathing solvents will be discussed.

4.6 Materials

All chemicals, including amantadine hydrochloride, were purchased from Sigma Chemical Company Ltd. Organic solvents were purchased from the same address. The phospholipids used were high-purity, stored at -70°C, and were obtained from Avanti, U.S.A. The M2 peptide used was native and was prepared as described in Section 2.7.

4.7 Experimental practice

A typical single-channel recording experiment began with the pipetting of lipid, which is dispersed in organic solvent, into an Eppendorf tube. The solvent was evaporated-off under a gentle stream of oxygen-free nitrogen and the lipid resuspended in decane and whirlimixed thoroughly.

The 'cup', ie. the machined styrene copolymer cylinder that houses the *cis* chamber, may be removed and cleaned with detergent then thoroughly rinsed. The *cis* and *trans* chambers in the perspex block were filled with the buffer of choice and the lipid 'painted' across the aperture (0.3 mm) between the two. Lipid painting is performed with a sharpened, plastic spatula.

The capacitance of the membrane is checked in order to ascertain optimum thickness. The ion channel of interest is added, in a minimal volume of solvent, to the *cis* chamber and the solution

is stirred briefly using a tiny, magnetic stirrer. With the experiments described here, it was observed that channel incorporation proceeded more rapidly if the system was exposed to a positive potential difference ($\approx$ +40 mV) at this point.

Successful channel reconstitution is deemed to have occurred when unit current flow is observed (events). The contents of the two chambers may now be changed, if so desired, by careful perfusion. A record of events is made on magnetic video tape for subsequent data analysis.

4.8 Results, subsequent data analysis, and discussion

The observation of proton channel activity

Initially, it was attempted to incorporate native M2 peptide into DOPC bilayers. However, this resulted in poor peptide incorporation and, after further trials, it was found that a equimolar mixture of palmitoyl-oleoyl phosphatidylethanolamine (POPE) and palmitoyl-oleoyl phosphatidylserine (POPS) (each at an initial concentration of 15 mg ml^{-1}) maximised channel reconstitution. In addition, after successful M2 reconstitution, if buffer solutions at approximately physiological pH were used in the *cis* and *trans* chambers then prohibitively small currents were observed. This was deemed to be due to a paucity of potential translocating ions and therefore, it was decided that experiments measuring proton flow characteristics would be performed at more acidic pH. To control for these rather non-physiological conditions, membranes of similar capacitance to those described above were held for up to one hour at pH's of between 2.3 and 7.0. In subsequent control experiments

it was observed that membrane stress occurred only if the pH dropped below 1. Bilayer stability was always monitored before the addition of peptide and the pH was only exceptionally reduced below 2.3.

When commencing such electrophysiological experiments as are described here, *cis* and *trans* chambers were both filled with 600 μl of 50 mM glycine HCl, pH 2.3. The *cis* chamber was voltage-clamped at a range of possible holding potentials relative to the *trans*, which was grounded. The bilayers were monitored by measuring their capacitance ($\approx$ 250 pF) and those used had resistances of at least 10^{11} Ohms. After successful M2 incorporation, the contents of the *trans* chamber was usually replaced by perfusion with 50 mM glycine HCl, pH 3.0. Transmembrane currents were commonly seen within thirty minutes of adding up to 1 μg of the peptide in 6 μl of methanol to the *cis* compartment. Channel incorporation could be accelerated by breaking and reforming the POPE/POPS membrane. Control bilayers exposed to 1% (v/v) methanol in the same buffer remained stable for up to three hours and exhibited no channel-like activity. All experiments described in this section were repeated many times and single-channel currents were obtained whenever successful reconstitution occurred (Figure 4.3).

The observation of current flow indicated that influenza A M2 protein, or, at least, the transmembrane region thereof, was indeed capable of proton translocation.

Importantly, such proton channel activity could be blocked by the addition of 20 μM amantadine hydrochloride. Furthermore, when the contents of both bilayer chambers were replaced by

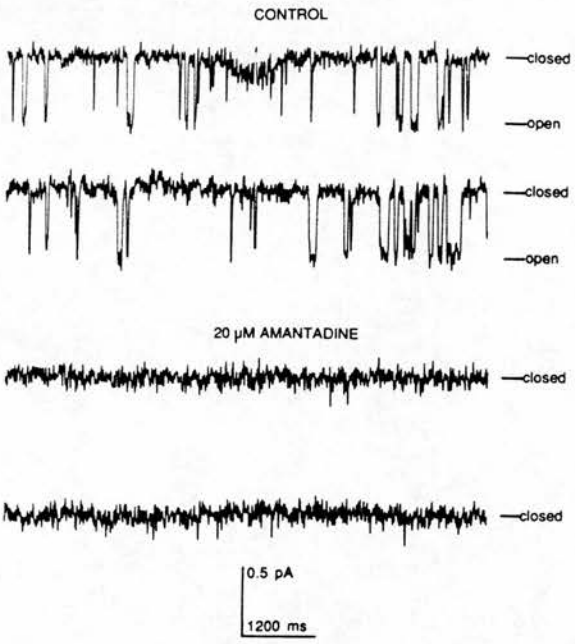

Figure 4.3 Single-channel currents (downward deflections) across a planar lipid bilayer with incorporated M2 peptide, subsequently inhibited by 20 μM amantadine HCl (added to both sides of the membrane). Holding potential +100 mV, glycine-HCl (pH 2.3 *cis* and 3.0 *trans*).

extensive perfusion with fresh buffer *after* amantadine block, channel activity was restored. A control experiment with the twenty-six amino acid peptide melittin (Tosteson and Tosteson, 1981) showed that, when it was incorporated in a similar manner under the same conditions, it acted as an anion channel but was insensitive to amantadine.

These results illustrate the *specific* action of amantadine upon the associated function of the transmembrane domain of influenza A M2 protein.

Lifetime distributions - a brief sojourn

For any two-state channel model, the gate in the channel opens and shuts randomly. If the gate is open, it has a certain probability of shutting. This probability is expressed as a *transition rate constant* (α) with units of s^{-1} (ie. per second). Conversely, if the gate is shut, it has a certain probability of opening, again expressed as a transition rate constant (ß) -

$$\text{open} \underset{\text{ß}}{\overset{\alpha}{<=>}} \text{shut} \qquad 4.10$$

The value of α shows that for every accumulated second that the channel is in the open state, it will on average shut α times, and conversely, for every accumulated second that the channel is shut, it will on average open ß times. For example, if the gate shuts on average one thousand times for every second that it is open, it means that the average length of time that the gate is open is 1 / 1000 seconds, or 1 ms. The mean length of time the channel stays

in a particular state, the 'sojourn' in that state, is the reciprocal of the transition rate constant that leads out of the state.

From the data illustrated in Figure 4.3, four and a half minutes of the pre-amantadine recording were inspected to identify discrete openings which were collected in a frequency histogram (Figure 4.4). [NB. The data collected in all these experiments were analysed using Axotape and PClamp software (Axon Instruments).] The mean open time (τ_0) was determined to have a duration of 20 msec. Therefore, from the above, it can be seen that the transition rate constant for channel closure ($1/\tau_0$) is $\approx$ 50 s^{-1}. Such lifetime analyses are consistent with a model for channel formation of the general type -

$$4p \underset{\beta}{\overset{\alpha}{<=>}} p4 \qquad 4.11$$

where incorporated peptide monomers (p) associate briefly to form an oligomeric channel (here shown as a tetramer, however, '4' may be replaced by 'n').

Closed lifetime distributions, on the other hand, appeared to contain at least two components, with mean lifetimes of about 10 msec and 1 msec. Because of the relatively small number of events, a complete analysis of the absolute values of the closed-state lifetimes proved impossible and it was observed that these values varied considerably between experiments, as would be expected for different peptide concentrations. However, the repeated finding of more than one component is consistent with the formation of clusters of peptides (eg. tetramers), with short 'intraburst' intervals reflecting the temporary dissociation of one monomer within a given group

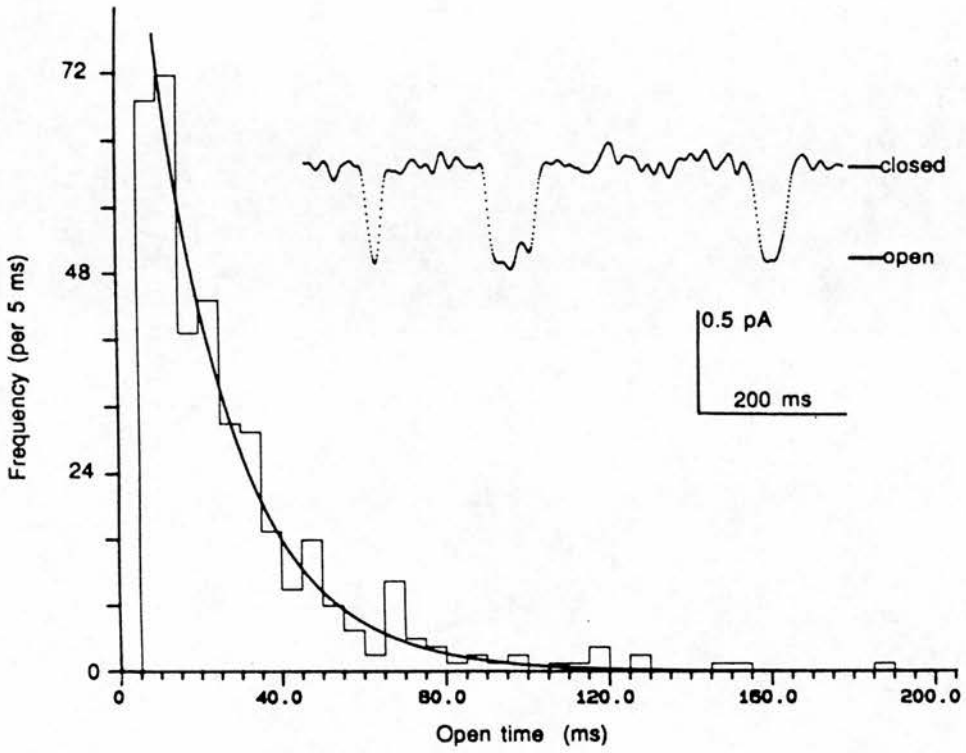

Figure 4.4 Frequency distribution of all the openings collected from 4.5 minutes of pre-amantadine recording (with typical events shown in detail). The smooth curve is a single exponential function with a time constant of 20 msec. Events lasting < 4 msec were discarded.

and longer 'interburst' intervals corresponding to more extensive disruption, eg. -

$$p + p <=> p^2 + p <=> p^3 + p <=> p^4 \qquad 4.12$$

With higher peptide concentrations, bursts of channel activity tended to overlap to give openings to more than one unit current level (see below). It was noted that channel activation showed little obvious voltage-dependence.

Multichannel currents

It was observed that peptide incorporation increased markedly on addition of >10 μg ml^{-1} but this usually resulted in the appearance of multichannel currents (up to 50 pA) which were difficult to analyse. However, occasionally, distinct conductance levels could still be resolved, and in the experiment shown in Figure 4.5, current transitions appear to occur between the closed level (which is more obvious after the application of amantadine) and several open levels. An amplitude histogram was constructed from one hundred seconds of these data (Figure 4.6) and it shows three main equally spaced peaks, consistent with the simultaneous formation of up to three channels in this bilayer. The third peak is not a single Gaussian, suggesting that some large events of $\approx$ 2.6 pA arose by a different mechanism (possibly ion channels formed from higher oligomers, eg. five peptides rather than four). In addition, apparently direct transitions between levels 1 and 3 occurred much more often than would be expected from the random superimposition of unit events (Krouse *et al.*, 1986). This is

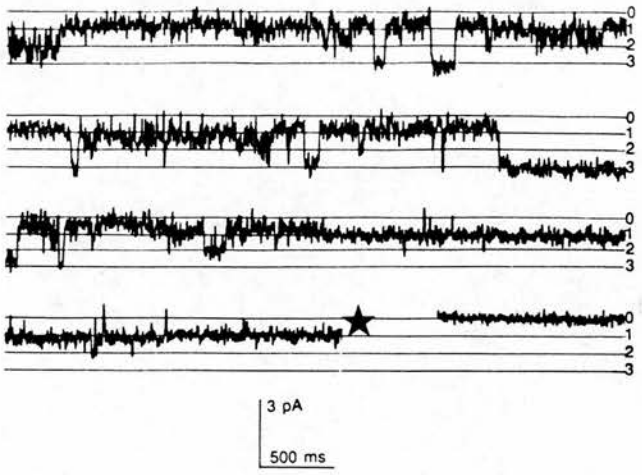

Figure 4.5 Current transitions in a peptide-containing bilayer voltage-clamped at +80 mV. The bilayer was formed in 25 mM Tris-HCl (pH 7) and the pH of the *cis* solution was then lowered to 1 by adding HCl. Downward proton currents flow *cis* to *trans*. Amantadine (20 mM), added to both chambers where indicated (*), confirmed the zero current level (0). Openings have been assigned to three marked current levels.

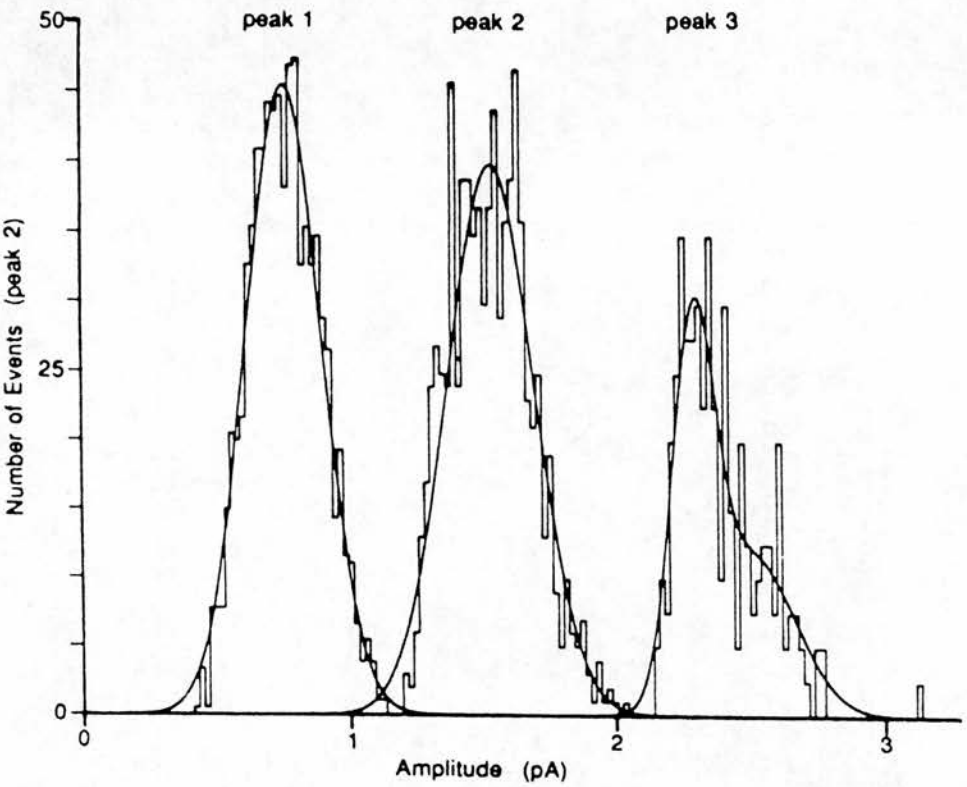

Figure 4.6 Amplitude histogram from 100 seconds of contiguous data displayed in Figure 4.5. Main peaks 1 and 2 were each fitted to a single Gaussian and peak 3 to two Gaussian distributions. Peaks 1:2:3 have been rescaled in the ratio 9:5:2 to share the same axis.

consistent with some cooperativity of oligomer association and dissociation or the formation of channel clusters.

If very large proton gradients were imposed across the bilayer (Figure 4.7), then highly nonlinear I/V relationships were produced (Figure 4.8) which appeared to be well described by electrodiffusion theory - Equation 4.9 (Hodgkin and Katz, 1949). Conductance could be seen to be ohmic (linear) in the more moderate gradients provided by citrate or glycine HCl buffers (eg. glycine HCl, pH 2.3 *cis* vs 3.0 *trans*, Figure 4.9, solid line). Reversal potentials were shifted slightly from the proton equilibrium potential but remained consistent with a H^+:Cl^- permeability ratio of at least 5:1 (derived from the GHK equation, Equation 4.9). On the same basis, the shift in the reversal potential when the *trans* chamber was perfused with 3.0 M NaCl (leaving glycine HCl, pH 2.3 *cis*) indicated a H^+:Na^+ permeability ratio of at least 3:1 (Figure 4.9, dotted line).

It must be pointed out that these values correspond to very unphysiological conditions for the peptide and for all the ions involved. Relative permeabilities in normal cellular conditions (and with the complete protein) may differ.

Nevertheless, these experiments, taken together, do provide clear evidence that the transmembrane domain of M2 protein can form proton-conducting ion channels which are blocked by amantadine and this therefore supports the original hypothesis of Hay and his colleagues that proton translocation by M2 plays an important part in viral pathogenesis (Sugrue and Hay, 1991; Hay, 1989).

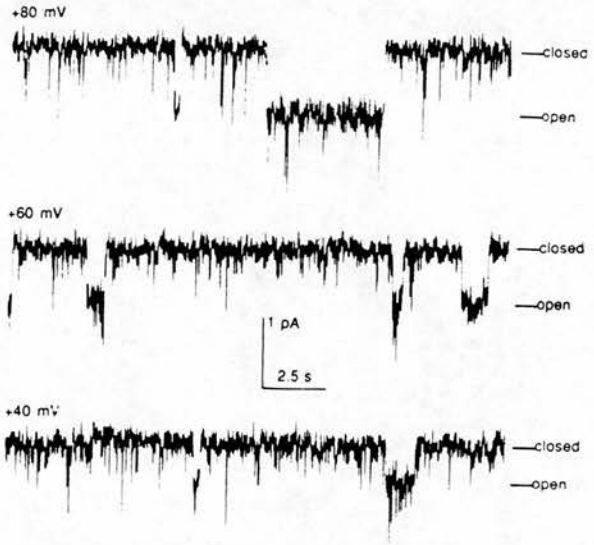

Figure 4.7 Single-channel currents across an M2-containing bilayer voltage-clamped at the indicated holding potentials (50 mM KCl both *cis* and *trans*, pH 1.5 and 7.0 respectively [adjusted with HCl or KOH]).

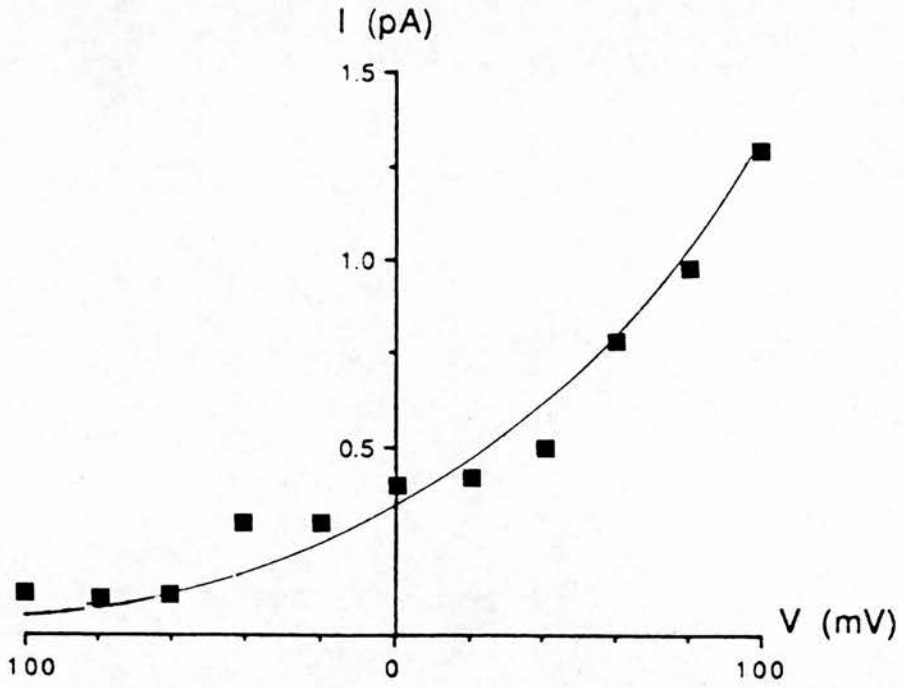

Figure 4.8 I/V plot from the experiment described in Figure 4.7. The smooth curve is a best-fit to the GHK equation (equation 4.9), assuming only protons are significantly permeant under these conditions.

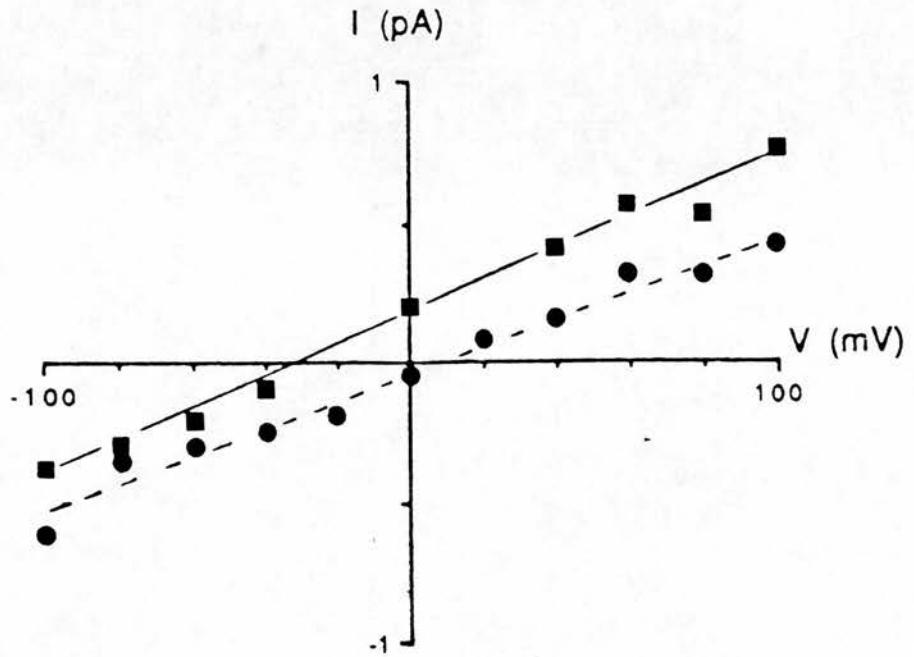

Figure 4.9 I/V relationship from an experiment with glycine HCl *cis* and *trans*, pH 2.3 and 3.0 respectively ■, and after changing the *trans* solution by perfusion with 3.0 M NaCl, pH 7.0 ●. The reversal potential shifted from -34 mV to +10 mV.

CHAPTER 5 CONCLUSION

5. Conclusion

An initial diffraction project investigated the position of amantadine in phospholipid multilayers (Duff et al., 1993). The thesis has then proceeded in a structure/function manner. The M2 transmembrane domain of influenza A has been demonstrated to adopt an α-helical secondary structure when incorporated into liposomes. This structure is influenced by phospholipid composition but not by temperature or the presence of amantadine. The M2 peptide, both native and mutant, has been shown to adopt a transmembrane position. Within this sequence a distinct area of amantadine interaction has been located which agrees spatially with such a proposed site deduced from recent molecular modelling studies. With amantadine-resistant mutant M2 sequences, peptide/drug interactions are not discernable in this area. The native M2 peptide, when incorporated into bilayers and studied from a functional perspective, has demonstrated an amantadine-sensitive proton channel ability.

It may therefore be reported that the results in this thesis indicate influenza A M2 transmembrane domain is an α-helical, membrane-spanning proton channel and that amantadine interacts with this channel, at a specific region, resulting in the blockade of its function.

At the outset of this thesis, January 1990, very little was known about M2. It had been recognised (Winter and Fields, 1980), been found in infected cells (Lamb and Chopin, 1981) and in virions (Zebedee and Lamb, 1988) and had been hypothesised to be involved in proton transfer at two possible stages in the infectivity

cycle (Hay, 1989). Three years later, after some extensive research from numerous workers, we now know that the transmembrane domain possesses α-helical secondary structure (Duff *et al.*, 1992), its precise orientation in the bilayer (Duff *et al.*, in prep.), that it forms tetrameric structures (Sugrue and Hay, 1991) and that it allows passage of protons (Duff and Ashley, 1992) and other cations (Pinto *et al.*, 1992), and, in addition, one of the possible areas of amantadine action has been described (Duff *et al.*, in prep; Sansom and Kerr, 1993).

It is expected that such diverse work will lead to a general understanding of the nature of enveloped virus infectivity and the basis of drug efficacy. It is hoped that the work described in this thesis has contributed in some measure to the achievement of this understanding.

REFERENCES

References

Allen, J.P., Feher, G., Yeates, T.O., Komiya, H. and Rees, D.C. (1987) Structure of the reaction centre from *Rhodobacter sphaeroides* R-26: the protein subunits *Proc. Natl. Acad. Sci. U.S.A. 84* 6162-6166

Anderson, R.G.W. and Orci, L. (1988) A view of acidic intracellular compartments *J. Cell Biol. 106* 539-543

Bacon, G.E. (1975) Neutron diffraction (third edition) Oxford University Press, London, U.K. pp. 48-50

Batenburg, A.M. and de Kruijff, B. (1988) Modulation of membrane-surface curvature by peptide-lipid interactions *Biosci. Rep. 8* 299-307

Bayley, P.M. (1973) The analysis of CD of biomolecules Progress in biophysics and molecular biology 27 3-79

Belshe, R.B., Hall-Smith, M., Hall, C.B., Betts, R. and Hay, A.J. (1988) Genetic basis of resistance to rimantadine emerging during treatment of influenza virus infection *J. Virol. 62* 1508-1512

Beveridge, W.I.B. (1977) Influenza - the last great plague Heinemann Books Ltd., London, U.K.

Blaurock, A.E. and Nelander, J.C. (1976) Disorder in nerve myelin : analysis of the diffuse X-ray scattering *J. Mol. Biol. 103* 421-431

Both, G.W., Sleigh, M.J., Cox, N.J. and Kendal, A.P. (1983) Antigenic drift in influenza virus H3 HA from 1968-1980 : multiple evolutionary pathways and sequential amino acid changes at key antigenic sites *J. Virol. 48* 52-60

Bradshaw, J.P., Edenborough, M., Sizer, P.J.H. and Watts, A. (1989) A description of the phospholipid arrangement intermediate to the humidity produced L_α and H_{II} phases in dioleoylphosphatidylcholine and its modification by dioleoylphosphatidylethanolamine as studied by X-ray diffraction *Biochim. Biophys. Acta 987* 101-110

Bragg, W.L. (1913) The diffraction of short electromagnetic waves by a crystal *Proc. Cambridge Philos. Soc. 17* 43-57

Bukrinskaya, A.G., Vorkunova, N.K. and Pushkarskaya, N.L. (1982) Uncoating of a rimantadine-resistant variant of influenza virus in the presence of rimantadine *J. Gen. Virol. 60* 61-66

Buldt, G., Gally, H.U., Seelig, A., Seelig, J., and Zaccai, G. (1978) Neutron diffraction studies on selectively deuterated phospholipid bilayers *Nature 271* 182-184

Buldt, G., Gally, H.U., Seelig, J. and Zaccai, G. (1979) Neutron diffraction studies on phosphatidylcholine model membranes *J. Mol. Biol. 134* 673-691

Campbell, I.D. and Dwek, R.A. (1984) Biological spectroscopy, Benjamin/Cummings Publishing Co., California, U.S.A.

Chang, C.T., Wu, C.-S.C. and Yang, J.T. (1978) Circular dichroic analysis of protein conformation; inclusion of the ß-turns *Anal. Biochem. 91* 13-31

Changeaux, J.P., Giraudat, J. and Dennis, M. (1987) The nicotinic acetylcholine receptor : molecular architecture of a ligand-regulated ion channel *Trends Pharmacol. Sci. 8* 459-465

Cheetham, J.J. and Epand, R.M. (1987) Comparison of the interaction of the antiviral chemotherapeutic agents amantadine and tromantadine with model phospholipid membranes *Biosci. Rep. 7* 225-230

Chen, Y-H, Yang, J.T. and Chau, K.H. (1974) Determination of the helix and beta forms of proteins in aqueous solution by circular dichroism *Biochemistry 13* 3350-3359

Curwen, M., Dunnell, K., Ashley, J. (1990) Hidden influenza deaths *Br. Med. J. 300* 896-897

Davies, W.L., Grunert, R.R., Haff, R.M., McGahen, J.W., Neumayer, E.M. and Paulshock, M. (1964) Antiviral activity of 1-adamantanamine [amantadine] *Science 144* 862-863

Deisenhofer, J., Epp, O., Miki, K., Huber, R. and Michel, H. (1985) Structure of the protein subunits in the photosynthetic reaction centre of *Rhodopseudomonas virdis* at 3Å resolution *Nature 318* 618-624

Dubowitz, V. (1958) Influenzal encephalitis *Lancet 1* 140-142

Duff, K.C. and Ashley, R.H. (1992) The transmembrane domain of influenza A M2 protein forms amantadine-sensitive proton channels in planar lipid bilayers *Virology 190* 485-489

Duff, K.C., Cudmore, A.J. and Bradshaw, J.P. (1993) The location of amantadine hydrochloride and free base within phospholipid multilayers : a neutron and X-ray diffraction study *Biochim. Biophys. Acta 1145* 149-156

Duff, K.C., Kelly, S.M., Price, N.C. and Bradshaw, J.P. (1992) The secondary structure of influenza A M2 transmembrane domain : a circular dichroism study *FEBS Lett. 311* 256-258

Duff, K.C., Saxena, A. and Bradshaw, J.P. (in prep.) The orientation of native and mutant influenza A M2 transmembrane domains in phospholipid multilayers and their interactions with amantadine hydrochloride : a neutron diffraction study

Epand, R.M., Epand, R.F., Orlowski, R.C., Boni, L.T. and Hui, S.W. (1983) Amphipathic helix and its relationship to the interaction of calcitonin with phospholipids *Biochemistry 22* 5074-5084

Ewald, P.P (1921) Das 'reziproca gitter' in der strukturtheorie *Z. Kristollagr. Miner 56* 129-156

Franks, N.P. and Leib, W.R. (1979). The structure of lipid bilayers and the effects of general anaesthetics : an X-ray and neutron diffraction study *J. Mol. Biol. 133* 469-500

Franks, N.P. and Lieb, W.R. (1981) X-ray and neutron diffraction studies of lipid bilayers Liposomes : from physical structure to therapeutic applications (Knight, ed) Elsevier/North-Holland Press pp. 243-272

Gilman, A.G., Rall, T.W., Nies, A.S. and Taylor, P. (1990) The pharmaceutical basis of therapeutics (8th Edition) Pergamon Press pp. 472-473

Gottschalk, A. (1957) The specific enzyme of influenza virus and *Vibrio cholerae Biochim. Biophys. Acta 23* 645-646

Gregoriades, A. (1973) The membrane protein of influenza virus : extraction from virus and infected cell with acidic chloroform-methanol *Virology 54* 369-383

Guo, Y., Jin, F., Wang, M. and Zhu, J. (1983) Isolation of influenza C virus from pigs *J. Gen. Virol. 64* 177-182

Hamill, O.P., Marty, A., Neher, E., Sakmann, B. and Sigworth, F.J. (1981) Improved patch-clamp techniques for high-resolution current recording from cells and cell-free membrane patches *Pfluegers Arch. Eur. J. of Physiol. 391* 85-100

Hay, A.J. (1989) The mechanism of action of amantadine and rimantadine against influenza viruses Concepts in viral pathogenesis III (A.L. Notkins and M.B.A. Oldstone, eds) Springer Verlag, New York, U.S.A. pp 361-367

Hay, A.J., Wolstenholme, A.J., Skehel, J.J. and Smith, M.H. (1985) The molecular basis of the specific anti-influenza action of amantadine *EMBO J. 4* 3021-3024

Hay, A.J., Zambon, M.C., Wolstenholme, A.J., Skehel, J.J. and Smith, M.H. (1986) Molecular basis of resistance of influenza A viruses to amantadine *J. Antimicrob. Chemother. 18 (suppl.)* 19-29

Hayden, F.G. and Hay, A.J. (1992) Emergence and transmission of influenza A viruses resistant to amantadine and rimantadine *Curr. Top. Microbiol. Immunol. 176* 119-130

Hers, J.F., Masurel, N. and Mulder, J. (1958) Bacteriology and histopathology of the respiratory and lungs in fatal Asian influenza *Lancet 2* 1141-1148

Hiebert, S.W., Patterson, R.G. and Lamb, R.A. (1985) Identification and predicted sequence of a previously unrecognised small hydrophobic protein, SH, of the paramyxovirus simian virus-5 *J. of Virol. 55* 744-751

Hille, B. (1992) Ionic channels of excitable membranes Sinauer Assoc, U.S.A.

Hodgkin, A.L. and Katz, B. (1949) The effect of sodium ions on the activity of the giant axon of the squid *J. Physiol. 108* 37-77

Huang, C., Charlton, J.P. and Litman, B.J. (1969) Studies on phosphatidyl choline vesicles : dye-lipid interaction *Biophys. J. 9* 37

Inglis, S.C., Carroll, A.R., Lamb, R.A. and Mahy, B.W.J. (1976) Polypeptides specified by the influenza virus genome I. Evidence for eight distinct core products specified by fowl plague virus *Virology 74* 489-503

Ito, T., Gorman, O.T., Kawaoka, Y., Bean, W.J. and Webster, R.J. (1991) Evolutionary analysis of the influenza A virus M gene with comparison of the M1 and M2 proteins *J. Virol. 65* 5491-5498

Jackson, D.C., Tang, X.-Li., Gopal Murti, K., Webster, R.G., Tregear, G.W. and Bean, W.J. (1991) Electron microscopic evidence for the association of M2 protein with the influenza virion *Arch. Virol. 118* 199-207

Jacobs, R.E. and White, S.H. (1989) The nature of the hydrophobic binding of small peptides at the bilayer interface : implications for the insertion of transbilayer helices *Biochemistry 28* 3421-3437

Kawakami, K. and Ishitama, A. (1983) RNA polymerase of influenza virus III. Isolation of RNA polymerase - RNA complexes of influenza PR8 *J. Biochem. 93* 989-999

Kilbourne, E.D. (1969) Future influenza vaccines and the use of genetic recombinants *Bull. WHO 41* 643-647

Kim, J., Mosior, M., Chung, L. A., Wu, H. and McLaughlin, S (1991) Binding of peptides with basic residues to membranes containing acidic phospholipids *Biophys. J. 60* 135-148

Kingsbury, D.W. (1990) Virology (second edition) Chapter 39 Orthomyxoviridae and their replication pp. 1075-1089

Krouse, M.E., Schneider, G.T. and Gage, P.W. (1986) A large anion-selective channel has seven conductance levels *Nature 319* 58-60

Lamb, R.A. and Choppin, P.W. (1981) Identification of a second protein (M2) encoded by RNA segment 7 of influenza virus *Virology 112* 729-737

Lamb, R.A., Lai, C.-J. and Choppin, P.W. (1981) Sequence of mRNA's derived from genome RNA segment 7 of influenza virus: colinear and interrupted mRNA's code for overlapping proteins *Proc. Natl. Acad. Sci. U.S.A. 78* 4170-4174

Lamb, R.A., Zebedee, S.L. and Richardson, C.D. (1985) Influenza virus M2 protein is an integral membrane protein expressed on the infected-cell surface *Cell 40* 627-633

Lear, J.D., Wasserman, Z.R. and Degrado, W.F. (1988) Synthetic amphiphilic peptide models for protein ion channels *Science 240* 1177-1181

Lesslauer, W., Cain, J.J. and Blaisie, J.K. (1972) X-ray diffraction studies of lecithin biomolecular leaflets with incorporated fluorescent probes *Proc. Natl. Acad. Sci. USA 69* 1499-1503

Markwell, M.K., Haas, S.M., Tolbert, N.E. and Bieber, L.L. (1981) Protein determination in membrane and lipoprotein samples: manual and automated procedures *Methods Enzymol. 72* 269-303

Martin, C.M., Kunin, C.M., Gottlieb, L.S., Barnes, M.W., Liv, C., Finland, M. (1959) Asian influenza A in Boston 1957-1958 *Arch. Intern. Med. 103* 515-518

Martin, K. and Helenius, A. (1991) Nuclear transport of influenza virus ribonucleoproteins: the viral matrix protein (M1) promotes export and inhibits import *Cell 67* 117-130

Matthews, R.E.F. (1982) Classification and nomenclature of viruses *Intervirology 17* 1-200

Miller, C. (Ed.) (1986) Ion channel reconstitution Plenum Press, New York, U.S.A.

Miller, D.K. and Lenard, J. (1981) Antihistaminics, local anaesthetics, and other amines as antiviral agents *Proc. Natl. Acad. Sci. USA. 78* 3605-3609

Mims, C.A. and White, D.O. (1988) Viral pathogenesis and immunology, Blackwell Scientific Publications, Oxford, U.K., pp. 292-293

Nernst, W. (1888) Zur kinetic der in losung befindlichen korper : theorie der diffusion *Z. Phys. Chem.* 613-637

O'Callaghan, E., Shan, P., Takai, N., Glover, G., Murray, R.M (1991) Schizophrenia after prenatal exposure to 1957 A2 influenza epidemic *Lancet 337* 1248-1250

O'Neill, G. (1991) Designer drugs to foil flu virus *New Scientist 132* 27

Obeso, J.A. and Martinez-Lage, J.M. (1987) Anticholinergics and amantadine The handbook of Parkinson's disease (W.C. Koller, ed) Marcel Dekker Inc., U.S.A. pp. 312-316

Oxford, J.S. and Galbraith, A. (1980) Antiviral activity of amantadine : a review of laboratory and clinical data *Pharmacol. Ther. 11* 181-262

Pacifici, G.M., Nardini, M. and Ferrari, P. (1976) Effect of amantadine on drug induced Parkinsonism : relationship between plasma levels and effect *Br. J. Clin. Pharmacol. 3* 883-889

Panayotov, P.P. and Schlesinger, R.W. (1992) Oligomeric organisation and strain-specific proteolytic modification of the virion M2 protein of influenza A H1N1 viruses *Virology 186* 352-355

Phonphok, Y. and Rosenthal, K.S. (1991) Stabilization of clathrin coated vesicles by amantadine, tromantadine and other hydrophobic amines *FEBS Lett. 281* 188-190

Pinto, L.H., Holsinger, L.J. and Lamb, R.A. (1992) Influenza virus M2 protein has ion channel activity *Cell 69* 517-528

Potter, C.W. (1982) Inactivated influenza virus vaccine Basic and applied influenza research (ed. Beare, A.S.) CRC Press, Florida, U.S.A.

Provencher, S.W. and Glöckner, J. (1981) Estimation of globular protein secondary structure from circular dichroism *Biochemistry 20* 33-37

Robinson, R.A. and Stokes, R.H. (1965) Electrolyte solutions p571 Butterworths, London, U.K.

Roth, M., Lewit-Bentley, A., Michel, H., Deisenhofer, J., Huber, R. and Oesterhelt, D. (1989) Detergent structure in crystals of a bacterial photosynthetic reaction centre *Nature 340* 659-662

Ruigrok, R.W.H., Hirst, E.M. and Hay, A.J. (1991) The specific inhibition of influenza A virus maturation by amantadine : an electron microscopic examination *J. Gen. Virol. 72* 191-194

Sacks, O. (1985) Awakenings, Pan Books, London, U.K.

Sakmann, B. and Neher, E. (1983) Single-channel recording Plenum Press, New York, U.S.A.

Sansom, M.S.P. and Kerr, I.D. (1993) Influenza virus M2 protein: a molecular modelling study of the ion channel *Protein Eng. 6* 65-74

Scadding, J.G. (1937) Lung changes in influenza *Q. J. Med. 6* 425-430

Schlegel, A., Omar, A., Jentsch, P., Morell, A. and Kempf, C. (1991) Semliki forest virus envelope proteins function as proton channels *Biosci. Rep. 11* 243-255

Schonberger, L.B., Bregman, D.J. and Sullivan-Bolyai, J.Z. (1979) Guillain-Barre syndrom following vaccination in the National Influenza Immunization Program, U.S., 1976-1977 *Am. J. Epidemiol. 110* 105-110

Schwartz, S., Cain, J.E., Dratz, E.A. and Blasie, J.K. (1975) An analysis of lamellar X-ray diffraction from disordered membrane multilayers with application to data from retinal rod outer segments *Biophys. J. 15* 1201-1233

Shaw, M.W. and Choppin, P.W. (1984) Studies on the synthesis of the influenza B virus NB glycoprotein *Virology 139* 178-184

Shinooka, T., Shibata, A. and Terada. H. (1992) The local anaesthetic tetracaine destabilizes membrane structure by interaction with polar headgroups of phospholipids *Biochim. Biophys. Acta. 1104* 261-268

Siegel, J.R., Steinmetz, W.E. and Long, G.L. (1980) A computer-assisted model for estimating protein secondary structure from circular dichroic spectra : comparison of animal lactate dehydrogenases *Anal. Biochem. 104* 160-167

Sizer, P.J.H., Miller, A. and Watts, A. (1987) Functional reconstitution of the integral membrane proteins of influenza virus into phospholipid liposomes *Biochemistry 26* 5106-5113

Smith, I.C., Auger, M. and Jarrell, H.C. (1991) Molecular details of anaesthetic-lipid interaction *Ann. N.Y. Acad. Sci. 625* 668-684

Stein, W.D. (1986) Transport and diffusion across cell membranes Academic Press, London, U.K.

Stein, W.D. (1990) Channels, carriers and pumps Academic Press, London, U.K.

Stuart-Harris, C.H., Schild, G.C., Oxford, J.S. (1985) Influenza : the viruses and the disease (second edition) , Edward Arnold Ltd, London, U.K.

Sugrue, R.J. and Hay, A.J. (1991) Structural characteristics of the M2 protein of influenza A viruses : evidence that it forms a tetrameric channel *Virology 180* 617-624

Sugrue, R.J., Bahadur, G., Zambon, M.C., Hall-Smith, M., Douglas, A. R. and Hay, A.J. (1990) Specific structural alteration of the influenza haemagglutinin by amantadine *EMBO. J. 9* 3469-3476

Tardieu, A., Luzzati, V. and Reman, F.C. (1973) Structure and polymorphism of the hydrocarbon chains of lipids: a study of lecithin-water phases *J. Mol. Biol. 75* 711-733

Terwilliger, E.F., Cohen, E.A., Lu, Y., Sodroski, J.G. and Haseltine, W.A. (1989) Functional role of human immunodeficiency virus type-1 *vpu Proc. Natl. Acad. Sci. U.S.A. 86* 5163-5167

Tominack, R.L. and Hayden, F.G. (1987) Rimantadine HCl and amantadine HCl use in influenza A virus infections *Infect. Dis. Clin. North Am. 1* 459-478

Torbet, J. and Wilkins, M.H.F. (1976) X-ray diffraction studies of lecithin bilayers *J. Theor. Biol. 62* 447-458

Tosteson, M.T. and Tosteson, D.C. (1981) The sting : melittin forms channels in lipid bilayers *Biophys. J. 36* 109-116

Tripos Associates (1991) SYBYL : A molecular modelling package Tripos Associates Inc., St. Louis, Missouri, U.S.A.

Warnick, J.E., Maleque, M.A., Bakry, N., Eldefrawi, A.T. and Albuquerque, E.X. (1982) Structure-activity relationships of amantadine : 1. Interaction of the N-alkylanalogues with the ionic channels of the nicotinic acetylcholine receptor and electrically excitable membrane *Mol. Pharmacol. 22* 82-93

Webster, R.G., Campbell, C.H., Granoff, A. (1971) The *in vivo* production of 'new' influenza A viruses *Virology 44* 317-328

Weiner, M.C. and White, S.H. (1991) Transbilayer distribution of bromine in fluid bilayers containing a specifically brominated analogue of dioleoylphosphatidylcholine *Biochemistry 30* 6997-7008

Weiner, M.C., King, G.I. and White, S.H. (1991) Structure of fluid dioleoylphosphatidylcholine bilayer determined by joint refinement of X-ray and neutron diffraction data *Biophys. J. 60* 568-576

White, J., Kartenbeck, J. and Helenius, A. (1982) Membrane fusion activity of influenza virus *EMBO J. 1* 217-222

Wiley, D.C. and Skehel, J.J. (1987) The structure and function of the haemagglutinin membrane glycoprotein of influenza virus *Ann. Rev. Biochem. 56* 365-394

Williams, M.A. and Lamb, R.A. (1986) Determination of the orientation of an integral membrane protein and sites of glycosylation by oligonucleotide-directed mutagenesis - influenza B virus NB glycoprotein lacks a cleavable signal sequence and has an extracellular NH_2-terminal region *Mol. Cell Biol. 6* 4317-4328

Wilson, I.A., Skehel, J.J. and Wiley, D.M. (1981) Structure of the haemagglutinin membrane glycoprotein of influenza virus at 3Å resolution *Nature 289* 366-373

Winter, G. and Fields, S. (1980) Cloning of influenza cDNA into M13 : the sequence of the RNA segment encoding the A/PR/8/34 matrix protein *Nucleic Acids Res. 8* 1965-1974

Wolstenholme, A.J., Barrett, T., Nichol, S.T. and Mahy, B.W.J. (1980) Influenza virus-specific RNA and protein synthesis in cells infected with temperature-sensitive mutants defective in the genome segment encoding nonstructural proteins *J. Virol. 35* 1-7

Woody, R.W. (1977) Optical rotary properties of biopolymers *J. Polymer Sci. 12* 181-321

Worcester, D.L. and Franks, N.P. (1976) Structural analysis of hydrated egg lecithin and cholesterol bilayers : II neutron diffraction *J. Mol. Biol. 100* 359-378

Zebedee, S.L. and Lamb, R.A. (1988) Influenza A virus M2 protein : monoclonal antibody restriction of virus growth and detection of M2 in virions *J. Virol. 62* 2762-2772

Zhirnov, O.P. (1990) Solubilisation of matrix protein M1/M from virions occurs at different pH for orthomyxo- and paramyxoviruses *Virology 176* 274-279

Zlychnikor, D.M., Kubar, O.I., Kovaleva, T.P. and Kamforin, L.E. (1981) Study of rimantadine in the USSR : a review *Rev. Infect. Dis. 3* 408-421

APPENDIX PUBLISHED PAPERS RESULTING FROM WORK PRESENTED IN THIS THESIS

Volume 311, number 3, 256–258 FEBS 11672 October 1992

The secondary structure of influenza A M2 transmembrane domain

A circular dichroism study

Kevin C. Duff[a], Sharon M Kelly[b], Nicholas C. Price[b] and Jeremy P. Bradshaw[a]

[a]*Department of Biochemistry, University of Edinburgh Medical School, Hugh Robson Building, George Square, Edinburgh, EH8 9XD, Scotland, UK* and [b]*Department of Biological and Molecular Sciences, University of Stirling, Stirling, FK9 4LA, Scotland, UK*

Received 7 September 1992

Using circular dichroism, this study investigated the secondary structure of the influenza A M2 transmembrane domain. When reconstituted into 1,2-dioleoyl-*sn*-glycero-3-phosphocholine liposomes, the M2 transmembrane domain was found to adopt a predominantly α-helical secondary structure which was unaffected by both temperature and the addition of 1-aminoadamantane hydrochloride. Reconstitution into 1,2-dioleoyl-*sn*-glycero-3-phosphoglycerol liposomes resulted in a marked decrease in helical content.

Spectrophotometry; Circular dichroism; Influenza M2 protein; Ion channel

1. INTRODUCTION

The influenza A virus M2 protein has recently been the focus of extensive research. This protein is expressed on the cell surface during viral synthesis [1] and has been identified in viral particles [2]. It is a disulphide-bonded homotetramer [3] of 97 amino acids and is important during two separate phases of the cell cycle [4]. Immediately after viral endocytosis, and concomitant with pH-induced fusion between the endosomal and viral membranes, mediated by hemagglutinin (HA) [5], M2 is thought to conduct protons into the interior of the virus, leading to uncoating, the release of ribonucleoprotein from the matrix protein (M1), and eventual nuclear infection [6]. When HA is transported to the cell surface in post-Golgi vesicles [7], M2 may also facilitate influenza synthesis and assembly by countering any vesicular acidification. The relative importance of these events, which occur at different stages of the infectivity cycle, may depend on the particular viral strain [4]. Amantadine (1-aminoadamantane hydrochloride), the only registered drug used in the prophylaxis and treatment of influenza infections, is thought to operate by impeding proton flow during these events, however, it is not yet clear if the mechanism of this action involves an alteration in the secondary structure of the membrane-spanning domain or physical blockade. Importantly, influenza A is thought to become resistant to amantadine via single amino acid substitutions in the membrane-spanning domain of M2 [8].

Regarding the thesis that M2 orchestrates proton flow, it has recently been shown that, when expressed in *Xenopus laevis* oocytes, it has an associated ion channel activity selective for monovalent cations [9]; using a two-electrode voltage-clamp procedure the Pinto study observed Na^+ and K^+ currents. In addition, a further electrophysiological study directly identified proton translocation when the transmembrane domain of M2 was incorporated into single-channel, voltage-clamped, planar lipid bilayers [10]. Both studies reported current negation upon addition of amantadine.

The premise that membrane-spanning regions are often α-helical is generally based on theoretical predictions and observations of such in bacterial photosynthetic reaction centres [11–13]. In addition, when the M2 transmembrane domain is modelled as an α-helix the residues which are substituted in amantadine-resistant mutants all appear on the same face of the helix [14]. Thus it is an attractive assumption that the M2 transmembrane domain is α-helical, however, several caveats exist. An amantadine-resistant influenza virus has been isolated that contains a proline substitution in the transmembrane domain, which is not usually thought to be compatible with a helical conformation [8]. In addition, Pinto et al. [9] observed that deletion of four transmembrane residues and addition of one extra residue still permitted ion channel activity.

The present study describes an investigation of the secondary structure of the native influenza A M2 transmembrane domain, and the influence of amantadine at different concentrations, using circular dichroism (CD).

Correspondence address: K.C. Duff, Department of Preclinical Veterinary Sciences, Royal 'Dick' School of Veterinary Science, University of Edinburgh, Summerhall, Edinburgh, EH9 1QH, Scotland, UK. Fax: (44) (31) 662 0790.

Published by Elsevier Science Publishers B.V.

The results are discussed in terms of the recent electrophysiological data available concerning the mode of action of the M2 protein.

2. EXPERIMENTAL

In order to investigate the secondary structure of the influenza A M2 transmembrane domain, a synthetic 25 residue peptide (sequence: SSDPLVVAASIIGILHLILWILDRL), corresponding to the predicted transmembrane sequence common to several strains of influenza A [15], was incorporated into 1,2-dioleoyl-*sn*-glycero-3-phosphocholine (DOPC) liposomes [16] and examined using CD. The peptide was synthesized in the MRC Cellular Immunology Unit, Oxford, UK, purified by reverse-phase HPLC and subsequently sequenced in the WelMet Unit, University of Edinburgh, UK. The lipid was chosen for this study because phosphatidylcholine is the most common phospholipid headgroup in mammalian systems and oleic acid represents the most frequently occurring fatty acyl chain. The possible effects of temperature, addition of amantadine, and liposomal lipid type used, were also investigated. M2 was also reconstituted into 1,2-dioleoyl-*sn*-glycero-3-phosphoglycerol (DOPG) liposomes.

CD spectra were recorded on a JASCO J-600 spectropolarimeter; analysis of the spectra in terms of secondary structure content was undertaken using the CONTIN procedure of Provencher and Glöckner [17], the methods of Chang et al. [18] and of Siegel et al. [19].

The liposomes were prepared in a 10 mM Tris-HCl, 0.1 mM EDTA buffer system, pH 7.4. Two concentrations of amantadine were added to the reconstituted liposomes, 4 and 12 μg/ml. These were designated low and high concentration, respectively. All chemicals were supplied by Sigma Chemical Co., UK.

Liposomal and control protein concentrations were determined colorimetrically following the Lowry modification of Markwell et al. [20], using bovine serum albumin as standard.

3. RESULTS AND DISCUSSION

The far UV CD spectrum at 20°C of the M2 transmembrane peptide incorporated into DOPC liposomes is shown in Fig. 1. Under these conditions, satisfactory data could be obtained down to 200 nm; below this wavelength, the noise levels precluded accurate measurements of ellipticity. The spectrum shows the characteristic double minima at 223 nm and 209 nm of α-helices [18]. Estimates of 92, 79 and 100% α-helix were obtained using the methods of Provencher and Glöckner [17], Chang et al. [18] and Siegel et al. [19], respectively. Although the exact values of these estimates should be treated with caution, in view of the fact that data could only be collected down to 200 nm instead of 190 nm, which is preferred [17,18], it is clear that under these conditions the M2 peptide exists largely, if not completely, in an α-helical form. In addition, estimates of helix approaching 100% have been obtained both when M2 peptide is dissolved in 0.4% (w/v) sodium dodecyl sulphate (SDS) and 50% (v/v) 2,2,2-trifluoroethanol (TFE) (see Table I). These solvents maximize possible secondary structure conformation. Such results are in direct contrast to those obtained when M2 is dissolved in buffer. In aqueous solution, the M2 peptide did not apparently adopt any stable secondary structure; the low value of the molar ellipticity at 225 nm (Table I) is typical of a random coil. The DOPC liposomal measurements were repeated at 37°C, and no change was observed in the spectrum when compared with the 20°C data.

On addition of amantadine to the liposomes, to give final concentrations of 4 or 12 μg/ml, there were no significant changes in the CD spectra (see the molar ellipticity values in Table I). Both low and high drug concentrations were used in order to examine any possible concentration dependence [21]. These results are significant in that they clearly demonstrate that amantadine itself has no discernable effect upon the helical nature of the M2 peptide, as was previously mooted [22]. This, along with recent findings that amantadine does indeed inhibit ion flow through M2 [9,10], augments the thesis that the efficacy of amantadine is due to its channel-blocking abilities and not to any conformational interference.

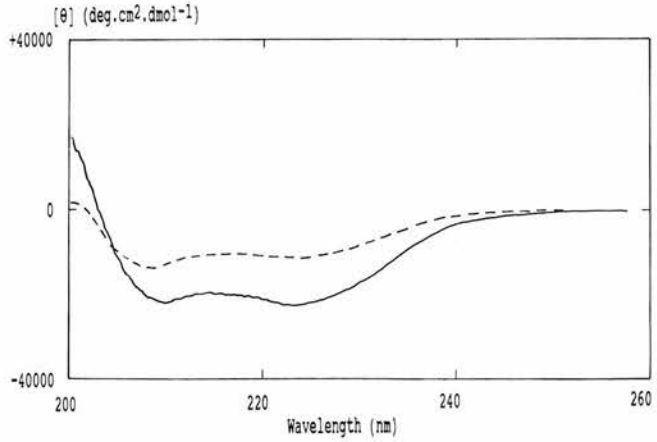

Fig. 1. Far UV CD spectra of M2 peptide incorporated into liposomes. Spectra were recorded at 20°C in a cell of path length 0.02 cm (—) DOPC liposomes; (– – –) DOPG liposomes. The liposomal peptide concentrations were 0.16 and 0.27 mg/ml, respectively.

Table I

Values of molar ellipticities at 225 nm for M2 peptide incorporated into liposomes

Sample	Ellipticity at 225 nm (deg·cm^2·dmol^{-1})
M2 peptide in DOPC liposomes (20°C)	−22,260
M2 peptide in DOPC liposomes (37°C)	−21,660
M2 peptide in DOPC liposomes (20°C) plus amantadine (4 μg/ml)	−21,970
M2 peptide in DOPC liposomes (20°C) plus amantadine (12 μg/ml)	−23,190
M2 peptide in DOPG liposomes (20°C)	−11,430
M2 peptide in 0.4% (w/v) SDS	−22,840
M2 peptide in 50% (v/v) TFE	−24,440
M2 peptide in buffer (20°C)	−700

Molar ellipticity values were calculated from the observed CD spectra using a value of 110 for the mean residue weight. The error in the ellipticity values is estimated to be ± 5%.

The M2 peptide incorporated into DOPG liposomes showed a considerably reduced CD spectrum (Fig. 1 and Table I). Analysis of this spectrum by the CONTIN procedure [17] yielded unacceptably high errors of estimates of secondary structure; the methods of Chang et al. [18] and of Siegel et al. [19] yielded values of 41 and 47% α-helix, respectively, in accord with the reduced values of the ellipticity at 225 nm (Table I). These experiments demonstrate a relationship between bilayer composition and the secondary structure of the peptide. Epand et al. [23] have demonstrated that the helical content of salmon calcitonin is dependent on the percentage of phosphatidylglycerol; altering the charge state of the membrane alters the helical content of the hormone. A similar phenomenon may also be found with peptide toxins where, for example, cardiotoxin and melittin are able to modulate lipid surface curvature and polymorphism in a lipid-specific manner [24].

In summary, the transmembrane domain of M2 adopts an α-helical conformation in DOPC liposomes, and this structure is not affected by the presence of the drug, amandatine. In view of recent developments in the study of M2 protein, these results answer the questions raised regarding M2 in bilayers [9,14,22], and help to explain its structural mechanism.

Acknowledgements: These measurements were carried out on the Scottish Universities CD Facility which is supported by the SERC.

REFERENCES

[1] Lamb, R.A., Zebedee, S.L. and Richardson, C. (1985) Cell 40, 627–633.
[2] Zebedee, S.L. and Lamb, R.A. (1988) J. Virol. 62, 2762–2772.
[3] Sugrue, R.J. and Hay, A.J. (1991) Virology 180, 617–624.
[4] Belshe, R.B. and Hay, A.J. (1989) J. Resp. Dis. (suppl.) 52–61.
[5] Skehel, J.J., Bayley, P.M., Brown, E.B., Martin, S.R., Waterfield, M.D., White, J.M., Wilson, I.A. and Wiley, D.C. (1982) Proc. Natl. Acad. Sci. USA 79, 968–972.
[6] Martin, K. and Helenius, A. (1991) Cell 67, 117–130.
[7] Sugrue, R.J., Bahadur, G., Zambon, M.C., Hall-Smith, M., Douglas, A.R. and Hay, A.J. (1990) EMBO J. 9, 3469–3476.
[8] Hay, A.J., Wolstenholme, A.J., Skehel, J.J. and Smith, M.H. (1985) EMBO J. 4, 3021–3024.
[9] Pinto, L.H., Holsinger, L.J. and Lamb, R.A. (1992) Cell 69, 517–528.
[10] Duff, K.C. and Ashley, R.H. (1992) Virology (in press).
[11] Deisenhofer, J., Epp, O., Miki, K., Huber, R. and Michel, H. (1985) Nature 318, 618–624.
[12] Allen, J.P., Feher, G., Yeates, T.O., Komiya, H. and Rees, D.C. (1987) Proc. Natl. Acad. Sci. USA 84, 6162–6166.
[13] Roth, M., Lewit-Bentley, A., Michel, H., Deisenhofer, J., Huber, R. and Oesterhelt, D. (1989) Nature 240, 659–662.
[14] Hay, A.J. (1989) in: Concepts of Viral Pathogenesis III (Notkins, A.L. and Oldstone, M.B.A. eds.) pp. 361–367, Springer Verlag, New York.
[15] Ito, T., Gorman, O.T., Kawaoka, Y., Bean, W.J. and Webster, R.J. (1991) J. Virol. 65, 5491–5498.
[16] Sizer, P.J.H., Miller, A. and Watts, A. (1987) Biochemistry 26, 5106–5113.
[17] Provencher, S.W. and Glöckner, J. (1981) Biochemistry 20, 33–37.
[18] Chang, C.T., Wu, C.-S. C. and Yang, J.T. (1978) Anal. Biochem. 91, 13–31.
[19] Siegel, J.R., Steinmetz, W.E. and Long, G.L. (1980) Anal. Biochem. 104, 160–167.
[20] Markwell, M.K., Haas, S.M., Tolbert, N.E. and Bieber, L.L. (1981) Methods Enzymol. 72, 269–303.
[21] Hayden, F.G. and Hay, A.J. (1992) Curr. Topics Microbiol. Immunol. 176, 119–130.
[22] Hay, A.J., Zambon, M.C., Wolstenholme, A.J., Skehel, J.J. and Smith, M. H. (1986) J. Antimicrob. Chemother. 18 (suppl.), 19–29.
[23] Epand, R.M., Epand, R.F., Orlowski, R.C., Boni, L.T. and Hui, S.W. (1983) Biochemistry 22, 5074–5084.
[24] Batenburg, A.M. and de Kruijff, B. (1988) Biosci. Rep. 8, 299–307.

Biochimica et Biophysica Acta, 1145 (1993) 149–156

BBAMEM 75860

The location of amantadine hydrochloride and free base within phospholipid multilayers: a neutron and X-ray diffraction study

K.C. Duff [a], A.J. Cudmore [a] and J.P. Bradshaw [a,b]

[a] *Department of Biochemistry, University of Edinburgh, Edinburgh (UK) and* [b] *Department of Preclinical Veterinary Sciences, University of Edinburgh, Edinburgh (UK)*

(Received 6 May 1992)
(Revised manuscript received 19 October 1992)

Key words: Amantadine free base; Amantadine hydrochloride; Phospholipid multilayer; X-ray diffraction; NMR, ^{2}H-

Concomitant neutron and X-ray studies were undertaken in order to locate accurately the anti-influenza and Parkinson's disease drug amantadine in multilayers of 1,2-dioleoyl-*sn*-glycero-3-phosphocholine. The X-ray data were phased using the swelling series method and the neutron data were phased using D_2O/H_2O exchange and a variation of the isomorphous replacement technique. The sets of data complement each other and reveal two populations of amantadine within the bilayer. One site is close to the bilayer surface, the other is much deeper. The majority of the amantadine occupies the surface site. The relative occupancy, but not the position, of the two locations appears to be dependent upon the initial protonation state of the drug. No evidence of bilayer perturbation was observed with either the protonated or the deprotonated forms of amantadine.

Introduction

Amantadine (1-aminoadamantane hydrochloride) is licensed for the prophylaxis of influenza A infection and for treatment of both influenza and Parkinson's disease [1,2]. In the case of influenza, the efficacy of amantadine is postulated to involve interruption of viral-host cell membrane fusion and/or interference in haemagglutinin maturation [3,4]. The mechanism of action of amantadine in Parkinson's disease is probably related to its ability to increase presynaptic synthesis and release of dopamine. This effect is potentiated by the drug inhibiting dopamine reuptake [5]. These therapeutic processes are thought to include the involvement of the hydrophobic, lipophilic properties of the molecule [6].

Amantadine studies undertaken so far have been wide-ranging, including its effect on influenza infection and, more recently, its specific molecular effect on the viral protein which is implicated in this drug-induced prophylaxis, namely M2 [7]. A recent study has examined the role of amantadine in the stabilisation of clathrin-coated membrane vesicles, similar to those formed upon initial viral penetration by influenza, Semliki Forest and vesicular stomatitus virus [6]. However, other authors have reported that, although tromantadine (an amantadine derivative: *N*-1-adamantyl-*N*-[2-(dimethylamino)ethoxy]acetamide hydrochloride) appears to stabilise phospholipid bilayers, amantadine itself slightly lowers the temperature of the bilayer to hexagonal phase transition. Also, NMR studies have shown that amantadine is perturbing to the organisation and motional properties of phospholipids in the bilayer phase [8]. These results indicate an amantadine-mediated increase in disorder. It can therefore be seen that a certain degree of ambiguity exists in the available data.

As a prerequisite of further mechanistic studies of amantadine, we have undertaken a series of experiments to investigate the location of the drug within bilayers of 1,2-dioleoyl-*sn*-glycero-3-phosphocholine (DOPC). To reduce possible ambiguity in the results a single lipid species was used, DOPC being the most physiologically representative. We have also examined any differences between amantadine hydrochloride (HCl) and amantadine in its free base form (FB).

This report describes the use of a specific deuterium labelling technique to locate amantadine in synthetic multilayer membranes using neutron diffraction. These

Correspondence to: J.P. Bradshaw, Department of Biochemistry, University of Edinburgh, Hugh Robson Building, George Square, Edinburgh, EH8 9XK, UK.

Abbreviations: amantadine FB, 1-amino adamantane free base; amantadine HCl, 1-amino adamantane hydrochloride; DOPC, 1,2-dioleoyl-*sn*-glycero-3-phosphocholine; DOPE, 1,2-dioleoyl-*sn*-glycero-3-phosphoethanolamine; NMR, nuclear magnetic resonance spectroscopy; rh, relative humidity.

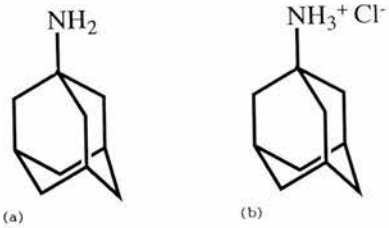

Fig. 1. The two forms of 1-aminoadamantane used in this study: (a) amantadine free base, (b) amantadine hydrochloride.

results are both quantitatively and qualitatively supported by a concomitant X-ray diffraction study using unlabelled amantadine.

Materials and Methods

1,2-Dioleoyl-*sn*-glycero-3-phosphocholine (DOPC) was purchased from Sigma (Fancy Road, Poole, UK) and confirmed to be a single species by thin-layer chromatography. Amantadine was obtained from the same source in both free base and hydrochloride forms (Fig. 1). Deuterated amantadine FB was obtained from Dr. M.R. Alecio of the Shell Research Centre (Sittingbourne, Kent, UK).

X-ray diffraction

Oriented phospholipid bilayer stacks were prepared as follows. Samples comprising 5 mg of DOPC with or without 5% (mol) amantadine were dissolved in methanol and applied to a curved glass support of approx. 1 cm^2 area. The solvent was allowed to evaporate before the slide was dried in vacuo for 2 h. Subsequently, the samples were hydrated for at least 2 h at 20°C and 100% humidity. Once fully hydrated, the samples were transferred to the sample cell of the X-ray camera.

For at least 1 h before and subsequently throughout the diffraction experiment, the samples were held in a purpose built environmental cell which allowed the temperature and humidity of the sample to be controlled. Temperature control was achieved by circulating water from a thermostat bath through tubes in the brass walls of the cell; all samples were run at 20°C at which DOPC adopts the L_α-phase. The humidity, and therefore the bilayer spacing, was controlled by passing air through containers of saturated salt solutions and then through the sample cell. Saturated solutions of $ZnSO_4$ (90% rh), KCl (81% rh), NaCl (74% rh) and NaBr (57% rh) were used in addition to distilled water (98% rh).

In the camera used to produce the diffraction patterns, 0.3 mm collimated, Nickel filtered copper K_α radiation of 1.54 Å from a Marconi-Elliot GX-13 rotating anode X-ray generator was scattered by the sample onto a pack of four 130 × 180 mm Agfa-Gevaert Osray X-ray films positioned 175 mm from the sample. The diffracted beam path was evacuated to reduce background noise from air-scattered radiation. To record the complete range of intensities without exceeding the films' dynamic range, each sample was exposed twice, typically for 20 h followed by a separate 4 min exposure. The developed films were scanned on a Joyce Loebl Chromoscan 3 microdensitometer.

Neutron diffraction

Sample preparation was essentially the same as described for the X-ray experiments, with the exception that each sample was 20 mg in weight and prepared on a quartz microscope slide. D_2O/H_2O exchange was achieved by dehydrating the samples in vacuo before re-equilibration over the new solvent.

Neutron diffraction data were collected using the D16 instrument at the Institut Max von Laue - Paul Langevin, Grenoble, France. After rehydration the quartz slide bearing its oriented multi-bilayer phospholipid sample was placed in the temperature controlled cell of the instrument along with water baths containing either D_2O or H_2O where it was allowed a further period of equilibration of 0.5–1 h. During this period the equilibration process was monitored by recording the angular position of the third or fourth order of lamellar diffraction which increased as the multilayers dehydrated and decreased as they took up water from the atmosphere. Each sample was judged to have achieved equilibrium when there was no further shift in the position of the Bragg peaks and the calculated lamellar repeat distance was that predicted for the experimental conditions by previous X-ray work. Any sample which did not fulfil both of these criteria was discarded. Each recorded diffraction pattern consisted of at least eight well defined orders. The mosaic spread of each sample was determined using the D16 software.

X-ray data analysis

The background scattering level was estimated by measuring the optical density of each X-ray film in the region immediately adjacent to a diffraction peak and interpolating across its base. Any peaks in which the dynamic range of the film had been exceeded were ignored. After integration of the diffracted intensities the films were scaled together using overlapping peaks and averaged to obtain the final set of intensities. A Lorentz factor was applied to take into account the spreading of the intensity in reciprocal space and the sampling of the peaks by the Ewald sphere. The diffraction peaks were discrete and well defined and were restricted to the meridional region of the film. In such situations, the Lorentz factor takes the form of $\sin(2\theta_h)$, where θ is the Bragg angle and h the order of diffraction. A further correction was applied for absorption of the incident and diffracted beams by the

lipid film [9]. Data sets of Bragg intensities (I_h) were scaled to each other using the expression:

$$\Sigma I_h = D/D_{\min}$$

where D is the Bragg spacing (bilayer repeat distance) and $D_{\min}$ represents the minimum Bragg spacing of a series run at different humidities.

D for each sample was determined using the Bragg equation. The instrument offset angle for each sample was calculated by iterative least squares regression of this equation over all observed orders of diffraction.

Neutron data analysis

Once the diffracted intensities had been corrected for detector response and background then integrated, the following corrections were applied:

(1) Acceptance angle. The projection of the quartz slide along the normal to the neutron beam is dependent upon its relative angle to the beam. If the slide presents a very low angle (θ) to the incident beam, it only samples a small fraction of the total neutron beam width and, therefore, flux. This means that the diffraction peaks recorded for the lower orders will be correspondingly weaker than if the slide were able to sample the whole width of the neutron beam. As long as the neutron beam is wider than the maximum projected width of the sample slide and the neutron flux constant across the width of the beam, the angular correction factor, takes the form:

$$C_{\mathrm{Ang}(h)} = 1/\sin\,\theta_h$$

(2) Lorentz factor. For the geometry used in this study, the appropriate correction factor is:

$$C_{\mathrm{Lor}(h)} = \sin(2\theta_h)$$

(3) Absorption. When the angle of diffraction is low, the incident and diffracted beam have a significant path length within the sample and thus will be subject to a greater degree of absorption than when the angle is high and the corresponding path lengths low. Moreover, the degree of absorption will also be affected by the H_2O/D_2O composition of the sample. The appropriate correction for absorption by the lipid film, was applied:

$$C_{\mathrm{Abs}(h)} = 1/(\sin\,\theta/2ut)(1 - \exp[-2ut/\sin\,\theta])$$

where $u = (6.04–0.75d)$, d being the mole fraction of D_2O [10]. The mass of lipid on each slide, the area over which it was spread and the unit cell size, as determined by diffraction, were used to calculate a value of 30 μm for t, the thickness of the lipid film.

(4) Sampling by the detector. As a result of lattice disorder in the sample, the diffraction peaks may be so wide that the whole of each diffraction peak is not recorded by the detector, and a correction must be applied to the data to account for this. In this study the mosaic spread of each sample was small enough to ensure that each diffraction peak was regular in shape and contained wholly within the central part of the detector so no correction was applied in this case.

The final neutron structure factor amplitudes were therefore calculated as:

$$F_h^2 = I_h \cdot C_{\mathrm{Ang}(h)} \cdot C_{\mathrm{Lor}(h)} \cdot C_{\mathrm{Abs}(h)}$$

Phasing

Electron density or neutron scattering profiles may only be obtained upon solving the individual phases of the recorded amplitudes. In this study three different techniques were employed to phase the data sets: swelling series, D_2O/H_2O exchange and isomorphous replacement.

The X-ray structure factors were phased using a five point swelling series [11]. Our methodology comprised of selecting from the swelling series one working set of eight diffraction peaks and using this to compute a continuous transform [12] against which the fit of all the other observed sets were compared. The best fit minimised the difference between the calculated and the observed intensities for each of the possible 256 phase combinations. The selected working set alternated until all five had been used and sampled against. The resulting transform represented the best, integrated fit for all data over all possible phases. This process was carried out independently for the DOPC, DOPC/amantadine HCl and DOPC/amantadine FB swelling series.

Neutron data are routinely phased by carrying out experiments hydrated at various H_2O/D_2O ratios [9,10,13,14]. This method was used in the present study, with additional phasing information coming from a variation of the isomorphous derivative technique [15] in which use was made of the presence or absence of amantadine in the multilayers. Assigning phases to the neutron data proceeded by altering the sign of the individual structure factors until a result was achieved in which both the differences caused by replacing H_2O with D_2O and the DOPC/amantadine minus DOPC differences were consistent within each set of comparable data.

The two techniques, using X-rays and neutrons, emphasise different features within the bilayer structure, and further confirmation that the correct phases had been assigned was given by the fact that the two methods agreed and thereby showed the complementary nature of the techniques.

White and his co-workers [16] have produced an elegant method for scaling neutron data. This approach was used in the present study and basically involved using the size of the D_2O and the amantadine distributions to scale the different sets of data to each other. The results put the profiles on a 'relative absolute' scale in which they are scaled with respect to the unit cell contents, but not on an absolute per volume scale. The method is also readily applicable to X-ray data, although for this there is no equivalent of the D_2O peak therefore scaling is carried out on the size of the amantadine distribution alone.

Results

Fig. 2 is a representative X-ray diffraction pattern, in this instance obtained from DOPC with 5% (mol) amantadine FB at 90% rh. Fig. 3 shows the relationship between the relative humidity of the sample chamber and the bilayer repeat distance as observed by X-ray and neutron diffraction. Fig. 4 shows the swelling series data used to phase the X-ray diffraction patterns of pure DOPC (a), DOPC with 5% (mol) amantadine HCl (b) and DOPC with 5% (mol) amantadine FB (c). In each case the continuous transform calculated from 98% rh data is shown superimposed upon the observed diffraction amplitudes for 98, 90, 81, 74 and 57% rh. Table I gives the corrected, scaled neutron diffraction structure factors for all three samples at 0% and 100% D_2O. Fig. 5 shows reconstructed transbilayer profiles of DOPC alone (a, b) and difference profiles calculated by subtraction of structure factor data sets of corresponding D-repeat to define the distribution of amantadine HCl (c, d) and FB (e, f), respectively.

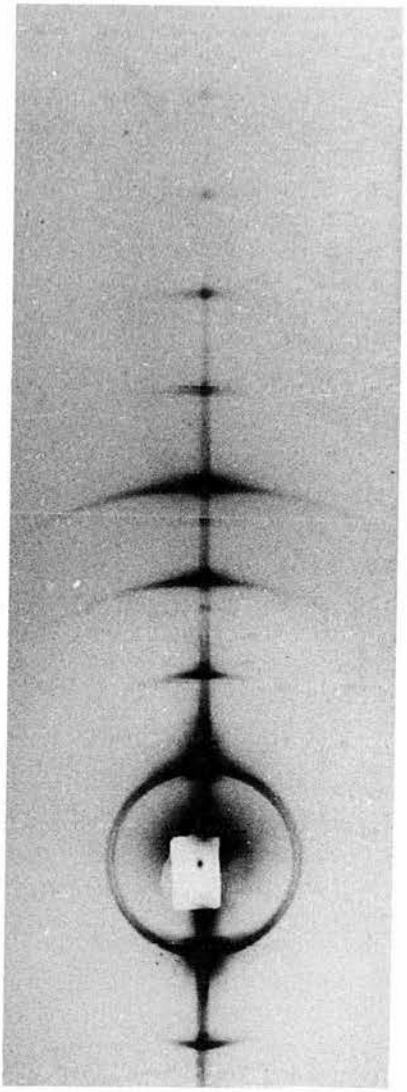

Fig. 2. X-ray diffraction pattern of lamellar arrays of DOPC with 5% (mol) amantadine FB at 90% relative humidity and 20°C.

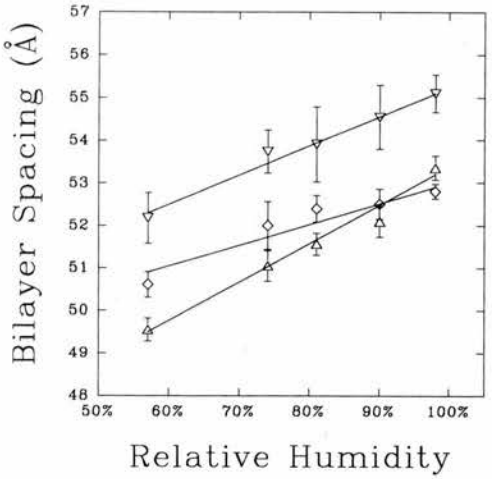

Fig. 3. The relationship between the relative humidity at 20°C of the sample and the observed bilayer spacing (in ångströms, Å). ▽, pure DOPC; △, amantadine hydrochloride; ◇, amantadine free base. The error bars represent the standard deviation for each point. Sample size varied from 3 to 9.

The mosaic spread of the DOPC bilayers ranged from 0.4° to 0.6°, these very low values being quite characteristic of unsaturated fatty acyl phospholipids. The mosaic spread was not significantly changed upon the addition of amantadine.

Discussion

DOPC

Fig. 5 displays both X-ray and neutron scattering density profiles across the phospholipid bilayer with the water component occupying the outer region of the graphs. With X-rays, the DOPC profile (a) agrees with previously published data [17,18] in that it displays the classic phospholipid leaflet form with a main peak representing the electron-dense region which encompasses the phosphate groups and fatty acyl ester bonds. A secondary peak appears within the hydrophobic region which corresponds to the double-bond in the oleic

acid chains. It can be seen from (b) that less detail results from the neutron data. This is probably due to the lower contrast characteristic of neutron scattering (all diffraction experiments were sampled through eight orders so this phenomenon does not involve the X-ray data being collected to a higher resolution than the neutron).

The differences between the X-ray and neutron profiles are due to inherent atomic scattering differences across the unit cell. X-rays are more strongly scattered by the phosphate groups in the repeat motif whereas maximum neutron scattering corresponds to the fatty acyl ester bond positions [19]. Profile (b) clearly displays this scattering dichotomy with the neutron data peak appearing markedly closer to the hydrophobic interior of the bilayer than the X-ray result (a). The sharper X-ray profile displays a second highly defined peak in the fatty acyl chain region of the leaflet.

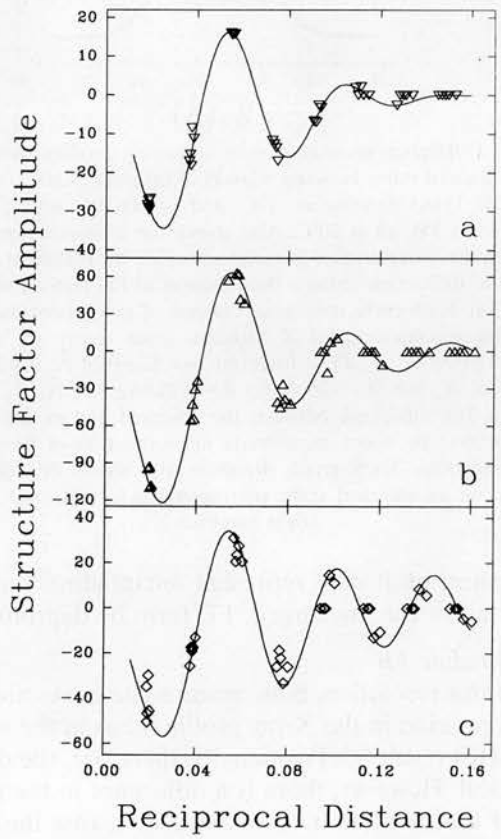

Fig. 4. Structure factors of lamellar arrays of bilayers of (a) pure DOPC, (b) DOPC with 5% (mol) amantadine HCl and (c) DOPC with 5% (mol) amantadine FB, plotted against corresponding reciprocals of Bragg spacings ($Å^{-1}$). The amplitudes of the structure factors are equal to the square roots of the Bragg intensities, their signs are those derived from the phasing procedure described in the text. The swelling series data sets were collected at 98, 90, 81, 74 and 57% relative humidity. The continuous transforms calculated from the 98% rh data is shown.

TABLE I

Relative absolute neutron structure factors of lamellar arrays of pure DOPC and DOPC with 5% (mol) amantadine HCl or FB at 98% rh and 20°C. The accuracy is estimated to be ± 0.15 units

Order	DOPC 20°C, 98%rh (D_2O)	DOPC+5 mol% amantadine HCl 20°C, 98%rh (D_2O)	DOPC+5 mol% D-amantadine FB 20°C, 98%rh (D_2O)
1	−89.31	−61.22	−96.41
2	25.56	10.02	18.80
3	−4.34	−1.68	−2.76
4	1.00	0.32	1.21
5	−2.84	−1.86	−2.97
6	0.77	0.06	0.57
7	−0.67	0.15	−0.16
8	0.00	−0.27	−0.15
Order	DOPC 20°C, 98%rh (H_2O)	DOPC+5 mol% amantadine HCl 20°C, 98%rh (H_2O)	DOPC+5 mol% D-amantadine FB 20°C, 98%rh (H_2O)
1	−6.47	−19.74	−13.55
2	−12.09	−8.66	−17.65
3	5.16	3.17	6.53
4	0.34	0.00	0.00
5	−1.44	−1.37	−1.98
6	0.33	−0.18	0.33
7	−0.30	0.26	0.00
8	0.00	−0.30	0.00

Amantadine HCl

Fig. 5. (c) to (f) are difference profiles which were calculated by subtracting the lipid component from the lipid + amantadine structure factors and therefore represent only the amantadine distribution across the bilayer. They are displayed in the same orientation as the pure DOPC but it can be seen that these profiles, both X-ray and neutron, are substantially different from the DOPC data. Amantadine, in both its hydrochloride and free base forms, appears to have been incorporated into the multilayer system.

The highest peak in the X-ray profile (c), representing the greatest distribution of amantadine HCl, lies between the phosphate and ester linkages. This surface location is also represented in the neutron (d) profile but its shape has changed with additional density encroaching into the water. It is proposed that the difference between the X-ray and neutron profiles is due to the relatively higher scattering length of nitrogen for neutrons compared to that for X-rays, which emphasises the amine group in the neutron profiles. These results therefore orientate amantadine HCl in the bilayer; the hydrophobic, cyclic region of the drug located between the phosphate and ester linkages of the phospholipids with the NH_3^+ group protruding into the water space.

This interpretation is supported by changes in the distribution of water between adjacent bilayers when amantadine HCl is added. Fig. 6 shows difference profiles representing the location of the deuterons of

heavy water, calculated by subtracting neutron scattering profiles of multi-bilayers containing H_2O from corresponding ones hydrated with D_2O. It can be seen that incorporation of amantadine HCl into the DOPC bilayers reduces the area under the water profiles, indicating that the drug is displacing some of the water from the system.

Both profiles (c) and (d) of Fig. 5 include additional features in the lipid tail region which may be caused by termination error. The resolution of the present study procludes unambiguous assignment of these features to the presence of amantadine deep within the bilayer, but it should be noted that evidence from the FB profiles (see below) indicates that full penetration of the bilayer by a proportion of the amantadine can occur. This is particularly noticeable in the neutron profiles and is either a product of the relatively high concentration of drug used saturating preferential surface sites, or it may represent amantadine which has reverted to the uncharged, FB form by deprotonation.

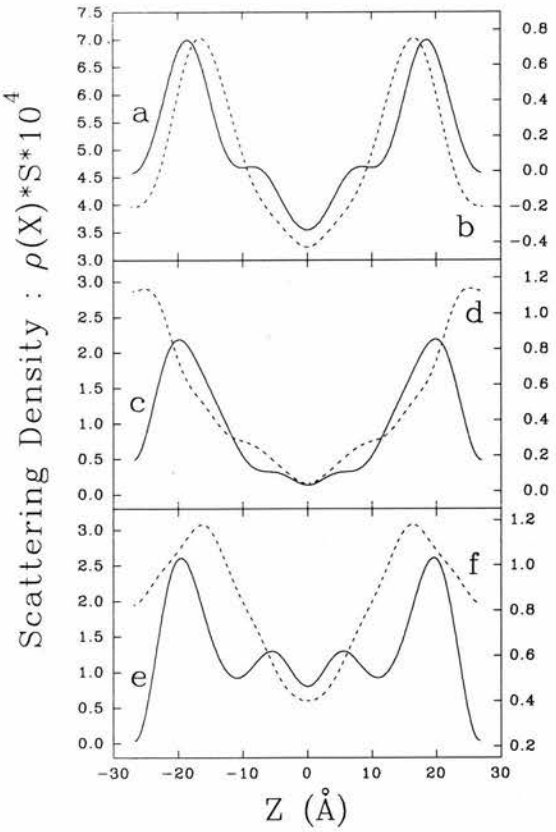

Fig. 5. Reconstructed trans-bilayer X-ray scattering profile of pure DOPC (a, left-hand scale) and neutron scattering profile of pure DOPC (b, right-hand scale) at 98% rh and 20°C. (d) and (f) are neutron scattering difference profiles of amantadine hydrochloride and amantadine free base, respectively. (c) and (e) are the corresponding X-ray scattering difference profiles. The difference profiles were calculated by subtracting structure factors of pure DOPC from those of DOPC with 5% (mol) amantadine, after correction for variations in bilayer repeat and placed on a relative absolute scale using the method of Weiner et al. [18]). The horizontal scale (Z) is distance, measured from the bilayer centre, in ångströms.

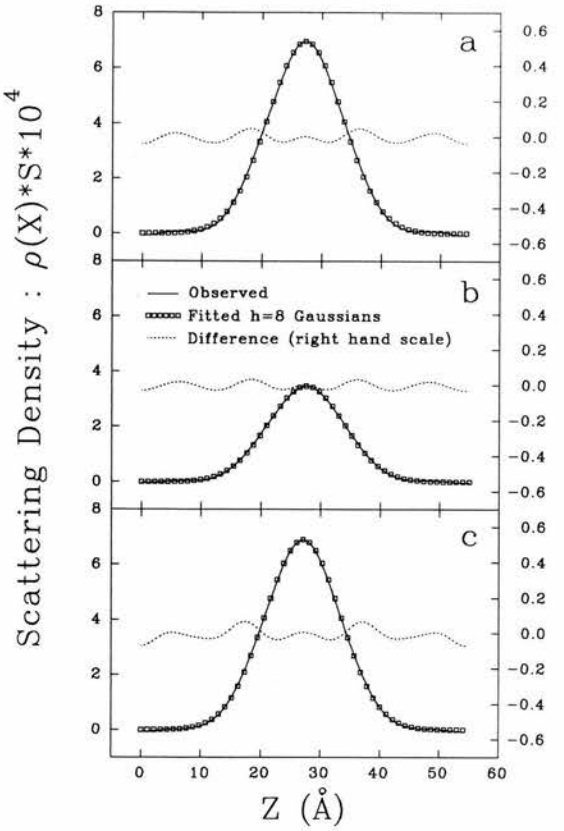

Fig. 6. Difference neutron density scattering profiles showing the distribution of water between bilayers of (a) pure DOPC, (b) DOPC with 5% (mol) amantadine HCl and (c) DOPC with 5% (mol) amantadine FB, all at 20°C. Also shown are Gaussian distributions fitted to the water profiles in reciprocal space over all eight observed orders of diffraction, using a development of the method of Wiener et al. [18]. Each curve consists of the sum of two Gaussians with the following parameters: (a) Z (distance from centre of bilayer) = $\pm 26.53 \pm 0.35$ Å, A_w (1/e halfwidth) = 8.82 ± 0.20 Å; (b) $Z = 26.04 \pm 0.55$ Å, $A_w = 8.75 \pm 0.25$ Å; (c) $Z = \pm 25.58 \pm 0.45$ Å, $A_w = 8.65 \pm 0.25$ Å. The difference between the observed and modelled water profiles may be taken as a crude approximation of error in the reconstructions. Each graph therefore also shows this difference, plotted on an enlarged scale, corresponding to that used in Fig. 5 (right-hand side).

Amantadine FB

At this resolution, both amantadine peaks are in the same position in the X-ray profile (e) as in the amantadine HCl result (c). Positionally, therefore, the data are identical. However, there is a difference in the proportional representation of amantadine across the bilayer with relatively more now appearing in the fatty acid tail region of the phospholipids. The neutron results (f) support these findings. Here the main scattering density at the surface location has moved slightly into the bilayer reflecting the fact that the amantadine FB is deuterated on the hydrophobic carbons only and that the NH_2 amine group is unlabelled and therefore scatters much less intensely compared to the labelled

mass; it can be observed as a shoulder on the water side of the main peak. This observation again orientates the amantadine with its NH_2 group at the lipid/water interface.

Profiles (e) and (f) clearly show that a proportion of amantadine has penetrated almost to the centre of the bilayer. Once again, the features in this region may represent some part of the amantadine structure, or may just be termination error. However, the height of the profiles above zero can only be explained in terms of a considerable mass of drug being present in this region. Consistent with this finding, the amount of water associated with the bilayers containing amantadine FB is much greater than that for bilayers containing amantadine HCl (Fig. 6) and almost equates with that present in the bilayers in the absence of either form of amantadine. Clearly a proportion of the drug has moved away from the water-penetrated surface of the bilayers to take up a deeper location in the bilayers. This evidence, taken together with the HCl results, leads us to propose that the interaction between amantadine and DOPC bilayers takes the form of an equilibrium between two possible regions. One of these is located at the water/bilayer interface, the other is less defined and broadly represents the fatty acid tail region. The balance of this equilibrium between the two sites appears to depend upon the starting protonation state of amantadine. However, this does not necessarily imply that the initial charge state of the amine is preserved throughout the experiment. This result compares with tetracaine where its interaction with phospholipids is also reported to be influenced by the charge state of the drug [20,21].

Amantadine–phospholipid interactions

If the optical parameters and the sample dimensions are kept constant throughout a series of diffraction experiments then the mosaic spread may be used as a measure of the macroscopic order of each sample; the smaller the mosaic spread, the less the degree of disorder of the bilayers [22,23]. The values obtained for stacked bilayers of pure DOPC in this study are in good agreement with previous observations [16,17]. The mosaic spread did not change upon the addition of 5 mol% amantadine, which indicates that the interaction between the drug and the bilayer did not disturb the macroscopic order of the system. There was no evidence of phase separation in the multilayers containing amantadine. Unfortunately, in the liquid phase, DOPC does not give discrete 4.5–4.8 Å reflections so we are unable to comment on the effect of amantadine on chain packing. We can, however, conclude that, under these experimental conditions, amantadine does not markedly perturb the bilayer system.

It has been reported that amantadine reduces the extent of dissociation of clathrin from coated vesicles [6] in a study which used relatively small amounts of the amine. The ability of amantadine and related compounds to stabilise or destabilise phospholipid bilayers has also been extensively investigated. Cheetam and Epand [8] concluded from NMR studies that amantadine perturbs the organisation and increases the fluidity of bilayers. Our present study, using a much lower drug/lipid molar ratio, does not indicate any such perturbation but it may be that this anomaly reflects the different drug concentrations used in such studies.

Another variable involves the lipid type used. The work reported here employed DOPC which has a large headgroup and two unsaturated chains giving the phospholipid a quasi-hourglass shape, creating an area of increased steric freedom in the neck region when the lipids are formed into a bilayer. The amantadine may be accomodated within such an area, fitting in between the phospholipid molecules. Our data, which indicate that the cyclic carbon component of amantadine orientates on the hydrophobic side of the phospholipid headgroup, support this model. This would suggest that the effects of amantadine upon bilayer structure and stability are likely to be complex and to be dependant upon intrinsic and environmental factors.

Fig. 2 shows that the bilayer repeat distance was reduced by up to 2.5 Å at low humidities. A similar effect is produced by the addition of 1,2-dioleoyl-*s*-glycero-3-phosphoethanolamine (DOPE) [17] to DOPC, where the smaller PE headgroup allows the choline moiety of DOPC to lie in a more perpendicular orientation and therefore closer to the plane of the bilayer surface (unpublished data). Amantadine may have a similar effect on DOPC. Unfortunately, the relatively low contrast between the PC headgroup and water makes it impossible to determine the headgroup conformation with the present data. However, this does mean that any drug-induced changes in headgroup conformation will not have an adverse effect on the profile subtractions. Future neutron work using specifically deuterated phospholipid headgroups may be able to resolve this question.

Our finding that uncharged, amantadine FB has the ability to penetrate more easily into the bilayer is supported by diffusion data performed on other similar compounds [24]. This phenomenon could be related to the zwitterionic nature of DOPC, the lipid chosen for our study. Further work will investigate the possible relationship between the lipid composition of the bilayer and the nature of its interaction with amantadine. For example, including a proportion of negatively-charged lipid may induce major changes [25] particularly with the charged amantadine HCl.

Acknowledgements

The deuterated amantadine was prepared by Dr. M.R. Alecio (Shell Research Centre, Sittingbourne,

UK) who also read and made helpful comments on the manuscript. Neutron data collection and initial reduction were performed on instrument DI6 at the Institut Max von Laue - Paul Langevin, Grenoble, France. The work was supported by both SERC and ILL grants.

References

1 Oxford, J.S. and Galbraith, A. (1980) Pharmacol. Therap. 11, 181–262.
2 Obeso, J.A. and Martinez-Lage, J.M. (1987) in: The Handbook of Parkinson's Disease (Koller, W.C., ed.), pp. 312–316, Marcel Dekker, New York.
3 Hay, A.J. (1989) in Concepts in Viral Pathogenesis, Vol. 3, pp. 561–567, Springer-Verlag, New York.
4 Sugrue, R.J., Bahadur, G., Zambon, M.C., Hall-Smith, M., Douglas, A.R. and Hay, A.J. (1990) EMBO. J. 9, 3469–3476.
5 Gilman, A.G., Rall, T.W., Nies, A.S. and Taylor, P. (1990) The Pharmaceutical Basis of Therapeutics, 8th Edn., pp. 472–473, Pergamon Press, New York.
6 Phonphok, Y. and Rosenthal, K.S. (1991) FEBS Lett. 281, 188–190.
7 Sugrue, R.J. and Hay, A.J. (1991) Virology 180, 617–624.
8 Cheetham, J.J. and Epand, R.M. (1987) Biosci. Rep. 7, 225–230.
9 Franks, N.P. and Lieb, W.R. (1979) J. Mol. Biol. 133, 469–500.
10 Worcester, D.L. and Franks, N.P. (1976) J. Mol. Biol. 100, 359–378.
11 Torbet, J. and Wilkins, M.H.F. (1976) J. Theor. Biol. 62, 447–458.
12 Lesslauer, W., Cain, J.J. and Blaisie, J.K. (1972) Proc. Natl. Acad. Sci. USA 69, 1499–1503.
13 Büldt, G., Gaily, H.U., Seelig, J. and Zaccai, G. (1979) J. Mol. Biol. 134, 673–691.
14 Jacobs, R.E. and White, S.H. (1989) Biochemistry 28, 3421–3437.
15 Büldt, G., Gaily, H.U., Seelig, A., Seelig, J. and Zaccai, G. (1978) Nature 271, 182–184.
16 Weiner, M.C., King, G.I. and White, S.H. (1991) Biophys. J. 60, 568–576.
17 Bradshaw, J.P., Edenborough, M., Sizer, P.J.H. and Watts, A. (1989) Biochim. Biophys.. Acta 987, 101–110.
18 Weiner, M.C. and White, S.H. (1991) Biochemistry 30, 6997–7008.
19 Franks, N.P. and Lieb, W.R. (1981) in Liposomes: From Physical Structure to Therapeutic Applications (Knight, ed.), pp. 243–272, Elsevier/North-Holland Press, Amsterdam.
20 Smith, I.C., Auger, M. and Jarrell, H.C. (1991) Ann. NY. Acad. Sci. 625, 668–684.
21 Shinooka, T., Shibata, A. and Terada, M. (1992) Biochim. Biophys. Acta. 1104, 261–268.
22 Schwartz, S., Cain, J.E., Dratz, E.A. and Blasie, J.K. (1975) Biophys. J. 15, 1201–1233.
23 Blaurock, A.E. and Nelander, J.C. (1976) J. Mol. Biol. 103, 421–431.
24 Miller, D.K. and Lenard, J. (1981) Proc. Natl. Acad. Sci. USA. 78, 3605–3609.
25 Kim, J., Mosior, M., Chung, L.A., Wu, H. and McLaughlin, S. (1991) Biophys. J. 60, 135–148.

VIROLOGY 190, 485–489 (1992)

The Transmembrane Domain of Influenza A M2 Protein Forms Amantadine-Sensitive Proton Channels in Planar Lipid Bilayers

K. C. DUFF[1] AND R. H. ASHLEY

Department of Biochemistry, University of Edinburgh, George Square, Edinburgh EH8 9XD, U.K.

Received March 12, 1992; accepted June 2, 1992

In a direct test of the hypothesis that the M2 coat protein of influenza A can function as a proton translocator, we incorporated a synthetic peptide containing its putative transmembrane domain into voltage-clamped planar lipid bilayers. We observed single proton-selective ion channels with a conductance of ~10 pS at a pH of 2.3, consistent with the association of several monomers around a central water-filled pore. The channels were reversibly blocked by the anti-influenza drug amantadine. These experiments imply a central role for M2 protein in virus replication and assembly and may explain the mechanism of action of amantadine. Analogous proteins may have a similar function in other viruses, and these may be susceptible to similar antiviral agents.

The surface of the influenza virus has been the focus of extensive research, leading to elucidation of the structure of the external spike proteins, hemagglutinin (HA) and neuraminadase (NA) (*1, 2*). Our knowledge of other viral envelope and interior proteins is much less complete (*3*). Several virus-coded proteins are present in infected cells (*4*), including M2. This protein is expressed on the cell surface during viral synthesis (*4*) and has recently been identified in virus particles (*5*). It is a homotetramer of 96 amino acid subunits which associate as a pair of membrane-spanning disulphide-linked dimers (*6*), and it has been suggested that the protein forms a proton-conducting pore (*7*). Proton translocation by M2 may be important during two separate phases of the viral cycle (*8*). Following endocytosis of the virus, and concomitant with pH-induced fusion between the endosomal and viral membranes mediated by HA (*9*), M2 may conduct protons into the interior of the virus, leading to uncoating, the release of ribonucleoprotein from the matrix protein (M1), and eventual nuclear infection (*10*). M2 may also facilitate viral synthesis and assembly when HA is transported to the cell surface in post-Golgi vesicles (*11*). Even minor acidification of these vesicles by cellular proton pumps is undesirable as the structure of HA might be compromised; this may be countered by M2 incorporated into the vesicle membrane. The relative importance of these effects, which occur at different stages in the viral cycle, will depend on the particular viral strain (*8*). Importantly, influenza A is thought to become resistant to amantadine (1-aminoadamantane hydrochloride), the only registered drug used in the prophylaxis and treatment of influenza infections, via single amino acid substitutions in the putative membrane-spanning domain of M2 (*12*).

In order to test the hypothesis that M2 protein can in fact act as a proton channel, a synthetic 25-residue peptide corresponding to the predicted transmembrane sequence common to several strains of influenza A (*13*) (Fig. 1a) was incorporated into voltage-clamped planar lipid bilayers. The peptide was synthesized in the MRC Cellular Immunology Unit, Oxford, U.K., purified by reverse-phase HPLC and subjected to confirmatory sequencing in the WelMet Unit, University of Edinburgh, U.K. Bilayers formed spontaneously at room temperature after decane suspensions of a mixture of palmitoyl-oleoyl phosphatidylethanolamine and palmitoyl-oleoyl phosphatidylserine (Avanti), each 15 mg/ml, were cast across a 0.3 mm hole in a polystyrene partition separating two solution-filled chambers designated *cis* and *trans* [e.g., (*14*)]. Both chambers contained 600 μl of 50 m*M* glycine–HCl, pH 2.3, unless otherwise indicated, which could be changed by perfusion (usually replacing the contents of the *trans* chamber with 50 m*M* glycine–HCl, pH 3.0). For simplicity we have not corrected salt concentrations for activity and have assumed throughout that $a_{H+} = 1.0$. The *cis* chamber was voltage-clamped (Biologic RK-300 patch clamp) at a range of holding potentials relative to the *trans* chamber, which was grounded. The bilayers were monitored by measuring their capacitance (~250 pF) and those used had resistances of at least 10^{11} Øhm. Unit transmembrane currents were usually seen within 30 min of adding up to 1 μg of the hydrophobic peptide in 6 μl of MeOH to the *cis* compart-

[1] To whom reprint requests should be addressed.

0042-6822/92 $5.00

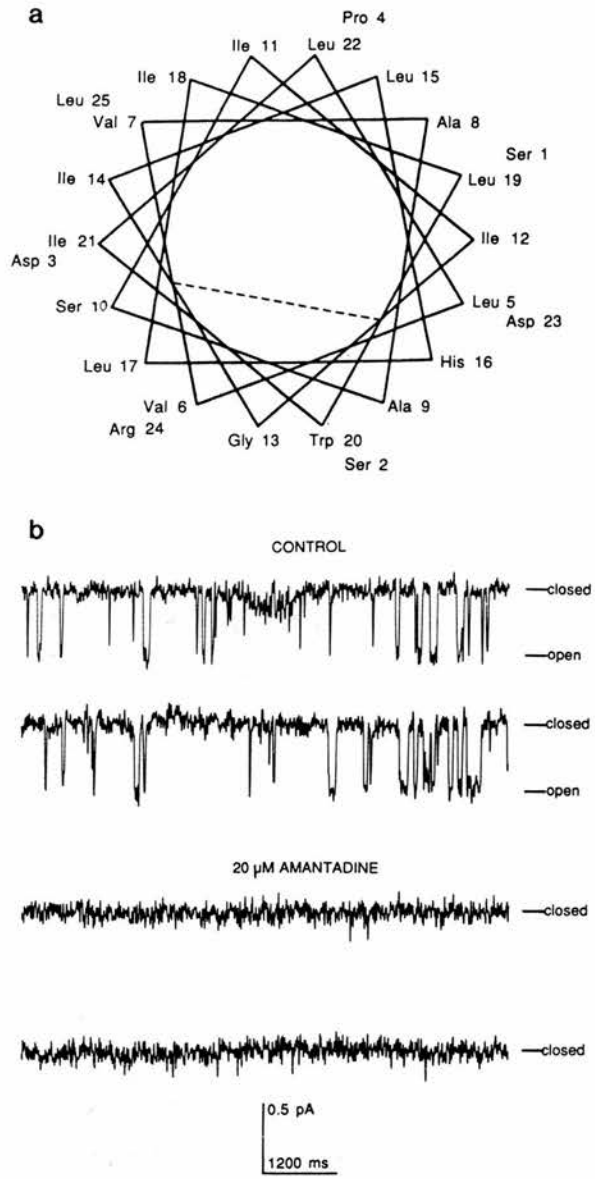

FIG. 1. (a) Sequence of synthetic 25-residue peptide containing the putative transmembrane domain of M2 protein (inner ring) with adjoining extramembrane residues. The helical wheel projection (*16*) is oriented with the strongly hydrophobic intramembrane sector above the dotted line. (b) Single-channel currents (downward deflexions) across a planar lipid bilayer with incorporated synthetic peptide, inhibited by 20 μM amantadine HCl (added to both sides of the membrane). Holding potential +100 mV, glycine–HCl, pH 2.3, *cis* and *trans*.

ment, and their appearance could be accelerated by breaking and reforming the membrane. Control bilayers exposed to 1% (v/v) MeOH in the same buffer remained stable for up to 3 hr and exhibited no channel-like activity. As another technical control, the 26-residue channel-forming peptide mellitin (*15*) was incorporated in the same manner into similar bilayers exposed to 50 mM glycine–HCl containing up to 300 mM NaCl or KCl. The pH was varied between 2.3 and 5.7. Mellitin channels became incorporated preferentially at low pH, were markedly anion-selective, and were insensitive to amantadine (results not shown). Overall approximately 6 hr of M2 channel data were recorded on magnetic tape or computer disc and analyzed using Axotape and PClamp software (Axon Instruments). Data were filtered with either an eight-pole Bessel low-pass analogue filter (−3 dB at 0.03 kHz, Frequency Devices) or, where indicated, a digital Gaussian filter (0.1 kHz).

Single-channel currents were obtained in more than 50 independent experiments and typical examples are shown in Fig. 1b. The channels were blocked within 30 sec by 20 μM amantadine (e.g., Fig. 1b). In several experiments the contents of both bilayer chambers were replaced by extensive perfusion with fresh buffer after amantadine block and channel activity was restored on each occasion. Four and a half minutes of the illustrated pre-amantadine recording were inspected to identify discrete openings which were collected in a frequency histogram (Fig. 2). The open lifetimes have been fitted to a single exponential distribution with a mean open time (τ_0) of 20 msec. The recording bandwidth limited our open time resolution to events lasting at least 8 msec (e.g., Fig. 2, inset), and typically only relatively few events (<1000) could be collected (effectively confining any numerical kinetic analysis to just one component). Lifetime analysis is,

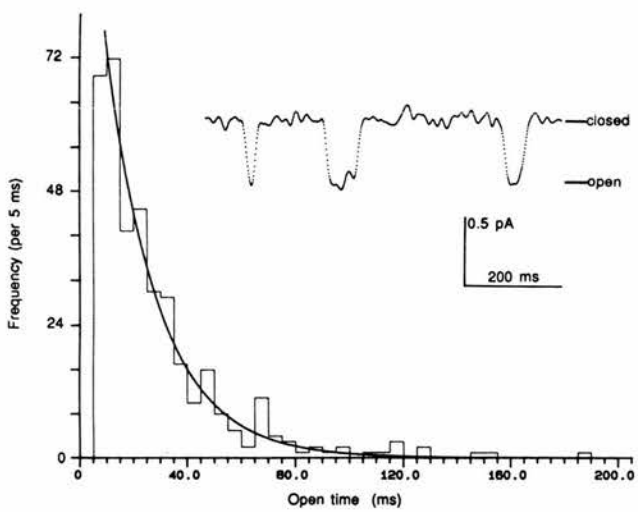

FIG. 2. Frequency distribution of all the openings collected from 4.5 min of pre-amantadine recording (with typical events in more detail). The smooth curve is a single exponential function with a time constant of 20 msec. Data were low-pass filtered at 0.1 kHz (digital Guassian filter) and events lasting <4 msec were discarded. In addition, the contents of the first bin were excluded from the fit.

however, consistent with a model for channel formation of the general type

$$4p \underset{\alpha}{\rightleftharpoons} p_4,$$

where incorporated peptides (p) associate briefly to form an oligomeric channel (here shown as a tetramer) and α, the rate constant for channel closure, is ~50 per second ($1/\tau_0$). Limited observations of single-channel currents in bilayers of the same lipid composition exposed to the same buffers at similar temperatures suggested that α was, as expected, independent of peptide concentration (40 ± 13 per second, mean ± SD, $n = 4$ independent experiments). Closed lifetime distributions, on the other hand, appeared to contain at least two exponential components, with mean lifetimes of about 10 msec and about 1 sec, respectively. Because of the small numbers of events these analyses are not detailed here, and the absolute values of the closed-state lifetimes varied considerably between experiments, as would be expected for different peptide concentrations. However, the constant finding of more than one component is consistent with the formation of clusters of peptides (e.g., tetramers), with short "intraburst" intervals reflecting the temporary dissociation of one monomer within a given group and longer "interburst" intervals corresponding to more extensive disruption. Of course, with higher peptide concentrations, bursts of channel activity tended to overlap to give openings to more than one unit current level (as described later). It was noted that channel activation showed little obvious voltage-dependence.

The membrane lipid composition and bathing solutions were varied to optimize channel incorporation and increase the amplitudes of single-channel currents. Bilayer stability was always monitored before adding the peptide. Diphytanoylphosphatidylcholine (Avanti) bilayers were exceptionally stable at low pH even when voltage-clamped at high potentials (up to ±150 mV), but the rate of channel incorporation was poor. The use of mixtures of phosphatidylethanolamine and phosphatidylserine greatly increased the rates of channel formation. These bilayers were sometimes unstable when exposed to a pH below ~1.0, and therefore the pH was only exceptionally reduced below 2.3 (Figs. 3a, 4a). Peptide incorporation increased markedly on addition of >10 μg/ml but this usually resulted in the appearance of multichannel currents (up to 50 pA) which were difficult to analyze. Occasionally distinct conductance levels could still be resolved and in the experiment shown in Fig. 3a current transitions appear to occur between the closed level (which is more obvious after the application of amantadine) and several open levels. The amplitude

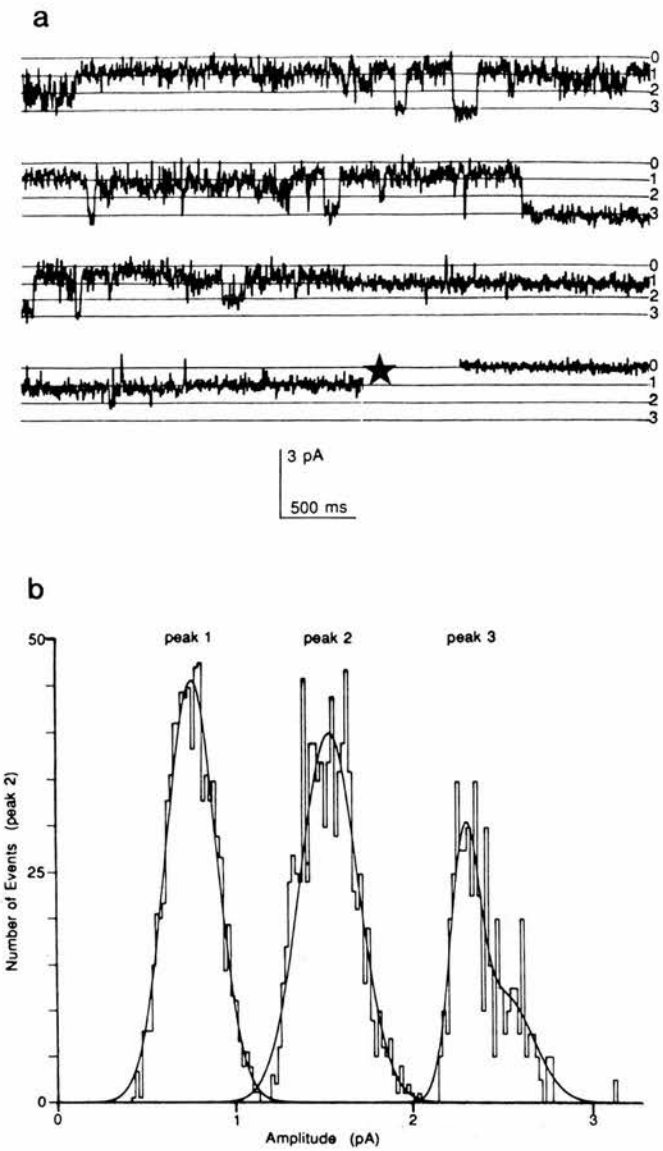

FIG. 3. (a) Current transitions in a peptide-containing bilayer voltage-clamped at +80 mV. The bilayer was formed in 25 m*M* TrisCl (pH 7.0) and the pH of the *cis* solution was then lowered to 1.0 by adding HCl. Downward proton currents flow *cis* to *trans*. Amantadine (20 μ*M*), added to both chambers where indicated (*), confirmed the zero-current level (0). Openings have been assigned to three marked current levels. Filtered at 0.1 kHz. (b) Amplitude histogram from 100 sec of contiguous data. Transitions from the marked levels which lasted <4 msec were ignored. Main peaks 1 and 2 were each fitted to a single Gaussian, and peak 3 to two Gaussian distributions. Peaks 1:2:3 have been rescaled in the ratio 9:5:2 to share the same axes.

histogram (Fig. 3b) shows three main equally spaced peaks, consistent with the simultaneous formation of up to three channels in this bilayer. The third peak is not a single Gaussian, suggesting that some large events of ~2.6 pA arose by a different mechanism

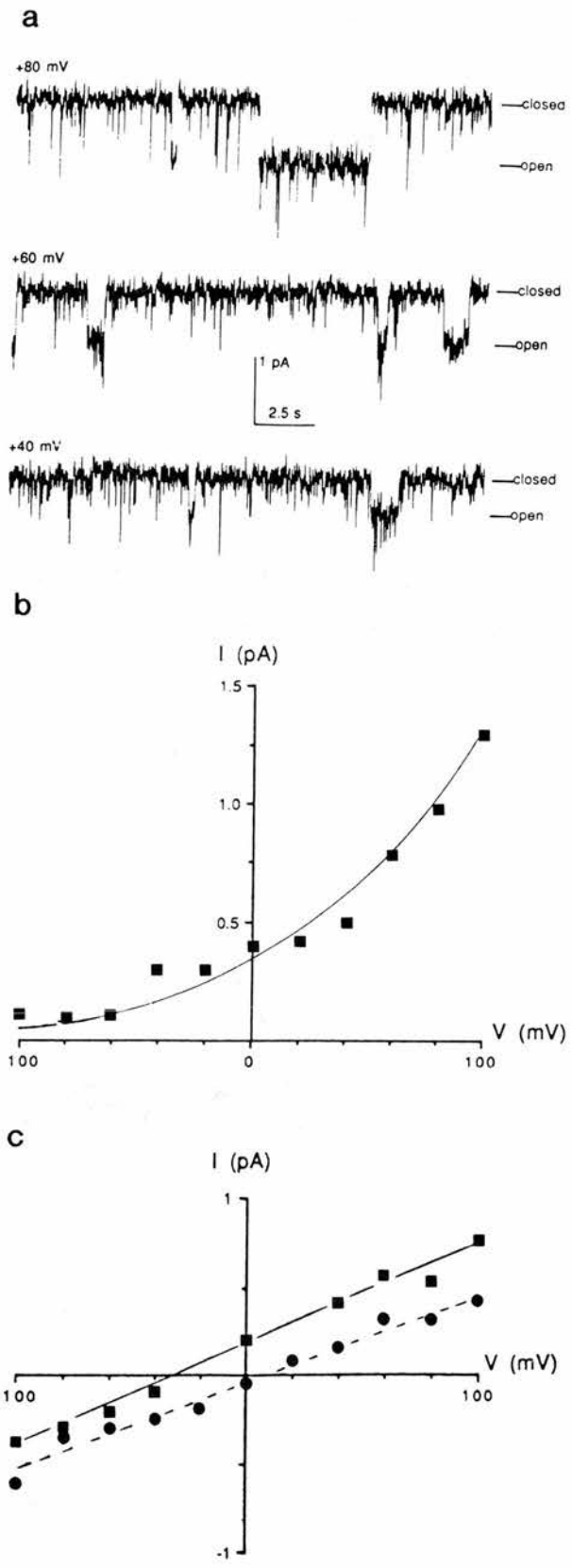

FIG. 4. (a) Single-channel currents (downwards deflexions) across a peptide-containing bilayer voltage-clamped at the indicated holding potentials with 50 m*M* KCl both *cis* and *trans*, pH 1.5 and 7.0, respectively (adjusted with HCl or KOH). (b) Current/voltage (I/V) relationship from the same experiment. The smooth curve is a best-fit to the Goldman–Hodgkin–Katz current equation (*18*) (assuming only protons are significantly permeant under these conditions). (c) I/V relationships from an experiment with glycine–HCl *cis* and *trans*, pH 2.3 and 3.0, respectively (■), and after exchanging the *trans* solution by perfusion with 3.0 *M* NaCl (pH 7.0) (●). The lines are fitted by linear regression and the reversal potential shifts from −34 mV to +10 mV. (Each figure is representative of at least four similar experiments.)

(possibly ion channels formed from higher oligomers, e.g., five peptides rather than four). In addition, apparently direct transitions between level 1 and level 3 occurred much more often than would be expected from the random superimposition of unit events (*17*), consistent with some cooperativity of oligomer association and dissociation or the formation of channel clusters.

We attempted to increase channel amplitudes by using high concentrations (up to 3.0 *M* both *cis* and *trans*) of neutral NaCl or KCl, but only obtained currents of ~0.25 pA at ±100 mV. We therefore continued to maintain a pH < 3.0 (usually 2.3) on at least one side of the bilayer. Unit currents with very large proton gradients (Fig. 4a) gave highly nonlinear I/V relationships (Fig. 4b) which appeared to be well-described by electrodiffusion theory (*18*). Conductance was ohmic in the more moderate gradients provided by citrate or glycine–HCl buffers (e.g., glycine–HCl, pH 2.3, *cis* vs 3.0 *trans*, Fig. 4c, solid line). Reversal potentials were shifted slightly from the proton equilibrium potential (which is −42 mV for Fig. 4c), even after taking liquid junction potentials of up to 5 mV into account, but remained consistent with a H^+:Cl^- permeability ratio of at least 5:1 (derived from the GHK voltage equation (*18*) and assuming glycine$^+$ is impermeant). On the same basis, the shift in reversal potential when the *trans* chamber was perfused with 3.0 *M* NaCl (leaving glycine–HCl, pH 2.3, *cis*) indicated a H^+:Na^+ permeability ratio of at least 3:1 (Fig. 4c, dotted line). It must be stressed that these values correspond to very unphysiological conditions for the peptide and all the ions involved. Relative permeabilities in normal cellular conditions (and with the complete protein) may differ.

These experiments have been carried out near the limits of useful resolution in a bilayer system (because of the small currents involved) although one advantage of this technique is a very stable current baseline. Better resolution of single-channel currents might be obtained by using smaller bilayers (for example, formed on the tips of patch pipettes (*19*)), but single-channel current transitions at more physiological pH values (~5–7) may only be revealed by fluctuation analysis. It is also important to draw attention to the fact that the

formation of ion channels in a bilayer does not necessarily prove that the peptide involved lines the pore *in vivo*. For example, a functional channel has been formed from peptides modeled on two quite different sequences from the nicotinic acetylcholine receptor (*20, 21*). Our experiments nevertheless do provide clear evidence that the "transmembrane" domain of M2 protein can form proton-conducting ion channels which are blocked by amantadine and therefore support the original hypothesis of Hay and his colleagues that proton translocation by M2 plays an important part in viral pathogenesis (*6, 7*). Our study thus adds to a wealth of convergent evidence to support an ion channel function for M2 and, in particular, its putative transmembrane domain. For example, while amantadine attenuates or prevents influenza infection (*22*), it is ineffective against mutant viruses with substitutions in the transmembrane domain of M2 (*12*), and the Na^+/H^+ exchanger monensin inhibits its action (*11*). Also, while the manuscript was in preparation, Pinto *et al.* (L. H. Pinto, L. J. Holsinger, and R. A. Lamb, *Biophys. J.* **61,** 1992, abstr. A11) reported that the expression of M2 RNA in *Xenopus* oocytes conferred amantadine-sensitive (whole-cell) currents. Amantadine may also interact with other channels, for example to inhibit K-currents in insulin-secreting cells (*23*).

The NB protein of influenza B (*24*), the SH protein of paramyxovirus SV5 (*25*) and the vpu protein of HIV-1 (*26*) are analogous to M2 and may have related functions. In conclusion, we anticipate that proton-conducting channels reconstituted from M2 peptides modelled on amantadine-resistant mutants will be unaffected by the drug, although the channel characteristics of whole M2 protein (when available in sufficient amounts for reconstitution) may differ significantly from those of the isolated transmembrane domain.

ACKNOWLEDGMENT

We thank Dr. Jeremy Bradshaw for comments on an earlier version of the manuscript.

REFERENCES

1. Wilson, I. A., Skehel, J. J., and Wiley, D. M., *Nature* **289,** 366–373 (1981).
2. Varghese, J. N., Laver, W. G., and Colman, P. M., *Nature* **303,** 35–40 (1983).
3. Kilbourne, E., "Influenza," Longman, New York, 1987.
4. Lamb, R., Zebedee, S., and Richardson, C., *Cell* **40,** 627–633 (1985).
5. Zebedee, S. L., and Lamb, R. A., *J. Virol.* **62,** 2762–2772 (1988).
6. Sugrue, R. J., and Hay, A. J., *Virology* **180,** 617–624 (1991).
7. A. J. Hay., *In* "Concepts in Viral Pathogenesis III" (A. L. Notkins and M. B. A. Oldstone, Eds.), pp. 561–567, Springer-Verlag, NY, 1989.
8. Belshe, R. B., and Hay, A. J., *J. Resp. Dis.* Supp. 52–61 (1989).
9. Skehel, J. J., Bayley, P. M., Brown, E. B., Martin, S. R., Waterfield, M. D., White, J. M., Wilson, I. A., and Wiley, D. C., *Proc. Natl. Acad. Sci. USA* **79,** 968–972 (1982).
10. Martin, K., and Helenius, A., *Cell* **67,** 117–130 (1991).
11. Sugrue, R. J., Bahadur, G., Zambon, M. C., Hall-Smith, M., Douglas, A. R., and Hay, A. J., *EMBO J.* **9,** 3469–3476 (1990).
12. Hay, A. J., Wolstenholme, A. J., Skehel, J. J., and Smith, M. H., *EMBO J.* **4,** 3021–3024 (1985).
13. Ito, T., Gorman, O. T., Kawaoka, Y., Bean, W. J., and Webster, R. G., *J. Virol.* **65,** 5491–5498 (1991).
14. Ashley, R. H., *J. Membrane Biol.* **111,** 179–189 (1989).
15. Tosteson, M. T., and Tosteson, D. C., *Biophys. J.* **36,** 109–116 (1981).
16. Schiffer, M., and Edmundson, A. B., *Biophys. J.* **7,** 121–135 (1967).
17. Krouse, M. E., Schneider, G. T., and Gage, P. W., *Nature* **319,** 58–60 (1986).
18. Hodgkin, A. L., and Katz, B., *J. Physiol.* **108,** 37–77 (1949).
19. Coronado, R., and Latorre, R., *Biophys. J.* **43,** 231–236 (1983).
20. Oiki, S., Danho, W., Madison, V., and Montal, M., *Proc. Natl. Acad. Sci. USA* **85,** 8703–8707 (1988).
21. Ghosh, P., and Stroud, R. M., *Biochemistry* **30,** 3551–3557 (1991).
22. Davies, W. L., Grunert, R. R., Haff, R. F., McGahen, J. W., Neumayer, E. M., Paulshock, M., Watts, J. C., Wood, T. R., Hermann, E. C., and Hoffman, C. E., *Science* **144,** 862–863 (1964).
23. Ashcroft, F. M., Kerr, A. J., Gibson, J. S., and Williams, B. A., *Brit. J. Pharmacol.* **104,** 579–584 (1991).
24. Williams, M. A., and Lamb, R. A., *Mol. Cell. Biol.* **6,** 4317–4328 (1986).
25. Hiebert, S. W., Patterson, R. G., and Lamb, R. A., *J. Virol.* **55,** 744–751 (1985).
26. Terwilliger, E. F., Cohen, E. A., Lu, Y., Sodroski, J. G., and Haseltine, W. A., *Proc. Natl. Acad. Sci. USA* **86,** 5163–5167 (1989).